Title
Design of a Biomimetic Hydrogel System for Tissue Engineering Application

Author
Kim, Soyon

Publication Date
2019

Peer reviewed|Thesis/dissertation

UNIVERSITY OF CALIFORNIA

Los Angeles

Design of a Biomimetic Hydrogel System for Tissue Engineering Application

A dissertation submitted in partial satisfaction of the

requirements for the degree Doctor of Philosophy

in Bioengineering

by

Soyon Kim

2019

ABSTRACT OF THE DISSERTATION

Design of a Biomimetic Hydrogel System for Tissue Engineering Application

by

Soyon Kim

Doctor of Philosophy in Bioengineering

University of California, Los Angeles, 2019

Professor Min Lee, Chair

A hydrogel platform using visible light inducible methacrylated glycol chitosan and riboflavin, an aqueous initiator from natural vitamins is biocompatible and supports proliferation of the encapsulated cells. However, the hydrogel platform has limited cell-matrix interaction, relatively slow degradation, and poor ability to deliver growth factors, which may hinder tissue regeneration. Therefore, the objective of this research is to design a hydrogel system which mimics native extracellular microenvironments, provides tunable degradation, and stabilizes bioactivity of growth factors.

The first study explores if the incorporation of native extracellular matrix components in chitosan hydrogel can promote cell-matrix interaction. The hydrogel is functionalized with cell adhesive motifs and cartilaginous or bony matrix. The modified hydrogels increase chondrogenic or osteogenic differentiation of the encapsulated cells by enhancing cell-matrix interaction. This

work suggests a hydrogel platform with a specific microenvironment tailored to promote cell differentiation.

Tuning hydrogel degradation enables effective and successful tissue regeneration by modulating cellular behaviors and matrix formation. A new degradable hydrogel system is developed based on a unique enzyme-substrate complex, lysozyme-chitosan. Incorporation of lysozyme accelerates hydrogel degradation in a dose dependent manner. This study proposes a novel strategy of incorporating an exogenous enzyme specific to the hydrogel which can control degradation kinetics in a cell-independent manner.

Bacterial infection during surgical processes leads to serious complications and continuously results in unsuccessful wound repair. A lysozyme-chitosan conjugate not only allows tunable degradation, but also exhibits antimicrobial properties. The lysozyme modified hydrogels successfully inhibit bacterial growth and delay its proliferation. This work verifies an advanced hydrogel platform with dual functions, tunable degradability and anti-infection.

Although heparin is widely used in controlled release system due to its strong binding ability and protective effect for growth factors such as bone morphogenetic protein-2 (BMP-2), it suffers from natural variability, difficulty in modification, and unknown physiological roles. Heparin mimetic sulfonated molecules can do a similar role of heparin by protecting BMP-2 against therapeutically relevant stressors and enhancing its bioactivity. This work demonstrates a new hydrogel system to improve clinical efficacy of BMP-2 and other heparin-binding growth factors.

These findings suggest great potentials of material-based therapeutics for tissue engineering application.

The dissertation of Soyon Kim is approved.

James C.Y. Dunn

Benjamin M. Wu

Tara Aghaloo

Min Lee, Committee Chair

University of California, Los Angeles

2019

TABLE OF CONTENTS

LIST OF FIGURES

LIST OF TABLES

ACKNOWLEDGEMENTS

First of all, I would like to thank my advisor, Professor Min Lee, for his guidance, giving me an opportunity, and support in my research. I also appreciate the valuable advices from the committee members, Professors James Dunn, Benjamin Wu, and Tara Aghaloo.

I was inspired and got a tremendous help from the Lee lab members who always encouraged and supported me. The time spent with my undergraduate and dental students was also very meaningful. I also would like to thank of the Wu and Dunn labs members for their help. I have also enjoyed the time with friends from Bioengineering and Korean community.

Last but not least, I want to express my sincere appreciation to my loved family for their patience and support. I would not be here without their love.

Parts of Chapter 2 were published in 1) *Biomaterials Science*, 2015, Choi B, Kim S, Fan J, Kowalski T, Petrigliano F, Evseenko D, Lee M: Covalently conjugated transforming growth factor-β1 in modular chitosan hydrogels for the effective treatment of articular cartilage defects, 2) *Acta Biomaterialia*, 2015, Choi B, Kim S, Lin B, Li K, Bezouglaia O, Kim J, Evseenko D, Aghaloo T, Lee M: Visible-light-initiated hydrogels preserving cartilage extracellular signaling for inducing chondrogenesis of mesenchymal stem cells, and 3) *Journal of Materials Chemistry B*, 2016, S. Kim, Z.-K. Cui, J. Fan, A. Fartash, T. Aghaloo, and M. Lee: Photocrosslinkable chitosan hydrogels functionalized with the RGD peptide and phosphoserine to enhance osteogenesis.

Chapter 3 was published in *ACS Applied Materials and Interfaces*, 2018, S. Kim, Z.-K. Cui, B. Koo, J. Zheng, T. Aghaloo, and M. Lee. “Chitosan-Lysozyme Conjugates for Enzyme-Triggered Hydrogel Degradation in Tissue Engineering Applications.”

Chapter 5 was published in *Acta Biomaterialia*, 2018, S. Kim, Z.-K. Cui, P. Kim, L. Jung, and M. Lee. “Design of hydrogels to stabilize and enhance bone morphogenetic protein activity by heparin mimetics.”

VITA

2008	Bachelor of Science, Biotechnology
	Yonsei University, Seoul, South Korea
2010	Master of Science, Environmental Materials Science
	Seoul National University, Seoul, South Korea
2012-2019	Graduate Student Researcher, Bioengineering
	University of California, Los Angeles
2015-2017	Teaching Assistant/Associate/Fellow
	University of California, Los Angeles

Publications (Most recent)

1. **Kim S**, Cui Z.-K., Koo B, Zheng J, Aghaloo T, Lee M, Chitosan-Lysozyme Conjugates for Enzyme-Triggered Hydrogel Degradation in Tissue Engineering Applications, ACS Applied Materials & Interfaces, 10 (48), 41138–41145, 2018.
2. **Kim S**, Cui Z.-K., Kim P, Jung L, Lee M, "Design of hydrogels to stabilize and enhance bone morphogenetic protein activity by heparin mimetics", *Acta Biomaterialia*, 72, 45-54, 2018.
3. Cui Z.-K., **Kim S**, Baljon J, Doroudgar M, Lafleur M, Wu B, Aghaloo T, Lee M, "Design and Characterization of a Therapeutic Non-Phospholipid Liposomal Nanocarrier with Osteoinductive Characteristics to Promote Bone Formation", *ACS Nano*, 11 (8), 8055−8063, 2017.

4. Fan J, Pi-Anruns J, Guo M, Im D. C, Cui Z.-K, **Kim S**, Wu B, Aghaloo T, Lee M, "Small molecule-mediated tribbles homolog 3 promotes bone formation induced by bone morphogenetic protein-2", *Scientific Reports*, 7 (1), 7518, 2017.
5. Cui Z.-K, Sun J, Baljon J, Fan J, **Kim S**, Wu B, Aghaloo T, Lee M, "Simultaneous Delivery of Hydrophobic Small Molecules and siRNA Using Sterosomes to Direct Mesenchymal Stem Cell Differentiation for Bone Repair", *Acta Biomaterialia*, 58:214-224, 2017.
6. Fan J, Guo M, Im C, Pi-Anfruns J, Cui Z.-K, **Kim S**, Wu B, Aghaloo T, Lee M, "Enhanced Mandibular Bone Repair by Combined Treatment of Bone Morphogenetic Protein 2 (BMP-2) and Small Molecule Phenamil", *Tissue Engineering Part A*, 23 (5-6):195-207, 2017. (Front Cover Article)
7. Arakawa C, Ng R, Tan S, **Kim S**, Wu B, Lee M. "Photopolymerizable chitosan collagen hydrogels for bone tissue engineering", *Journal of Tissue Engineering and Regenerative Medicine*, 4:164-174, 2017.
8. **Kim S**, Cui Z.-K, Fan J, Fartash A, Aghaloo T, Lee M, "Photocrosslinkable chitosan hydrogels functionalized with RGD peptide and phosphoserine to enhance osteogenesis", *Journal of Materials Chemistry B*, 4:5289-5298, 2016.
9. Fan J, Im C, Guo M, Cui Z.-K, Fartash A, **Kim S**, Patel N, Bezouglaia O, Wu BM, Wang C.-Y, Aghaloo T, Lee M, "Enhanced osteogenesis of adipose-derived stem cells by regulating BMP signaling antagonists and agonists", *Stem Cells Translational Medicine*, 5:539-551, 2016.
10. Cui Z.-K, Fan J, **Kim S**, Bezouglaia O, Fartash A, Wu BM, Aghaloo T, Lee M, "Delivery of siRNA via cationic Sterosomes to enhance osteogenic differentiation of mesenchymal stem cells", *Journal of Controlled Release*, 217:42-52, 2015.

Chapter 1. Introduction

1.1. Background

1.1.1. Photocrosslinkable Chitosan Hydrogel Platform

Hydrogel has a lot of advantages to use in biomedical applications including tissue engineering. It has a biomimetic three-dimensional microenvironment and is applicable as a minimally invasive manner[1]. In addition, it is easy to form in any desired shape, and mixable with cells and stimulating factors which are parts of tissue engineering triangle.

Chitosan is a naturally occurring polysaccharides with a high biocompatibility and biodegradability. Therefore, it is widely used in biomedical applications including tissue engineering. Glycol chitosan is a water-soluble molecules, which provides hydrophilic nature and easy to form hydrogels with proper crosslinking pathway[2, 3]. Photocrosslinking has mild processing conditions, rapid reactions with minimal heat production, and is easy to control spatiotemporal environment of hydrogels[4]. Due to these features, photocrosslinkable hydrogels are also broadly used in tissue engineering. The abundant amine groups in glycol chitosan can be modified with glycidyl methacrylate to integrate photocrosslinkable moiety[5]. This methacrylated glycol chitosan (MeGC) can form a hydrogel after proper photocrosslinking. Visible blue light (VBL) is 400-500 nm spectrum wavelength with non-thermogenic property, low cytotoxicity, and high transmittance compared with ultra violet (UV). As a result of these aspects, VBL is extensively used in dentistry application to polymerize light-curable resin composites. The last factor for photocrossking is radical generation from photoinitiators. There are several VBL specific photoinitators such as camphoquinone, fluorescein, and riboflavin. Camphorquinone is the most commonly used initiators in dentistry application but has a hydrophobic characteristic. For

hydrophilic initiators, fluorescein is used as a fluorescent tracer in biomedical researches, and riboflavin is a vitamin B2 derivative. Among those three photoiniators, riboflavin (RF) showed the most favorable cell viability and mechanical strength, which it was combined with MeGC and VBL[6]. Therefore, photocrosslinkable chitosan hydrogel platform is ready by integrating MeGC, RF, and VBL (Figure 1-1). In our previous study, MeGC hydrogel platform showed a great potential for tissue engineering application by supporting cell proliferation and extracellular matrix (ECM) deposition[7]. However, this MeGC platform still has several challenges of poor cell-matrix interaction, imperfect delivery ability of bioactive molecules, and relatively slow degradation[8-10].

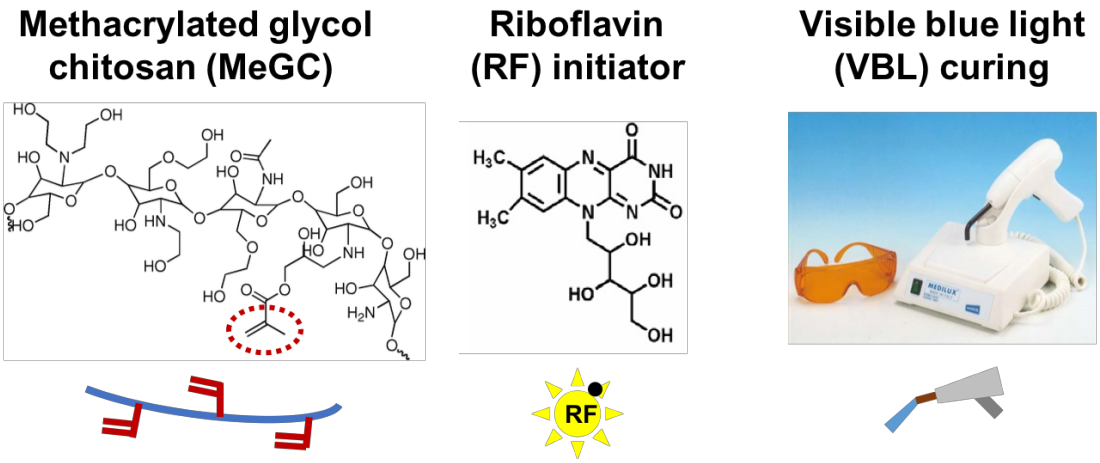

Figure 1-1. Photocrosslinkable chitosan hydrogel platform including methacrylated glycol chitosan, riboflavin as a photointiator, and visible blue light.

1.1.2. Bone Extracellular Matrix Microenvironment

Bone microenvironment is composed of many ECM molecules, cells, and bioactive molecules. The bone ECM provides three-dimensional structure of cell adhesion and anchorage, becomes a

template of mineral initiator and propagation, and regulates various signaling process by interacting with growth factors[11, 12].

Type I collagen is the most abundant protein in bone ECM which is secreted by osteoblast during ossification and assists cell interactions with integrin cell receptors[13, 14]. Many previous studies used type I collagen for biomimetic scaffold such as hydrogel or sponge[10, 15-18]. Specifically, Arg-Gly-Asp (RGD)-containing cell adhesion motif in type I collagen[19] is essential to stimulate osteoblast proliferation and differentiation. Cell adhesion and migration are mediated by integrins, transmembrane receptors clustering to form focal adhesions combining with actin cytoskeleton[20]. Activation of integrin β1 and β3, which are receptors for type I collagen, triggers osteogenesis by forming focal complexes to initiate FAK phosphorylation[21]. Intracellular signaling pathways triggered by integrins (αvβ3, αvβ5 and αIIbβ3) can mediate mesenchymal cell commitment and osteoblast differentiation[22].

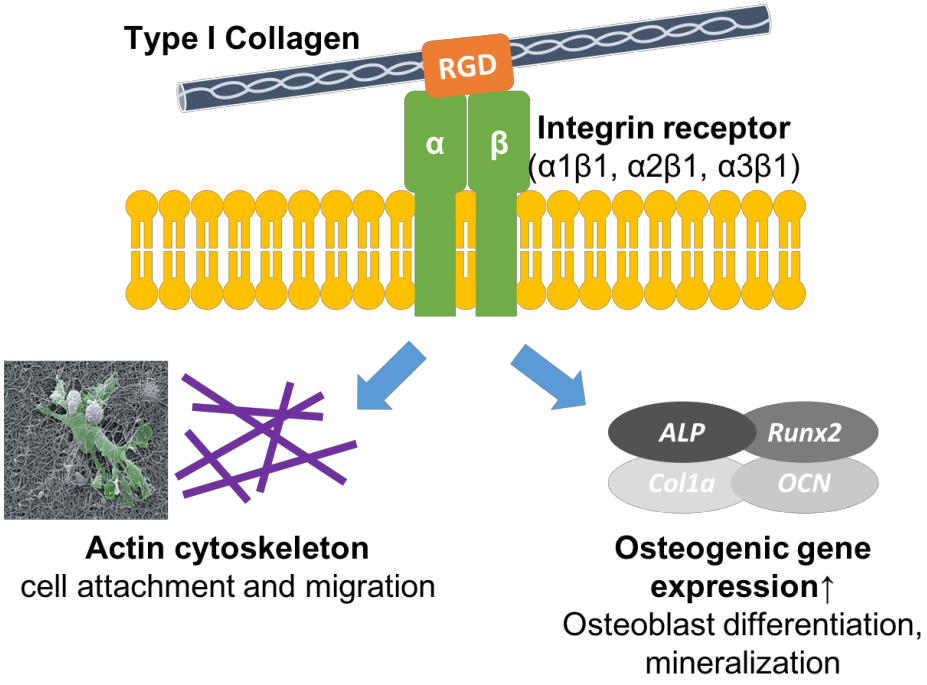

Figure 1-2. Cell adhesion triggered by RGD-integrin signalling pathway.

Non-collagenous phosphoproteins such as bone sialoprotein or osteocalcin is critical for mineralization[23]. High amounts of phosphorylated serine residues in phosphoproteins have a specific interaction with calcium ion to form hydroxyapatites. These phosphate and calcium phosphate molecules trigger osteogenesis and mineral deposition. From the review, osteogenesis can be promoted by PO_4 group and shown spreading morphology while adipogenesis is by t-butyl group and rounded shape[24, 25]. From another review, tethered chemical groups in scaffolds can direct particular chemical interactions which may nucleate cell-secreted molecules[21, 26].

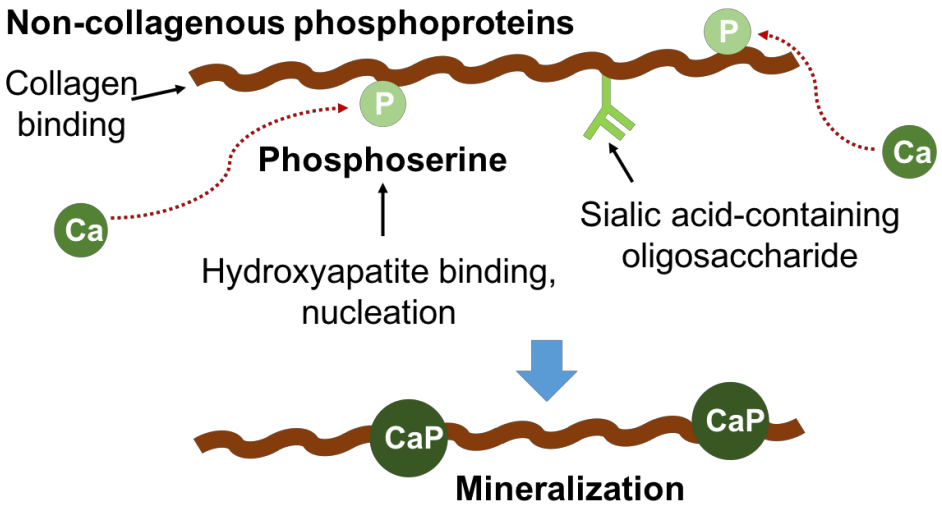

Figure 1-3. Mineral initiation from phosphoserine groups in non-collagenous phosphoproteins.

Mineralization process is very dynamic and heterogenic involving both inorganic apatite formation and organic matrix accumulation. Collagen and non-collagenous proteins start nucleation of crystal whose size is decided by surface area of site of collagen and mineral interaction occurring[23]. The size and three-dimensional distribution of apatite are controlled by collagen matrix and also affects to atomic scale structure[27].

1.1.3. Degradation of Hydrogels

Native ECM is spatiotemporally heterogenic and dynamic[28]. Hydrogels are widely used as model system of extracellular matrix (ECM), and physical properties of hydrogels is one of the key parameters to define architectures in biological tissues. In order to modulate cell invasion, density of matrix and ligand, and matrix stiffness are suggested as key parameters[29, 30]. For two-dimensional setting, cell spreading, proliferation, migration as well as differentiation are influenced by the stiffness of the substrate[31, 32]. For three-dimensional setting, crosslinking degree of hydrogel affects both matrix stiffness and degradability which directly impacted the locomotion and spreading of cells[33]. Besides, three-dimensional microenvironment responds to alteration of healthy matrix and this may affect the result of stem cell based therapy[28]. Hydrogel three-dimensional microenvironment can be controlled by various native ECM cues such as adhesion, degradation, mechanics, growth factors, and mechanical loading[28]. Mesenchymal stem cell fate *in vitro* can be modulated by matrix elasticity such as mechanotransduction[31, 34]. In case of osteogenesis, without exogenous growth factor, mechanotransduction signaling can act synergistically with basal endogenous osteogenic cytokines[35]. For instance, MAPK signaling and *in vitro* osteogenesis is strongly correlated[34].

Transition from initial stable structure to resorbable and soluble products are key concepts of tissue engineering hydrogels[36]. Hydrogel degradation can change property of mechanics, swelling as well as encapsulated cell survival and spreading[33, 37]. Degradable hydrogels have been studied widely with a variety of materials such as poly(ethylene glycol), poly(vinyl alcohol), poly(propylene fumarates) or hyaluronic acid[38-41]. For tissue engineering application, ideal nature of hydrogel is being unbroken till cells to produce extracellular matrix but not staying forever to hinder tissue regeneration. It allows cell infiltration into hydrogels, tissue ingrowth and

ultimately replaced by host tissues[26]. The shortcoming of current scaffolds is their resorption scale do not meet the scale of ECM deposition[42, 43]. When degradability was tuned independently to matrix stiffness, it was still a key factor of multicellular invasion[29]. Degradable hydrogels can be applied to on-demand drug release system with a concept of erosion release which possibly avoid burst release[44]. In addition, after complete drug release correlated with full degradation of hydrogels, it can avoid foreign-body reactions compared with non-degradable implants[45].

The localization of encapsulated cells in hydrogels are highly dependent on hydrogel degradation kinetics. The initial mesh size ($\xi \sim 25$ nm) of hydrogel is usually ~2-3 orders smaller than cell size (~ 20 μm) which can constrain cell migration[46]. Therefore, hydrogel is required to meet a critical mesh size to allow integration of host tissue and migration of encapsulated cells. With spatiotemporal control of cell movement by tunable hydrogel degradation, we can investigate the role of transplanted cells in tissue regeneration such as guiding integration of tissue[47].

1.1.4. Enzyme-Mediated Hydrogel Degradation

The mechanism of degradation varies from hydrolytic degradation occurring throughout the whole hydrogel to local enzymatic break down. Hydrolysis occur across the bulk of a material specifically targeting unstable chemical bonds and physical properties such as crosslinking density during fabrication affect the rate of hydrolysis. Enzyme-mediated hydrogel degradation occurs more locally and mimic tissue remodeling in the body[48]. Enzymatic degradation was mostly mediated matrix metalloproteinases (MMPs), elastases, aggrecanase, or plasmin which are actively regulated in natural ECM remodeling[33, 49, 50]. MMP-cleavable hydrogel incorporated MMP-specific linker in hydrogel structure and degradation was initiated by cell-secreted MMP[42, 51].

However, MMP-cleavable hydrogel has some limitations that degradation is restricted to localized cells which can secrete high enough MMP concentration to cleave a linker, and control of MMP production is very challenging due to association with cell types and its metabolic activity.

To overcome these issues, the incorporation of exogenous hydrogel-specific enzyme which can control degradation kinetics regardless of cell encapsulation can be a great strategy. Lysozyme is endo-carbohydrase cleaving 1,4-beta linkages of chitosan backbone and presents ubiquitously in saliva, tears, or other body secretions[52]. It has a stable three-dimensional structure at various pH (5-9) and due to its degradability of chitosan, chitosan-lysozyme conjugates were used to modulate release of insulin from chitosan nanogel with lysozyme-mediated degradation[53].

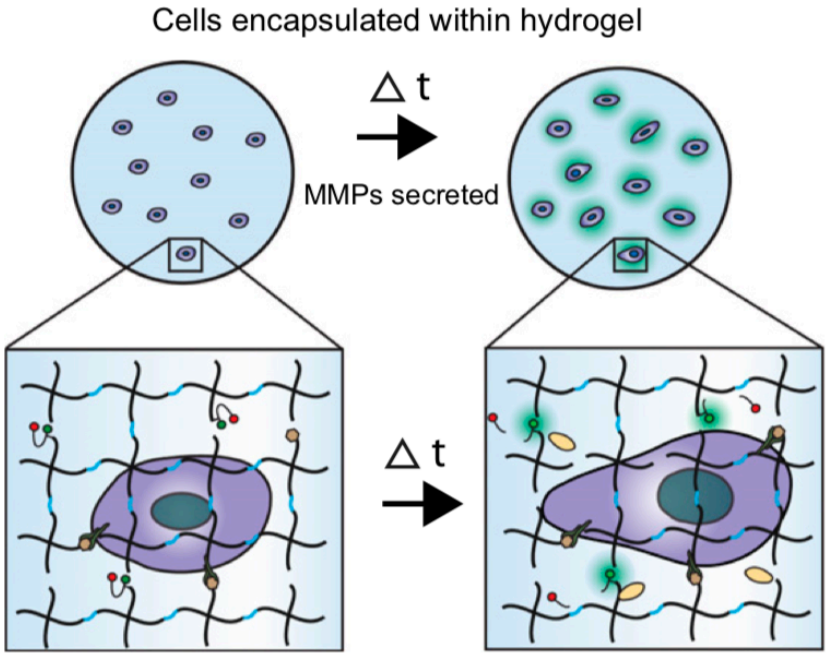

Figure 1-4. Scheme of MMP sensor peptide-functionalized hydrogels[51].

1.1.5. Current Challenges of BMP-2 Applications

BMP-2 is the only Food and Drug Administration (FDA)-approved osteoinductive growth factor and demonstrated extraordinary potential in bone formation. However, its clinical applications

required supraphysiological milligram-level doses which possibly lead to various side effects such as ectopic bone and bone cyst formation, osteoclast-mediated bone resorption, complicate inflammation, and inappropriate adipogenesis etc[54]. In addition, premature release from conventional collagen carrier with a short half-life under various stressed conditions is a key issue[55].

Table 1-1. Clinical and pre-clinical side effects of BMP-2

Adverse effect	Discovery	References
Ectopic bone formation	Soft tissue ectopic bone in spinal application	[56]
Osteoclast activation	Osteoclast-mediated bone resorption and osteolysis Osteoclastogenesis stimulation	[57]
Inflammation	Cervical spine swelling Increase in various cytokines	[58]
Cyst formation and adipogenesis	PPARγ expression induction	[59]

FDA has warned of the potential complications of BMP-2 and there is still ongoing discussion of BMP-2's adverse clinical effects. BMP-2 concentration for consistent bone formation in nonhuman primates is 0.75–2.0 mg/mL which is substantially higher than 0.02–0.4mg/mL required for rodents[60, 61]. By nonhuman primate efficacy testing, 1.5 mg/mL BMP-2 concentration was determined for human trial[62].

Ectopic bone formation was mostly caused by premature leakage into epidural space from spinal application[56]. Osteoclast activation was observed highly in anterior lumbar interbody fusion (ALIF) by enhanced osteoclastic activity in cancellous bone environment[57]. BMP-2 affected osteoclast differentiation stimulated by receptor activator of nuclear factor kappa-B ligand (RANKL) and upregulated osteoclast activity by peroxisome proliferator-activated receptor

gamma (PPAR-γ) pathway[63, 64]. Different types of inflammatory complications including seroma formations to cervical spine swelling, FDA-boxed warning, was reported[54]. Numerous cytokines including IL-1a, IL-1b, IL-6, IL-10, IL-18, TNF-a, macrophage inflammatory protein-1a (MIP-1 a) and monocyte chemotactic protein-1 (MCP-1) were increased and alter the balance of pro-inflammatory and anti-inflammatory cytokines[58]. Bone cyst formation was only reported in pre-clinical studies by antagonistic balance between Runx2, key transcription factor associated with osteogenesis, and PPAR-γ, the master transcriptional regulator of adipogenesis[59].

Besides these multiple side effects, BMP-2 is still a gold standard and there is no suitable alternatives so better understanding of these effects and persistent research to improve BMP-2 use will help both scientists and clinicians[65]. Different strategies for BMP-2 delivery were studied such as dosage alteration, scaffold application, and the implementation of additional proteins etc. There is a recent proof that vascular endothelial growth factor (VEGF) was not only induce angiogenesis but also cross-talked with BMP-2 pathway to influence osteogenesis[66]. Bisphosphonates supplementation with BMP-2 was demonstrated to decrease osteoclast[67, 68] and anti-inflammatory drugs such as corticosteroids addition was directed to drop the inflammatory side effects of BMP-2[69, 70].

The key of biomaterials system for BMP-2 delivery is to retain it at the defect site and control the release and activity[71]. Pharmacokinetics of BMP-2 was affected by the carrier and supraphysiologic concentrations dosages application may influence additional side effects. In addition, recently used recombinant human (rh) forms of BMP-2 were produced deficient of heparin-binding domain which likelihood decrease its clinical bioactivity[72]. There were general requirements of BMP-2 delivery systems; biocompatibility, biodegradability, low immunogenicity, high affinity to BMP-2, maintenance of BMP-2 activity, controlled release, ease

of manufacture, safety and cost-effectiveness etc[73, 74]. FDA approved BMP-2 delivery system is bovine collagen-based devices with limited applications such as spinal interbody fusion and open tibial non-unions due to large doses requirement which may cause severe side effects[74, 75]. An ideal BMP-2 carrier material was necessarily osteoconductive, osteoinductive and osteogenic as well[76, 77]. Alternative carriers for BMP-2 including natural and synthetic polymers, inorganic materials and composites were steadily studied.

1.1.6. Stressors Affecting BMP-2 Stability

Recently, protein-based pharmaceutic industry grew largely due to its superb potential for treatment. However, because of its distinct nature, protein is fragile from intrinsic physical and chemical stress so different strategies to enhance protein's stability and activity was studied[78]. Protein structure was stabilized by different kinds of covalent and non-covalent interactions such as electrostatic interactions, van der waals forces, pi stacking as well as hydrophobic interactions.

Table 1-2. Chemical interactions building protein structure influenced by various stressors

Interactions	Types	Stressors
Covalent	Peptide bond	Proteolytic degradation, chemical crosslinking
	Electrostatic interactions (hydrogen bond, salt bridges, helix capping etc.)	Charge repulsion by pH change, oxidation
Non-covalent	Van der waals forces	Temperature change
	Hydrophobic interactions	Temperature change, oil/water transfer

Development of long-term security of protein drugs can be achieved by the addition of stabilizers such as sugars, polyols and amino acids etc. and chemical modifications such as glycosylation and pegylation etc.

Table 1-3. Various stressors affecting protein stability

Instability	Main stress factors
Proteolytic degradation	Protease exposure
Oxidation	Active oxygen-based radicals (metals, atmospheric oxygen)
Chemical crosslinking	Disulfide and non-disulfide crosslinking
pH denaturation	Extremes of pH (far from pI)
Chemical denaturation	Chemical denaturants to disrupt non-covalent bonds
Thermal denaturation	Extreme temperature, freeze and thaw
Precipitation	High protein concentration, pH, temperature etc.
Kinetic inactivation	Extremes of pH, temperature
Aggregation	Hydrophobic surfaces, phase separation

1.1.7. Heparin Interacting with BMP-2

Heparin is a glycosaminoglycan, a component of ECM, and consisted of a variable sulfated repeating disaccharide. Heparin-binding growth factors regulate diverse biological activities including cellular proliferation and differentiation[79]. Heparin-binding cytokines can preserve molecules from pH, protease related degradation mechanisms[80]. The BMP-2 dimer has two heparin binding sites on N-terminal segments and also binds strongly to ECM and cell surfaces[81]. BMP-2 binds to heparin or heparan sulfate through gathered basic residues in short N-terminal sequences[80].

BMPs, heparin-binding proteins, influence osteoblast differentiation of mesenchymal cells. Homodimers of BMP-2 or BMP-4 or heterodimers of BMP-2/6 or BMP-2/7 induced osteogenesis

with heparin in a dose dependent manner. Signaling of BMPs is started by receptors binding, type I and type II serine/threonine kinase receptors[82, 83]. Constitutively active BMP type I receptor can stimulate BMP signaling without ligand binding which means not affected by heparin. Sulfated polysaccharides such as heparin or heparan sulfate and dextran sulfate have been shown to directly contact with BMPs via charge interaction [81, 84]. Desulfated heparin-derivatives have lost the capacity of stimulation of BMP signaling. Those polysaccharides decreased BMP-2 amount binding to the cell layer or receptors and kept its level in the culture medium which is able to prolong BMP-2 biological activity[85]. Heparin enhance FGFs biological activity by acting as co-receptors and triggering ligand binding to the signaling receptors[86, 87]. Not only the total amount of sulfur but also its position and/or structure is essential to alter BMP-2 stimulating ability. Based on structural analysis of BMP-2, conversed region in BMP-2 mature domain is critical for binding with receptors and basic amino acid stretch located at N-terminal region is critical for heparin-binding[84, 88]. Sulfates are recognized to form stronger salt bridges with lysine and arginine side chains than carboxylates[89]. In addition, pattern of the sulfation groups is important which suggest non-specific electrostatic interaction is not the only mechanism. Sulfated polysaccharides also manage Noggin activity by binding to Noggin and save BMPs signaling[90].

There are also studies that pharmacological agents preventing glycosaminoglycans synthesis or function reverse the effect of GAG binding proteins such as Hurler syndrome which is occurred by partially degraded haparan sulfate[91]. Both endogenous and exogenous GAGs straightly control BMP-2 bioactivity depending on GAGs sulfate residues. In addition, to lower the dose of BMP-2, haparan sulfate, lacking the anti-coagulant effect of heparin, was used to enhance BMP-2 activity by extending BMP-2 half-life, decreasing interaction with noggin and

regulating BMP-2 distribution on cell surface[92]. Heparan sulfate on cell surface can both positively and negatively control BMP-2 activity by increasing heteromeric BMP receptor assembly and signaling or managing BMP-2 internalization and decreasing its binding to the receptor or confining noggin and its inhibitory effects[93, 94].

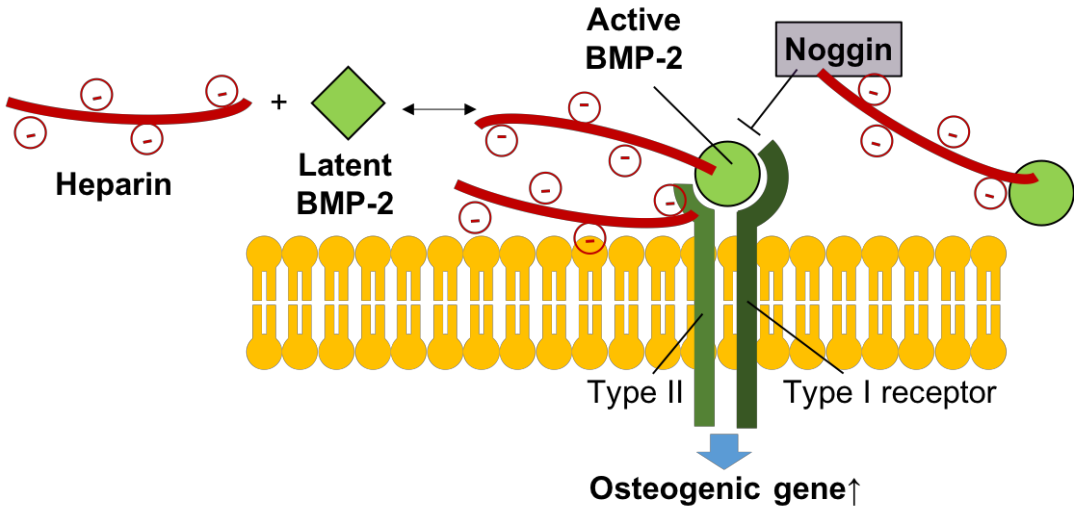

Figure 1-5. Heparin interacting with BMP-2 and modulating its bioactivity by changing BMP-2 to bioactive form, inducing BMP-2 receptor recruitment, and educing BMP-2 antagonist interaction with prolonged half-life.

Basic fibroblast growth factor (bFGF) participating in mesenchymal and neuroectodermal cells proliferation, migration and differentiation strongly binds with heparin[95, 96]. Heparin secures bFGF activity from enzymatic degradation and denaturation[97]. bFGF signaling is induced through high affinity (K_d = 2 - 20 x 10^{-11} M) cell surface receptors[98]. In addition, there are low affinity receptors (K_d = 2 x 10^{-9} M) to heparin sulfate proteoglycans, found on cell surface and extracellular matrix[99, 100]. Heparin and heparin sulfate can reform a low affinity receptor

required for high affinity binding of bFGF and interchangeably act as accessory molecules to enhance bFGF binding by conferring an active, receptor-compatible conformation to bFGF[86]. These cell surface and ECM-bound bFGF contributes to a sustained ligand source to FGF receptors. The degree of sulfation is important that different sulfated polysaccharides such as chondroitin sulfate, hyaluronic acid have no effect to enhance bFGF activity. Heparin's protective effect of bFGF is due to significant tertiary structure changes when it binds to polysaccharide.

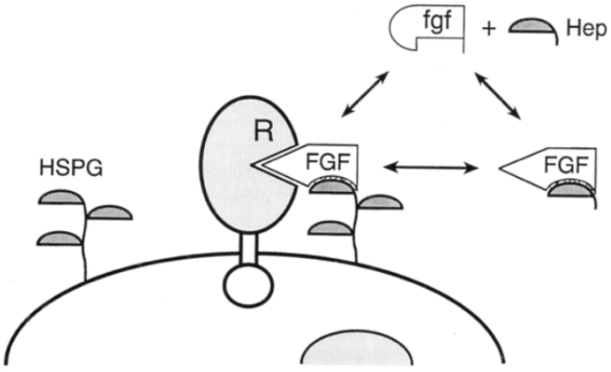

Figure 1-6. An induced model for heparin-dependent high affinity receptor binding of bFGF[86].

Heparin is required for bFGF binding to high affinity receptors on cells even without heparin sulfate proteoglycan[101]. Heparin, bFGF and receptors build a stable trimolecular complex by binding of heparin to both bFGF and receptors[102]. Therefore, heparin itself stabilized FGF dimers and also promotes receptor dimers[101, 103]. The biologically active minimum length of heparin oligosaccharide is eight sugar residues but longer oligosaccharides presented more effective binding by presenting numerous binding sites[102]. In addition, highly sulfated polysaccharides such as heparin or polysulfonates are able to enhance receptors even without FGF ligand[104].

1.1.8. Heparin-Mimicking Polysulfonates

Synthetic polysulfonated compounds has been used with some benefits in clinical trials. Heparin-mimicking polymer by conjugating sulfated group into backbone polymer could stabilize basic fibroblast growth factor (bFGF) from environmentally and therapeutically relevant stressors[105]. Cyanoxyl-mediated polymerized glycopolymers mimicked macromolecular chaperone and showed effective sequestering and protecting fibroblast growth factor-2 (FGF-2) from proteolytic, acid or heat-induced degradation by selective promotion of FGF-2 and fibroblast growth factor receptor (FGFR-1) reaction and it also induces FGF-2 specific proliferative cell response[106]. Polyanionic compounds which mimic heparin were able to replace heparan sulfate proteoglycan (HSPG) for growth factor interaction so it is capable to use sulfonic acid polymers to control interaction with FGF-2 and affect its biological activity *in vitro*[107]. Negatively charged sulfate groups in heparin were found to interact with basic amino acid residues of FGF-2. Polysulfonates mimic heparin or heparin sulfate by binding to FGF-2 and avoiding its interaction with HSPGs and FGFR.

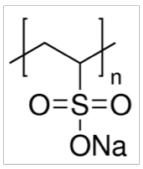

Poly-vinylsulfonic acid (PVSA)

- Mw: 2 kDa
- Repeating unit Mw: 130 Da
- Sulfonate group in 1mol: 15

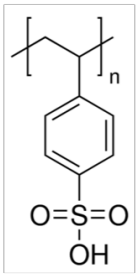

Poly-4-styrenesulfonic acid (PSS)

- Mw: 75 kDa
- Repeating unit Mw: 196 Da
- Sulfonate group in 1mol: 383

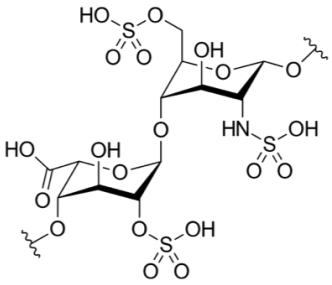

Heparin

- Mw 17-19 kDa
- Repeating unit Mw: 529
- Sulfonate group in 1mol: 34

Figure 1-7. Heparin-mimicking polysulfonates, PVSA and PSS in comparison with heparin.

1.2. Innovation

- A visible blue light inducible hydrogel platform was developed using a photocrosslinkable methacrylated glycol chitosan, methacrylated lysozyme, and a riboflavin initiator. The new hydrogel system is biocompatible and bioactive.
- Tuning hydrogel degradation enables effective and successful tissue regeneration by modulating cellular behaviors and matrix formation. A novel chitosan hydrogel system incorporating an exogenous hydrogel-specific enzyme, lysozyme, can control degradation kinetics in a cell-independent manner.
- Bacterial infection during surgical process leads to serious complications and continuously results in unsuccessful wound repair. The conjugated form of lysozyme in hydrogel could provide antimicrobial properties in an optimized concentration range.

1.3. Research Objectives

Although a hydrogel platform using visible light inducible methacrylated glycol chitosan and riboflavin is biocompatible and supports proliferation of the encapsulated cells, it still has limited cell-matrix interaction, relatively slow degradation, and poor ability to deliver growth factors, which may hinder tissue regeneration. Therefore, the objective of this research is to design a hydrogel system which mimics native extracellular microenvironments, provides tunable degradation, and stabilizes bioactivity of growth factors. This objective was accomplished by completing the following specific aims which were elaborated in Chapter 2, 3, 4 and 5.

Aim 1: To develop hydrogels surface mimicking cartilage and bone extracellular matrix microenvironments.

A. To investigate the chondrogenic efficacy of hydrogel modified with type II collagen.
B. To develop hydrogels modified with bone-specific chemical moieties and investigate the osteogenic efficacy *in vitro* and *in vivo*.

Aim 2: To modulate degradation of hydrogels for bone tissue engineering.

A. To develop and characterize a hydrogel based on a specific enzyme-substrate pair with photocrosslinkable chitosan and lysozyme.
B. To investigate the osteogenesis of encapsulated mesenchymal stem cells in modified hydrogels *in vitro* and *in vivo*.

Aim 3: To verify antimicrobial function of lysozyme-chitosan conjugate.

A. To develop and characterize a hydrogel based on a specific enzyme-substrate pair with photocrosslinkable RGD modified chitosan and lysozyme.
B. To investigate the antibacterial properties of hydrogel *in vitro*.

Aim 4: To stabilize and enhance bone morphogenetic proteins-2 (BMP-2) activity in hydrogels by synthetic heparin mimetics.

A. To investigate BMP-2 stabilizing effect of sulfonated molecules.
B. To determine the enhancement of BMP-2 activity with sulfonated molecules in hydrogels *in vitro*.

Chapter 2. Photocrosslinkable Chitosan Hydrogels Functionalized with Native Extracellular Matrix Components

2.1. Introduction

Hydrogels derived from naturally occurring polymers are attractive three-dimensional networks for tissue engineering applications due to their high biocompatibility and hydrophilicity[2, 108, 109]. Moreover, progenitor or stem cells can be delivered into lesions in a minimally invasive manner. Photopolymerization has been widely employed to crosslink hydrogels due to its rapid and mild reactions with minimal cytotoxicity and possible in situ polymerization[4, 15, 17, 110-115].

We have previously developed a visible blue light (VBL) inducible hydrogel system using methacrylated glycol chitosan (MeGC) and riboflavin (RF, vitamin B2) as a photocrosslinkable polymer and an initiator[5, 116]. In contrast to current photocuring systems using UV light[4, 117], our hydrogel could be prepared under mild conditions, reducing potential adverse effects associated with UV exposure and toxic initiators. Although the hydrogel system supported proliferation and extracellular matrix (ECM) deposition of encapsulated mesenchymal stem cells[6, 7, 118], lack of specific cell binding domains on chitosan surfaces and their highly hydrophilic nature with resultant low protein adsorption can limit cell-matrix interactions, leading to poor osteogenic cellular responses[6, 119]. Recently, numerous strategies have been employed to facilitate osteogenesis in hydrogels, including addition of osteogenic growth factors[120] or bioactive filler materials[117, 121], but the hydrogel in itself showed minimal bone forming ability without the additional osteogenic factors or bioactive materials. Thus, there is a need to develop chitosan hydrogel surfaces that present a favorable osteogenic microenvironment.

During cartilage development, chondrogenic differentiation is regulated by cell–cell and cell–matrix interactions in the presence of various soluble factors. Type II collagen is a main structural protein in articular cartilage and has been proven to play a crucial role in chondrogenesis[122]. Although collagen can form a gel spontaneously, the use of collagen alone is limited in tissue engineering applications due to its significant shrinkage and rapid degradation. Chemical modification can enhance the physical stability of collagen, but this can reduce the bioactivity of natural collagen[123].

During osteogenic development, mesenchymal stem cells produce various fibrous ECM proteins such as collagen, in particular, type I collagen, the main structural protein in bone tissue[117, 124, 125]. Type I collagen is known to enhance cellular attachment due to its abundant Arg-Gly-Asp (RGD) residues and to induce osteogenic differentiation[19, 20, 22, 117, 120, 126, 127]. In addition, non-collagenous bone ECM proteins such as bone sialoprotein and osteocalcin are known to play an important role in mineral nucleation and osteogenic differentiation[128]. Phosphorylated amino acid residues (e.g. phosphoserine) abundant in such proteins are thought to be responsible for inducing nucleation of hydroxyapatite, resulting in enhance bone formation[23, 26].

Although the incorporation of collagen in MeGC hydrogels greatly enhanced cellular attachment, proliferation, and osteogenic differentiation of bone marrow stromal cells (BMSCs) in our previous study, use of natural collagen as tissue scaffolds is limited by their potential immune-and pathogenic effects, material variability, and inadequate mechanical strength[124]. As an alternative, numerous studies have focused on the employment of cell adhesion motifs containing RGD to enhance cell-matrix interactions[20]. The incorporation of RGD-containing peptides onto biomaterial surfaces has been shown to enhance cell adhesion and osteogenic

differentiation[129]. Moreover, recent studies suggest that phosphoserine is an effective functional group in inducing biomineralization[24]. Surface functionalization with phosphoserine induced highly mineralized matrix that increased osteogenic differentiation and osseointegration on the implant surface[21, 115].

In this study, we introduce photopolymerizable hydrogel systems functionalized with ECM components. First part of study investigated whether the incorporation of type II collagen into hydrogel, it can enhance chondrogenesis. Second part of study hypothesized hypothesized that incorporation of RGD and phosphoserine to MeGC hydrogels will synergistically enhance osteogenic differentiation of encapsulated cells and bone regeneration. To test the hypothesis, we will evaluate the ability of the MeGC hydrogels functionalized with type II collagen or RGD peptide and phosphoserine to enhance proliferation and osteogenic differentiation of encapsulated BMSCs.

2.2. Materials and Methods

2.2.1. Materials

Glycol chitosan (GC, ~100 kDa) was purchased from Wako Chemicals USA, Inc. (Richmond, VA). Glycidyl methacrylate (GMA), type II collagen (from chicken sternal cartilage), O-phospho-L-serine (phosphoserine), 1-ethyl-3-(3-dimethylaminopropyl)-carbodiimide (EDC), alizarin red S and ethylene-diaminetetraacetic acid (EDTA) were supplied from Sigma-Aldrich (St. Louis, MO). Succinimidyl-4-(N-maleimidomethyl) cyclohexane-1-carboxylate (SMCC) was purchased from Pierce (Rockford, IL) and Ac-GCGYGRGDSPG-NH_2 peptide (RGD peptide) was obtained from Anaspec, Inc. (Fremont, CA).

2.2.2. Preparation of photocrosslinkable chitosan hydrogel

2% (w/v) GC in distilled water (DW) was mixed with GMA at 1.1 molar ratio of GMA to the amino groups in GC. The mixture was adjusted to pH 9.0 and located on a shaker at room temperature. After 40 h, the solution was adjusted to pH 7.0 and dialyzed with 50 kDa tubes against with DW for 16 h. The purified solution was lyophilized and rehydrated with 1×phosphate-buffered saline (PBS) to obtain a 2 % (w/v) methacrylated glycol chitosan (MeGC) solution[7, 110].

Type II collagen/MeGC composite contained as 0.4% and 2% w/v each. It was prepared by mixing the stock solutions of MeGC (4% w/v in PBS) with type II collagen (1.0% w/v in 0.05% acetic acid).

RGD peptide conjugated photocrosslinkable chitosan (RGD-MeGC) was prepared by SMCC crosslinking reaction. SMCC stock solution was prepared as 7.4 μg/μL in dimethyl sulfoxide (DMSO) and 20 μL of SMCC stock solution was firstly conjugated with 20 mL of 1 % (w/v) MeGC in PBS for 16 h, dialyzed with 50 kDa tubes for 16 h and lyophilized. SMCC conjugated MeGC was rehydrated to 1 % (w/v) in PBS and reacted with 1 mg/mL of RGD peptide in DW for 16 h, dialyzed with 50 kDa tubes for 16 h and lyophilized. Phosphoserine conjugated photo-crosslinkable chitosan (PS-MeGC) was prepared by EDC activated reaction. EDC solution was prepared as 84 mg/mL and 1 mL of EDC solution was reacted with 50 μL of 200 mg/mL phosphoserine in DW for 30 min and mixed with 1 % (w/v) MeGC in PBS for 16 h, dialyzed with 50 kDa tubes for 16 h and lyophilized. Both phosphoserine and RGD peptide conjugated photo-crosslinkable chitosan (PSRGD-MeGC) was prepared by the same method of RGD-MeGC and PS-MeGC preparation. In brief, PS-MeGC was reacted with SMCC and then modified with RGD peptide.

2.2.3. Characterization of hydrogels

To observe the distribution of Col II in hydrogels, disk-shaped hydrogels (diameter = 5 mm, height = 2 mm) were embedded in the optimal cutting temperature medium (OCT) and frozen at −80 °C. The frozen blocks were sectioned along the plane of the construct at 20 μm thickness and mounted on glass slides. The cryo-sections collected from the top, middle, and bottom of the construct were stained with 0.1% picrosirius red solution (Polysciences, Inc., Warrington, PA) and specimens were observed under a polarized light microscope. To observe the stability of Col II incorporated in hydrogels over time, MeGC/Col II hydrogels were incubated in PBS at 37 °C for up to 21 days, stained with picrosirius red solution, and observed under the polarized light microscope.

The conjugation of RGD peptide and phosphoserine to the MeGC backbone was analyzed via ^{1}H NMR in D_2O (Bruker ARX400 spectrometer). RGD peptide conjugation was quantified based on the integration of the peaks at 3.8 - 3.9 ppm ($A_{3.8\text{-}3.9}$, protons in proline ring in RGD peptide). Phosphoserine conjugation was quantified based on the reduction of the peaks at 3.4 - 3.7 ppm ($A_{3.4\text{-}3.7}$, protons in NH_2). The degree of substitution was reported as relative to total amine groups. The degree of substitution of RGD peptide and phosphoserine was 3.8% and 5.5%, respectively.

2.2.4. *In vitro* cell proliferation in hydrogels

Chondrocytes were isolated from the knees of 3-month old male New Zealand white rabbits (Charles River Laboratories, Wilmington, MA). The mouse bone marrow stromal cell line (BMSCs, D1 ORL UVA [D1], D1 cell, CRL-12424) was purchased from American Type Culture Collection (ATCC, Manassas, VA). All cells were cultured in culture medium (CM) including

Low Glucose Dulbecco's Modified Eagle's Medium (DMEM, Life Technologies, Grand Island, NY), 10 % (v/v) Fetal Bovine Serum (FBS, Mediatech Inc, Manassas, VA), 1 % (v/v) Penicillin/Streptomycin (Life Technologies) at 37 ^{o}C with 5 % CO_2 humidified atmosphere. cells were trypsinized and encapsulated in hydrogels with 1×10^7 cells/mL concentration. Hydrogels encapsulated with cells were incubated in CM for 2 weeks and medium was changed twice a week. The viability of cells was imaged after calcein/ethidium homodimer staining for 15 min using Live/Dead staining kit (Invitrogen, Carlsbad, CA). Cells in hydrogels were imaged under fluorescent microscope. Encapsulated Cells in hydrogels were fixed in 10% neutral buffered formalin (NBF) for 16 h, embedded in paraffin and cut into sections of 5 μm thickness. Sectioned slides were deparaffinized and stained with hematoxylin and eosin (H&E) to assess cell proliferation. All the images were obtained with Olympus IX71 microscope (Olympus, Tokyo, Japan).

2.2.5. *In vitro* cell differentiation in hydrogels

To induce chondrogenic differentiation, cells encapsulated in hydrogels were incubated in chondrogenic medium consisting of DMEM with 10% FBS, ITS+ Premix supplement (BD Biosciences, Bedford, MA), 100 nM dexamethasone, 40 μg mL^{-1} L-proline, 1 mM sodium pyruvate and 50 μg mL^{-1} L-ascorbic acid 2-phosphate.

To induce osteogenic differentiation, cells encapsulated in hydrogels were incubated in OM for 3 weeks and medium was changed twice a week. Cells encapsulated in hydrogels were fixed in 10 % neutral buffered formalin for 16 h and stained with picrosirius red (Polysciences, Inc.) to assess collagen deposition and alizarin red S to assess mineralization. Macroscopic images were taken using Olympus SZX16 Stereomicroscope.

2.2.6. Statistical analysis

Statistical analysis was performed using one-way analysis of variances (ANOVA), with the Tukey's post hoc test. A value of $p < 0.05$ was considered as significant.

2.3. Results

2.3.1. Incorporation of type II collagen into hydrogel and its effect to the encapsulated cells

The cationic nature of chitosan hydrogel made it easy to modify with native ECM molecules such as type II collagen (Col2), the most abundant ECM molecules in cartilage tissue. Chitosan hydrogel had a simple affinity binding with Col2 (Figure 2-1a) and its distribution inside hydrogel was studied after picrosirius staining of cryosections (Figure 2-1b). The MeGC/Col2 hydrogel displayed a highly birefringent area as compared to the pure MeGC hydrogels, indicating the presence of Col2 in the gels after crosslinking. The distribution of Col2 was relatively homogeneous throughout the hydrogels as shown by picrosirius red stained sections obtained from various regions of the hydrogels. The stability of the incorporated Col2 over time was confirmed by incubating the hydrogels in PBS for up to 21 days (Figure 2-1c). The feasibility of MeGC/Col 2 to support chondrogenic differentiation was further investigated by histological examination (Figure 2-1d). H&E staining revealed that encapsulated chondrocytes maintained their characteristic round shape over the culture period in hydrogel. Cartilaginous ECM deposition was evaluated by safranin-O staining to observe sGAG and immunohistochemistry for Col2, Col1, and Col10. Accumulation of sGAG increased over the culture period and positive safranin-O staining was observed immediately adjacent to chondroid cell clusters in MeGC after 6 weeks. In contrast, the region of safranin-O positive ECM extended throughout the hydrogel matrix as well as around

cellular aggregates in MeGC/Col2, indicating increased sGAG accumulation. Immunostaining showed Col2 production was higher for MeGC/Col2 compared to MeGC. The markers of immature and hypertrophic chondrocytes (Col1 and Col10) were minimally detected in MeGC/Col2, suggesting the presence of mature chondrocytes that are not hypertrophic in the hydrogels and a stable hyaline phenotype.

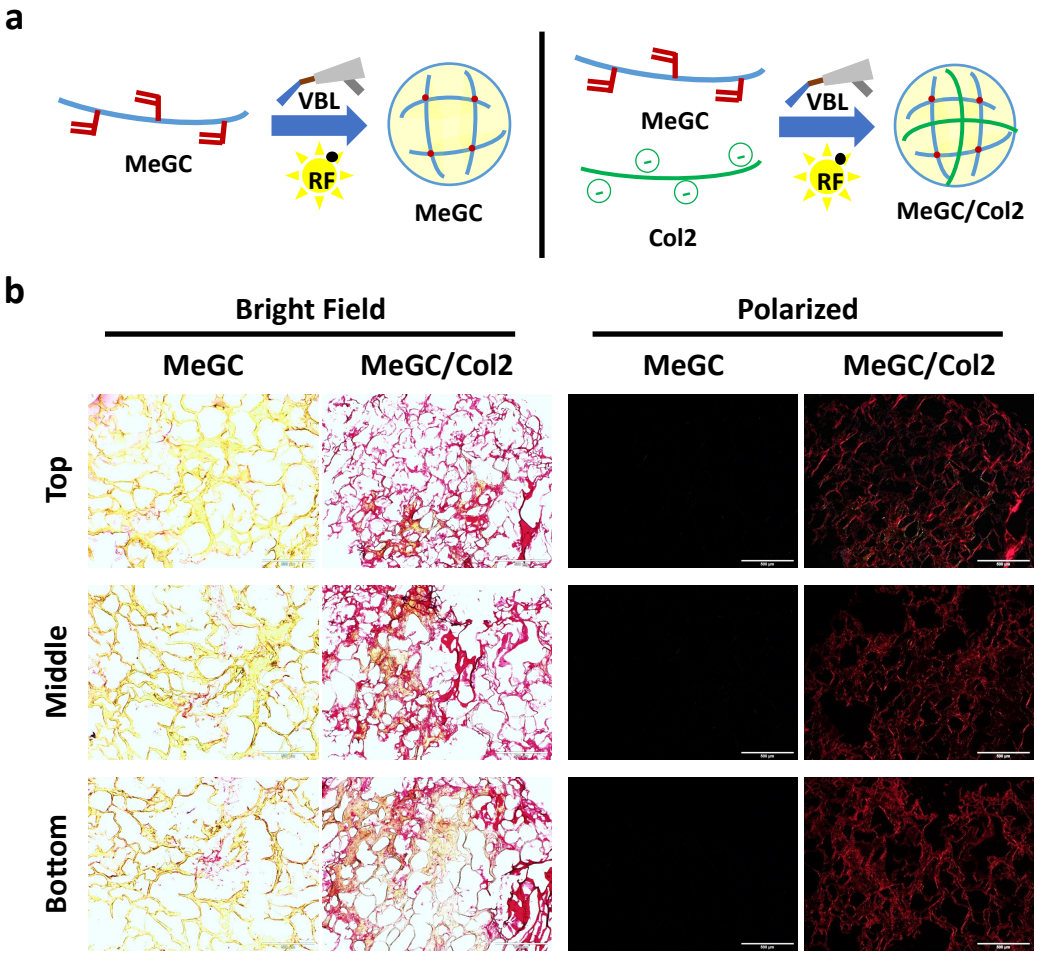
a
MeGC
VBL
RF
MeGC
MeGC
Col2
VBL
RF
MeGC/Col2
b
Bright Field
Polarized
MeGC
MeGC/Col2
MeGC
MeGC/Col2
Top
Middle
Bottom
c
MeGC
MeGC/Col2
Day1
Day1
Day7
Day21
d
H&E
sGAG
Col2
Col1
Col10
MeGC
MeGC/Col2

Figure 2-1. (a) The scheme of hydrogel preparation modified with type II collagen. (b) Incorporation of Col2 in hydrogels verified with picrosirius staining. Bright field (left) and polarized light (right) microscopic images performed on the cryosections (2 μm) collected from the top, middle, and bottom of disk-shaped hydrogels (diameter = 5 mm, height = 2 mm). Scale bars are 200 μm. (c) Polarized light microscopic images of hydrogels after incubation in PBS at 37 °C and subsequent picrosirius red staining. (d) Histological analysis of three-dimensional cultured chondrocytes in hydrogel system after six weeks culture. Sections are stained with H&E, safranin-O (sGAG; orange red), and immunohistochemically stained with Col2, Col1, and Col10. Scale bar is 200 μm.

2.3.2. Incorporation of RGD peptide and phosphoserine into hydrogels

Adhesion ligands containing RGD peptide were covalently coupled into MeGC using SMCC crosslinkers and the RGD incorporation were verified with ^{1}H NMR (Figure 2-2b). The ^{1}H NMR spectra of RGD-MeGC and PSRGD-MeGC exhibited the appearance of the peaks corresponding to the functional groups contained in the grafted peptide sequence, indicating successful conjugation of RGD peptide.

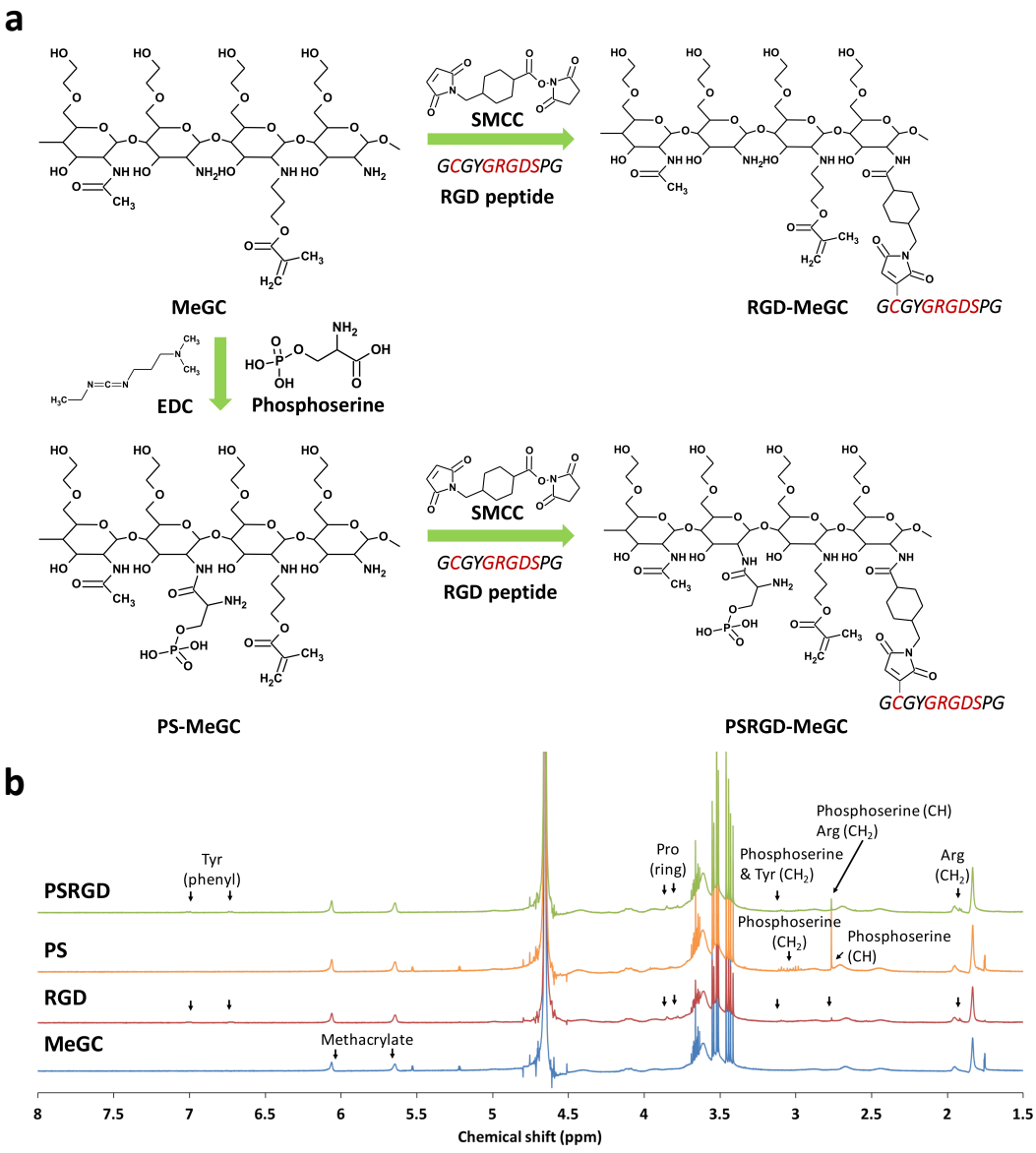

Figure 2-2. Modification of hydrogels with the RGD peptide and/or phosphoserine (RGD-MeGC, PS-MeGC and PSRGD-MeGC). (b) ^{1}H NMR spectra of MeGC, RGD-MeGC and PSRGD-MeGC (400 MHz, D_2O) to analyze conjugation of RGD peptide.

2.3.3. Proliferation and osteogenic differentiation of encapsulated cells in hydrogels

BMSCs encapsulated in hydrogels were round in shape and formed large clusters over the 14-day culture period with no indication of cell spreading (Figure 2-3a). Similar cell growth was observed in the hydrogels conjugated with phosphoserine only. In contrast, cells cultured in RGD-modified hydrogels exhibited extensive spreading with a spindle-like shape at day 14. A high level of viability (over 95%) of encapsulated cells was observed in all experimental groups by Live/Dead staining. The hydrogels modified with RGD peptide significantly enhanced cell proliferation compared with unmodified hydrogels. The incorporation of phosphoserine did not result in significant differences in cell proliferation over the culture period. Morphology of BMSCs cultured in the hydrogels was observed by histological examination (Figure 2-3b). H&E staining exhibited large cell aggregated near the surface of unmodified MeGC hydrogels or hydrogels modified with phosphoserine only at day 14. In contrast, BMSCs cultured in the hydrogels modified with RGD peptide extensively spread with a spindle-like shape and proliferated along the surface of the hydrogel. Moreover, cells in hydrogels co-modified with RGD peptide and phosphoserine formed dense cellular layers near the periphery of the hydrogel and intense cell growth extended toward the center of the hydrogel.

Osteogenic differentiation of BMSCs in hydrogels was determined by collagen and mineral staining. The extent of collagen deposition and mineralized matrix was confirmed by picrosirius red and alizarin red S staining appeared in MeGC hydrogels modified with RGD peptide or phosphoserine (Figure 2-3c). Especially, BMSCs cultured in hydrogels co-modified with RGD peptide and phosphoserine exhibited highly intense positive throughout the entirety of the hydrogel, indicating strong collagen deposition and mineralization.

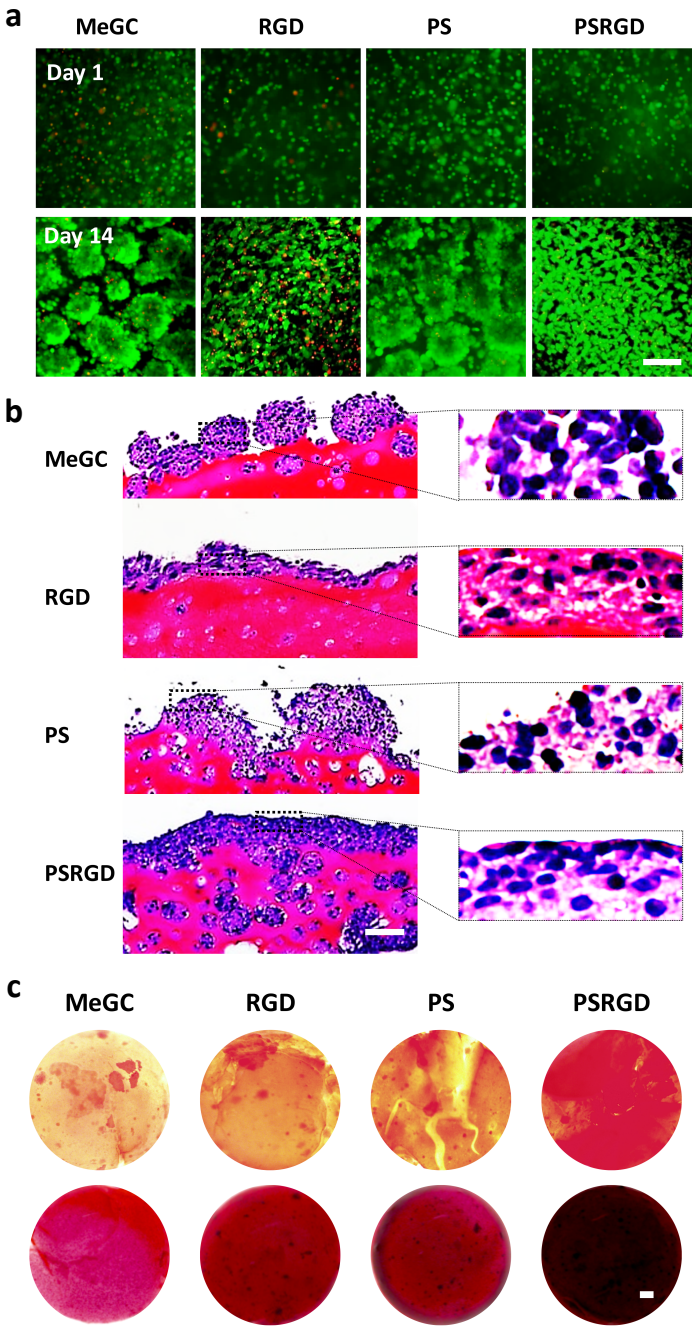

Figure 2-3. Proliferation of BMSCs encapsulated in hydrogels for 2 weeks culture. (a) BMSCs viability and morphology in hydrogels observed with Live/Dead staining. (b) Histological analysis of BMSCs in hydrogels. (c) Picrosirius red (top) and alizarin red S (bottom) staining of hydrogel sections. The scale bar is 100 μm.

2.4. Discussion

The primary goal of this study is to create hydrogel matrix that mimic natural extracellular microenvironment by introducing cartilage specific type II collagen or bone specific RGD peptide and phosphoserine into MeGC which is already developed in our previous study.

Type II collagen is one of the major ECM components in cartilage tissue and is proven to play a crucial role in mediating an early mesenchymal condensation process during chondrogenesis[130]. The homogenous mixture of Col2 in crosslinked MeGC successfully enhanced cartilaginous ECM deposition in hydrogel which was confirmed by safranin-O staining. Histologic staining revealed a high cell cluster density in the outer region of the hydrogels, while the cluster density remained low in the interior region. The observed heterogeneous cell distribution in the hydrogels might be due to mass transport and nutrient exchange limitations whereby insufficient oxygen and soluble factors are transported to the interior regions of the hydrogels, resulting in cell death.

Cell-matrix interactions play important roles in cell growth, survival, and differentiation in bone tissue engineering. Although high cell viability was observed in all experimental MeGC hydrogels as shown by Live/Dead staining, BMSCs encapsulated in pure MeGC hydrogels remained round in shape and formed clusters along the hydrogel surface, indicating minimal cell-matrix interaction. In contrast, BMSCs near the periphery of the MeGC hydrogels modified with RGD peptide greatly spread and proliferated over time. This is mostly mediated by binding of the cell surface integrin receptors to RGD motif present on hydrogel networks, allowing cells to attach and proliferate[131, 132]. Moreover, BMSCs in hydrogels co-modified with RGD peptide and phosphoserine not only spread and proliferate extensively along the hydrogel surface but also

penetrated toward the interior of the hydrogels. It is possible that the employed phosphate groups promoted protein adsorption and integrin-matrix interactions on the hydrogel surface, resulting in increased cell proliferation and matrix remodeling as hydrogels degraded by cell-secreted enzymes. Similar cell growth with dense cellular layers was observed on the MeGC hydrogels modified with collagen in our previous study[124].

2.5. Conclusions

We developed injectable biomaterial systems that mimic specific tissue extracellular environment by incorporating ECM proteins or cell adhesion motifs and phosphorylated groups to photocrosslinkable chitosan hydrogels. These modified hydrogels successfully enhance cell-matrix interaction and guide specific differentiation. The present work suggests that our hydrogel system functionalized with RGD peptide and phosphoserine has a great potential as a biomaterial for bone tissue engineering applications.

2.6. Acknowledgement

This work has been published in 1) *Biomaterials Science*, 2015, Choi B, Kim S, Fan J, Kowalski T, Petrigliano F, Evseenko D, Lee M: Covalently conjugated transforming growth factor-β1 in modular chitosan hydrogels for the effective treatment of articular cartilage defects, 2) *Acta Biomaterialia*, 2015, Choi B, Kim S, Lin B, Li K, Bezouglaia O, Kim J, Evseenko D, Aghaloo T, Lee M: Visible-light-initiated hydrogels preserving cartilage extracellular signaling for inducing chondrogenesis of mesenchymal stem cells, and 3) *Journal of Materials Chemistry B*, 2016, S. Kim, Z.-K. Cui, J. Fan, A. Fartash, T. Aghaloo, and M. Lee: Photocrosslinkable chitosan hydrogels functionalized with the RGD peptide and phosphoserine to enhance osteogenesis.

Chapter 3. Chitosan-Lysozyme Conjugates for Enzyme-Triggered Hydrogel Degradation in Tissue Engineering Applications

3.1. Introduction

Tissue-engineered hydrogels mimicking native extracellular matrix (ECM) microenvironments offer a spatiotemporally heterogenic and dynamic nature[10, 28, 46]. The nature of hydrogels can direct the fate of the encapsulated cells such as migration, infiltration, proliferation, differentiation, and tissue rearrangement[8, 33, 36]. Cell migration and infiltration are favored in porous structure which can provide enough space for cell movement as well as ECM depositions guiding differentiation pathways[34, 133, 134].

The porous architecture of hydrogels can be obtained by modulating hydrogels degradation via various mechanisms. Hydrolytic degradation originated from water-susceptible functional groups may encounter high initial mass loss which makes it difficult to interact with the encapsulated cells[135]. Photoactive degradation triggered by photolabile groups is challenging to apply in tissue engineering due to a need of additional light activation[136]. Protease-mediated degradation mimics local enzymatic breakdowns such as matrix metalloproteinases (MMP) regulation in tissue remodeling of natural ECM[137]. However, MMP-mediated degradation is limited to the localized cells where the MMP concentration is high enough to cleave MMP-sensitive bonds, as well as hard to control MMP production level correlated with cell types, numbers, and metabolic activities[42]. Therefore, incorporation of exogenous hydrogel-specific enzymes that can control degradation kinetics regardless of cell encapsulation is an appealing strategy[138].

Chitosan is a well-proven polysaccharide with high biocompatibility and has numerous primary amines that can be conjugated with diverse functional groups such as the photo-crosslinkable methacrylate group[6, 8]. Chitosan hydrogels have been used in various tissue engineering applications including bone, cartilage, and neural regeneration[125, 139]. Lysozyme, a well distinguished endo-carbohydrase, ubiquitously presents in saliva, tears, or other body secretions[140] and cleaves 1,4-beta-linkages between N-acetylmuramic acid and N-acetyl-D-glucosamine of a chitosan backbone. Moreover, lysozyme is capable of destructing bacterial cell walls that contain peptidoglycan[141]. It also exhibits a stable three-dimensional structure and maintains stability at various pH (5-9), suitable to utilize in tissue remodeling environments[142]. Lysozyme is widely applied in chitosan scaffolds or films to modulate its material characteristics since *in vivo*, chitosan is mainly degraded by lysozyme targeting the acetylated part, and the final product of degradation, glucosamine, is nontoxic to cells[52, 143-145]. Therefore, lysozyme incorporated chitosan hydrogels can potentially induce porous structure by causing degradation.

We have previously developed a visible blue light-crosslinkable hydrogel system using methacrylated glycol chitosan (MeGC) and riboflavin, an aqueous initiator from natural vitamins[110]. Enhanced proliferation and osteogenic or chondrogenic differentiation of mesenchymal stem cells (MSCs) encapsulated in MeGC hydrogel were demonstrated[8, 110, 118, 119]. However, it had relatively slow degradation profile which may interfere with tissue regeneration.

In this work, we report a novel hydrogel system with fine-tuned degradability based on a unique enzyme-substrate pair, lysozyme-chitosan. Lysozyme was modified with photo-crosslinkable moiety for stable conjugation in MeGC hydrogel. Degradation profiles and morphological changes of MeGC hydrogels were evaluated using cryogenic scanning electron

microscopy (cryo-SEM). Cryo-SEM preserves native structures in a frozen hydrated state through rapid freezing and provides a direct imaging of samples in nanometer resolution. The degree of degradation with various lysozyme concentration was examined by analyzing the pore size change in the cryo-SEM micrographs. The effects of hydrogel degradation on cell proliferation, migration, and construct modulus were assessed by encapsulation or seeding of bone marrow stromal cells (BMSCs). We further investigated whether the hydrogel modification with lysozyme can promote osteogenesis of mesenchymal cells *in vitro* and bone regeneration in a mouse calvarial defect model.

3.2. Materials and Methods

3.2.1. Materials

Glycol chitosan (GC, B100 kDa), glycidyl methacrylate (GMA), lysozyme from chicken egg white, tween-20, *p*-nitrophenol phosphate, β-glycerophosphate, L-ascorbic acid, dexamethasone, riboflavin (RF), nitro blue tetrazolium (NBT), 5-bromo-4-chloro-3-indoxylphosphate, alizarin red S and ethylene diaminetetraacetic acid (EDTA) were supplied by Sigma-Aldrich (St. Louis, MO). Low glucose dulbecco's modified eagle's medium (DMEM), penicillin/streptomycin (P/S, 100 U mL^{-1}) and trypsin were purchased from Life Technologies (Grand Island, NY). Fetal bovine serum (FBS) was obtained by Mediatech Inc. (Manassas, VA). All solvents and products were used without further purification.

3.2.2. Preparation of Lysozyme Incorporated Hydrogel

Methacrylated glycol chitosan (MeGC) was prepared by following the previously developed method[6, 8]. Methacrylated lysozyme (MeLyz) was prepared by reaction of 200 mg mL^{-1}

lysozyme and GMA at a 1.1 molar ratio in distilled water (DW) for 18 h on a shaker at room temperature. After reaction, it was dialyzed in 3 kDa tubes against DW for 24 h, lyophilized and rehydrated in 1x phosphate buffered saline (PBS) at 200 mg mL^{-1}.

3.2.3. Bioactivity of Methacrylated Lysozyme

Vancomycin-resistant *Staphylococcus aureus* Mu50 (*S. aureus*, ATCC 700699) was used to test bioactivity of MeLyz[146]. The bacterial culture was diluted to 5 x 10^7 colony-forming units (CFU) mL^{-1} with sterile Luria-Bertani (LB). Lysozyme solution was prepared as 0, 0.01, 0.1, 0.5, 1, and 5 mg mL^{-1} with sterile LB. 500 µL of the bacterial solution was added to 500 µL of lysozyme solution and cultured for 5 h at 37 °C. The counts of bacteria were quantified by measuring the optical density of medium at 600 nm (OD_{600}) by UV/Vis spectrophotometer (Beckman Coulter). Based on the OD_{600} value, bacterial survival rate was quantified and calculated as bacterial survival percentage.

3.2.4. Degradation Kinetics of Hydrogels

Degradation kinetics of hydrogels were measured by the dry weight change of hydrogels. The hydrogels with different MeLyz concentrations (0, 0.1, 1, and 10 mg mL^{-1}) were incubated in DW for two weeks at 37 °C. At day 0, 1, 7, and 14, hydrogels were collected (n = 4), and after lyophilization, the dry weight was weighed. The degradation of hydrogels was calculated by the following equation (1).

$$Gel\ degradation\ (\%) = \frac{W_0 - W_t}{W_t} \times 100 \qquad (1)$$

where W_0 and W_t, refers to the dry weight of a hydrogel at day 0 and each time point.

3.2.5. Theoretical Mesh Sizes of Hydrogels

The theoretical mesh sizes of hydrogels were calculated based on Flory-Rehner theory. First of all, the swelling ratio based on hydrogel mass (Q_M) was computed by the following equation.

$$Q_M = \frac{M_s}{M_D}$$

where M_s is the hydrogel mass after swelling and M_D is the dry hydrogel mass. The volume swelling ratio of hydrogel (Q_v) was calculated by the following equation.

$$Q_v = 1 + \frac{\rho_s}{\rho_p}(Q_M - 1)$$

where ρ_s is the density of the solvent (1 g/cm^3 for water) and ρ_p is the density of the hydrogel (1.12 g/cm^2 for PEG and 0.8 g/cm^2 for chitosan)[135]. The specific volume of the polymer ($\bar{\nu}$) is calculated by the following equation.

$$\bar{\nu} = \frac{\rho_s}{\rho_p}$$

Second, $\bar{M}_c$, the molecular weight of the polymer chain between two neighboring crosslinking points, was calculated by the following equation.

$$\frac{1}{\bar{M}_c} = \frac{2}{\bar{M}_n} - \frac{\frac{\bar{\nu}}{V_1}\left(\ln\left(1 - \nu_{2,s}\right) + \nu_{2,s} + \chi_1 {\nu_{2,s}}^2\right)}{{\nu_{2,s}}^{1/3} - \frac{\nu_{2,s}}{2}}$$

where $\bar{M}_n$ is the number-average molecular weight of the un-crosslinked hydrogel (the molecular weight of the polymer), $\bar{\nu}$ is the specific volume of the polymer, V_1 is the molar volume of solvent (18 cm^3/mol for water), $\nu_{2,s}$ is the polymer volume fraction in the equilibrium swollen hydrogel, which is equal to $1/Q_v$, and χ_1 is the polymer-solvent interaction parameter (0.426 for PEG-water and assumed constant for PEG $\nu_{2,s}$ is 0.04 to 0.2; chitosan $\nu_{2,s}$ is 0.01 to 0.04). The correlation between χ_1 and $\nu_{2,s}$ is given below[147]:

$$\chi_1 = \frac{\ln(1 - \nu_{2,s}) + \nu_{2,s}}{{\nu_{2,s}}^2}$$

In the presence of water, it may modify the chemical potential change due to elastic forces which will change the volume fraction density of the chains during crosslinking so Flory-Rehner equation can be adjusted like the following equation[148].

$$\frac{1}{\bar{M}_c} = \frac{2}{\bar{M}_n} - \frac{\frac{\bar{\nu}}{\bar{V}_1}(\ln(1 - \nu_{2,s}) + \nu_{2,s} + \chi_1 {\nu_{2,s}}^2)}{\nu_{2,r}\left[\left(\frac{\nu_{2,s}}{\nu_{2,r}}\right)^{1/3} - \left(\frac{\nu_{2,s}}{2\nu_{2,r}}\right)\right]}$$

Here, $\nu_{2,r}$ is the polymer volume fraction in the relaxed state, which is defined as the state of the polymer right after crosslinking but before swelling.

Hydrogel mesh size (ξ) was then calculated by the following steps. The root-mean-square end-to-end distance of the polymer chain in the unperturbed state ($({\bar{r}_0}^2)^{1/2}$) was calculated by the following equation.

$$({\bar{r}_0}^2)^{1/2} = l{C_n}^{1/2} n^{1/2}$$

where l is the average bond length (0.146 nm for PEG, 0.154 nm for vinyl polymers, and 0.4 nm for chitosan), C_n is the Flory characteristic ratio of the polymer (typically 4.0 for PEG, 60 for chitosan), and n is the number of bonds (or links) in the cross-link.

$$n = 2\frac{\bar{M}_c}{M_r}$$

where M_r is the molecular weight of the repeat unit (44 for PEG and 250 for chitosan). Then mesh size was calculated by the following equation.

$$\xi = {\nu_{2,s}}^{-1/3}({\bar{r}_0}^2)^{1/2}$$

where $\nu_{2,s}{}^{-1/3}$ is elongation ratio of the polymer chains in any direction for isotropically swollen hydrogel. By customizing the molecular structure of hydrogels ($\nu_{2,s}$, $\bar{M}_c$, and ξ), their mechanical, responsive, and diffusive properties will be varied.

3.2.6. Morphological Observations of Hydrogels

The morphology of hydrogels was observed with a Cryogenic-Scanning Electron Microscopy (Cryo-SEM, TESCAN Mira 3 filed emission SEM coupled with a Leica cryogenic system). Hydrogels were sandwiched between two freezer planchettes (Type "A", Ted Pella, Inc.) with 100 μm depth. The total volume of the hydrogel should be enough (at least 5.6 μL) to fill the gap created by both planchettes. The hydrogel-loaded planchettes were vitrified in liquid ethane (~ -170 °C) for ~ 5 s and then transferred to a freeze fracture/sputtering coater (Leica ACE 600). The samples were freeze fractured and sublimated at -105 °C for 90 min to reveal the structure of hydrogel. The sublimation condition was optimized to observe the underlying surface feature of the hydrogel without distorting their native morphology. Following the sublimation, an approximately 5 nm of gold layer was sputter-coated. The sample was imaged in the pre-cooled (~ -142 °C) TESCAN Mira 3 FE-SEM operated at 5 kV. An area less than 20 μm away from the planchette wall was imaged to minimize insufficient freezing. The size of pore created by hydrogel degradation was quantified by ImageJ (NIH, Bethesda, Maryland) after processing images to the binary mode and analyzing particles.

3.2.7. *In vitro* Cell Viability and Proliferation in Hydrogels

The mouse bone marrow stromal cell line (BMSC, CRL-12424, ATCC, Manassas, VA) were cultured in culture medium (CM) consisting of DMEM with 10% (volume per volume) FBS and

1% (volume per volume) P/S at 37 °C under 5% CO_2 humidified atmosphere. The BMSCs were encapsulated in hydrogels with 2 x 10^6 cells mL^{-1} concentration. The hydrogels with different MeLyz concentrations (0, 0.1, and 1 mg mL^{-1}) were incubated in CM for two weeks at 37 °C. At day 1, 7, and 14, the viability of cells was pictured with Live/Dead staining kit (Invitrogen, Carlsbad, CA). To quantify the cell viability, the ratio of live cells to total cells were calculated based on green and red color by ImageJ software (NIH, Bethesda, Maryland). The alamarBlue assay was performed to quantify the cell growth by following the manufacture's protocol. The relative cell growth was measured by the following equation (2).

$$Relative\ cell\ growth = \frac{F_e - F_b}{F_c - F_b} \qquad (2)$$

where F_e, F_c, and F_b refer to fluorescence emission value at 585 nm after excitation at 570 nm of experimental, control (MeGC at day 0) and blank groups, respectively. To evaluate the change in mechanical properties of hydrogels by cell growth, the compressive modulus of cell-laden hydrogels was measured via an indentation test at day 1, 7, and 14 by Instron Electromechanical Testing Machine (Instron, Model 5564, Norwood, MA) using a 1.6 mm diameter indenter as described previously[8, 149].

3.2.8. *In vitro* Cell Migration on Hydrogels

The BMSCs were seeded on the top surface of hydrogels with 2 x 10^4 cells per hydrogel (300 μL, molded in 48-well plate) and cultured for 14 days to observe cell migration from the top to the bottom of hydrogel. At each time point, cells were stained with Live staining kit and imaged by Confocal Multiphoton STED microscope (Leica TCS-SP5 AOBS, Buffalo, IL) to track on Z direction.

3.2.9. *In vitro* Osteogenesis of Cells in Hydrogels

The BMSCs encapsulated hydrogels were cultured in osteogenic medium (OM) including CM, 10 mM of β-glycerophosphate, 50 μg mL^{-1} of L-ascorbic acid and 100 nM of dexamethasone for three weeks to induce osteogenic differentiation. After four days of culture, hydrogels were collected and fixed in 10% NBF for alkaline phosphatase (ALP) staining. The hydrogels were incubated in AP solution (100 mM Tris, pH 8.5, 50 mM $MgCl_2$, 100 mM NaCl) with NBT and 5-bromo-4-chloro-3-indoxylphosphate[150]. For ALP activity test, the hydrogels were digested in 0.02% tween-20 solution in 1x PBS, mixed with *p*-nitrophenol phosphate for 10 min and an absorbance at 405 nm was measured. ALP activity was normalized by total protein expression from Pierce BCA Protein Assay Kit (Thermo Scientific, Rockford, IL). After three weeks of culture, hydrogels were collected and fixed for alizarin red S staining for mineral deposition measurement. The fixed hydrogels were incubated in 2% alizarin red S solution for 5 min and washed in 1x PBS for 2 h. All stained hydrogels were imaged by Olympus SZX16 Stereomicroscope. The osteogenic genes, *Runx2*, *Col1a* and osteocalcin (*OCN*), expression was measured by qRT-PCR. For *Runx2* and *Col1a*, hydrogels were collected at day 4 and for *OCN*, they were collected at day 21. After incubation, total RNA was extracted using Trizol (Invitrogen, Ca) and RNeasy mini kit (Qiagen, CA). Total RNA was reverse transcribed with cDNA transcription kit (Invitrogen, CA) and quantitative real-time polymerase chain reaction (qRT-PCR) was performed to evaluate the expression of osteogenic critical markers in a LightCycler 480 PCR (Indianapolis, IN) with SYBR Green. It was amplified 45 cycles and *GAPDH* was used for normalization. The primer sequence of each gene was as following: *GAPDH*: AGGTCGGTGTGAACGGATTTG (forward), TGTAGACCATGTAGTTG AGGTCA (reverse); *ALP*: GTTGCCAAGCTGGGAAGAACAC (forward), CCCACCCCGCTATTCCAAAC (reverse); *Runx2*: CGGTCTCCTT CCAGGATGGT

(forward), GCTTCCGTCAGCGTCAACA (reverse); *Col1a*: AACCCGAGGTATGCTTGATCT (forward), CCAGTTCTTCATTGCATTGC (reverse); *OCN*: GGGAGACAACAGGGAGGAAAC (forward), CAGGCTTCCTGCCAGTACCT (reverse). All experiments were triplicated.

3.2.10. *In vivo* Bone Forming Ability of Hydrogels

All operations were executed by the Guide for the Care and Use of Laboratory Animals of the University of California, Los Angeles approved by the Chancellor's Animal Research Committee. To decrease the host immune response to implanted cells, the adult nude mice (CD-1, 2 months old, Charles River Laboratories) were used. The adult nude mice (n = 4 per groups) were anesthetized and 3 mm diameter craniotomy defects were created with trephine drill following our previous study[151]. Each defect was washed with saline solution, filled with hydrogels containing MSCs and crosslinked with VBL for 40 s. After surgery, all animals were placed on a warm sheet and moved to the vivarium for postoperative care. All mice received subcutaneous injection of buprenorphine with 0.1 mg kg^{-1} for three days and drinking water including trimethoprim-sulfamethoxazole for seven days.

3.2.11. Three-Dimensional Microcomputed Tomography Scanning

After six seeks (for bone formation study) of implantation, all mice were sacrificed and calvarial tissues were collected. The calvarial tissues were fixed in 4% formaldehyde for 48 h at room temperature, washed with PBS and stored in 70% ethanol at 4 ^{o}C till imaging. The resolution of high-resolution microcomputed tomography (μCT40; Scanco USA, Inc., Southeastern, PA) was 10 μm (57 kVp and 180 μA radiation source with 0.5 mm aluminum filtration). Reconstruction of

μCT images was done by OsiriX MD (Pixmeo SARL, Switzerland) and new bone growth area was analyzed by ImageJ. The percent bone volume (BV TV^{-1}) and trabecular number (Tb.N) were assessed by CTAn (Bruker MicroCT).

3.2.12. Histological Examination

For *in vitro* cell migration study, hydrogels at day 0, 7, and 14 were fixed in 10% neutral buffered formalin (NBF) for 16 h and embedded in paraffin to cut into 5 μm thickness. The sections were imaged after deparaffinizing and hematoxylin and eosin (H&E) staining. For *in vivo* bone healing study, the fixed calvarial tissues were decalcified in 10% EDTA solution for a week under gentle shaking. The decalcified tissues were embedded in paraffin to cut into 5 μm thickness, deparaffinized, and stained with H&E and Masson-goldner trichrome to investigate new bone formation.

3.2.13. Statistical Analysis

The one-way analysis of variance (ANOVA) with Tukey's *post hoc* test was used for statistical analysis. A value of $p < 0.05$ was considered as significant.

3.3. Results

3.3.1. Preparation of Lysozyme Incorporated Hydrogels

For lysozyme incorporated hydrogel fabrication, methacrylated lysozyme (MeLyz) was prepared by the reaction of lysozyme with glycidyl methacrylate (GMA), and integrated into MeGC hydrogel[110] by visible blue light crosslinking (Figure 3-1a). Under various concentrations of MeLyz (0, 0.01, 0.1, 0.5, 1, and 5 mg mL^{-1}), the survival rate of *S. aureus* is similar for natural

lysozyme and MeLyz, which confirmed that the bioactivity of MeLyz is comparable to natural lysozyme (Figure 3-1b). Then, MeLyz was incorporated in MeGC at the concentration of 0, 0.1, 1, and 10 mg mL^{-1} respectively, for hydrogel degradation study. The introduction of MeLyz in MeGC accelerated the degradation rate in a dose dependent manner (Figure 3-1c).

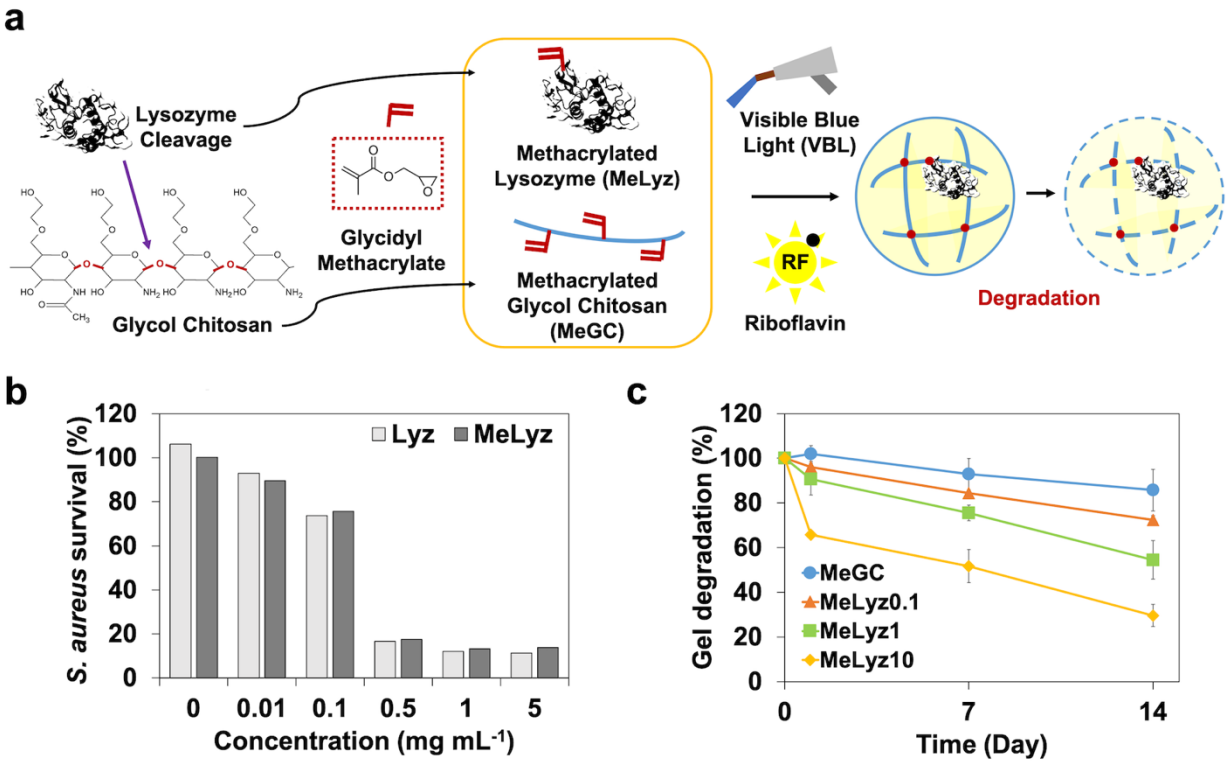

Figure 3-1. a) The scheme of degradable hydrogel preparation with MeLyz incorporation. Lysozyme degrades chitosan by cleaving 1,4-beta-glycosidic bond in chitosan backbone. b) Bioactivity of MeLyz in comparison to lysozyme tested by antibacterial effect on *S. aureus* for 5 h. c) Degradation kinetics of hydrogels for 14 days by measuring dry weight.

3.3.2. Theoretical Mesh Sizes of Hydrogels

Based on Flory-Rehner equation, hydrogel mesh size, associated with swelling ratio, was calculated (Figure 3-2). With the incorporation of MeLys and over time, the mesh sizes of hydrogels were increased due to enhanced swelling ratio as a result of degradation.

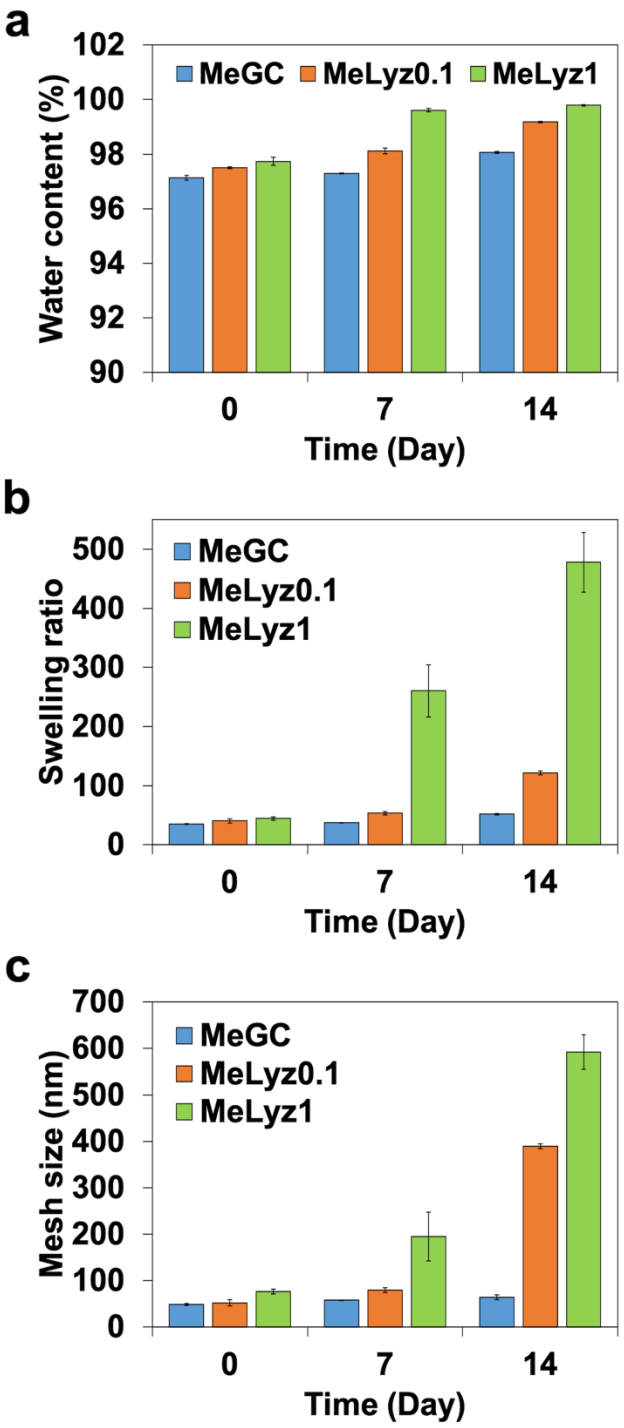

Figure 3-2. a) Water content and b) swelling ratio of MeGC, MeLyz0.1, and MeLyz1 for 14 days. c) Theoretical mesh sizes of hydrogels calculated by swelling ratio.

3.3.3. Morphological Observations of Hydrogels

Cryo-freezing and cryo-SEM allows the study of dynamic process of hydrogels degradation with improved ultra-structural preservation and nanometer resolution. Variety of pores were generated in hydrogel scaffold when the degradation occurred. The degradation of the three hydrogels was examined by measuring pore size from cryo-SEM micrographs (Figure 3-3a). At day 0, all three hydrogels yielded comparable pore sizes of 39 ± 14, 37 ± 15, and 38 ± 14 nm respectively for MeGC, MeLyz0.1, and MeLyz1; thereafter increased to 68 ± 27, 86 ± 49, and 409 ± 396 nm respectively, after 10 days (Figure 3-3b). A clear trend was observed where both the average pore size and size distribution increased as MeLys dose increases for MeLys0.1 and MeLys1. Yet, MeLys1 hydrogel showed the greatest distribution in pore size with a larger fraction of outliers, reaching up to 1,200 nm at day 10.

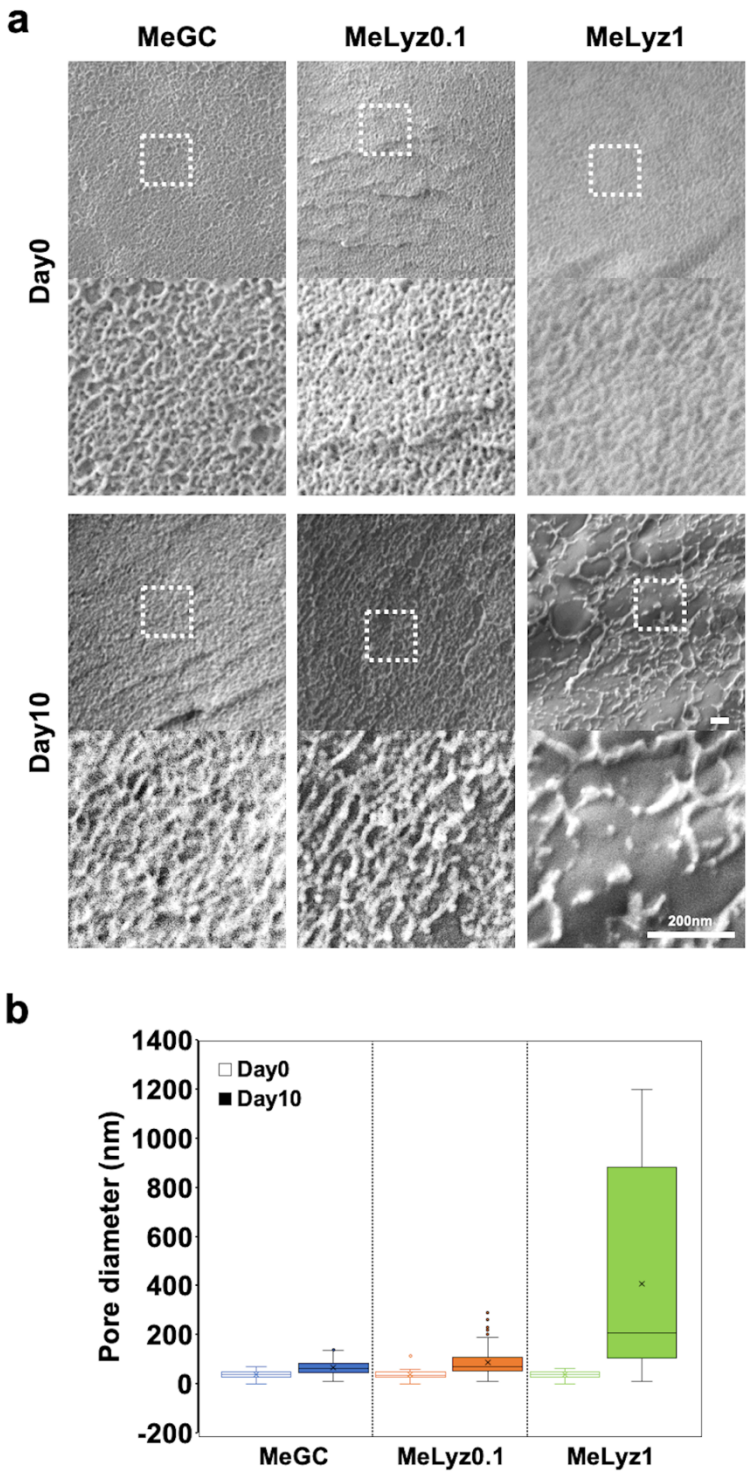

Figure 3-3. a) Morphological observations of MeGC, MeLyz0.1, and MeLyz1 hydrogels by Cryo-SEM at day 0 and 10. b) The box graph of pore diameter from Cryo-SEM analysis.

3.3.4. *In vitro* Cell Viability and Proliferation in Hydrogels

The BMSCs were mixed with hydrogel solution (MeGC, MeLyz, and RF) before visible blue light (VBL) crosslinking for cell encapsulation (Figure 3-4a). The viability of BMSCs encapsulated in hydrogels was observed over two weeks, and both fluorescent images and the quantitative analysis demonstrated that cell viability in all hydrogels was above 90% over two weeks (Figure 3-4b). This indicated that regardless of MeLyz incorporation, hydrogels have biocompatible environments. In spite of the high viability of cells, fluorescent images at day 14 showed larger green-colored areas for MeLyz0.1, and MeLyz1 compared with those for MeGC. This result can be clarified by the cell proliferation result (Figure 3-4c) pointing out the higher cell proliferation of MeLyz0.1, and MeLyz1 than that of MeGC, with intensified the green fluorescence in cell viability images (Figure 3-4b). To investigate the change of mechanical strength of hydrogel *via* cell encapsulation, a compressive modulus test was performed with or without the encapsulation of BMSCs (Figure 3-4d). The initial compressive modulus of MeGC, MeLyz0.1, and MeLyz1 without cells at day 1 was 7.9, 7.4, and 7.1 kPa, which are similar around 7.5 kPa. However, after two weeks, the modulus of MeLyz0.1 and MeLyz1 without cells decreased to 2.6 and 1.4 kPa, which are significantly lower than that of MeGC, 6.9 kPa. We already observed the mass loss of hydrogels with degradation (Figure 3-1c), hence the decrement of compressive modulus can also be explained as a consequence of degradation. However, with the encapsulation of cells, all MeGC, MeLyz0.1, and MeLyz1 showed enhanced compressive modulus over the time compared to that of hydrogels without cells. Particularly, MeLyz0.1 and MeLyz1 at day 14 had significantly risen, which represented that the production of ECM from the proliferated cells as a result of hydrogel degradation supported the mechanical strength.

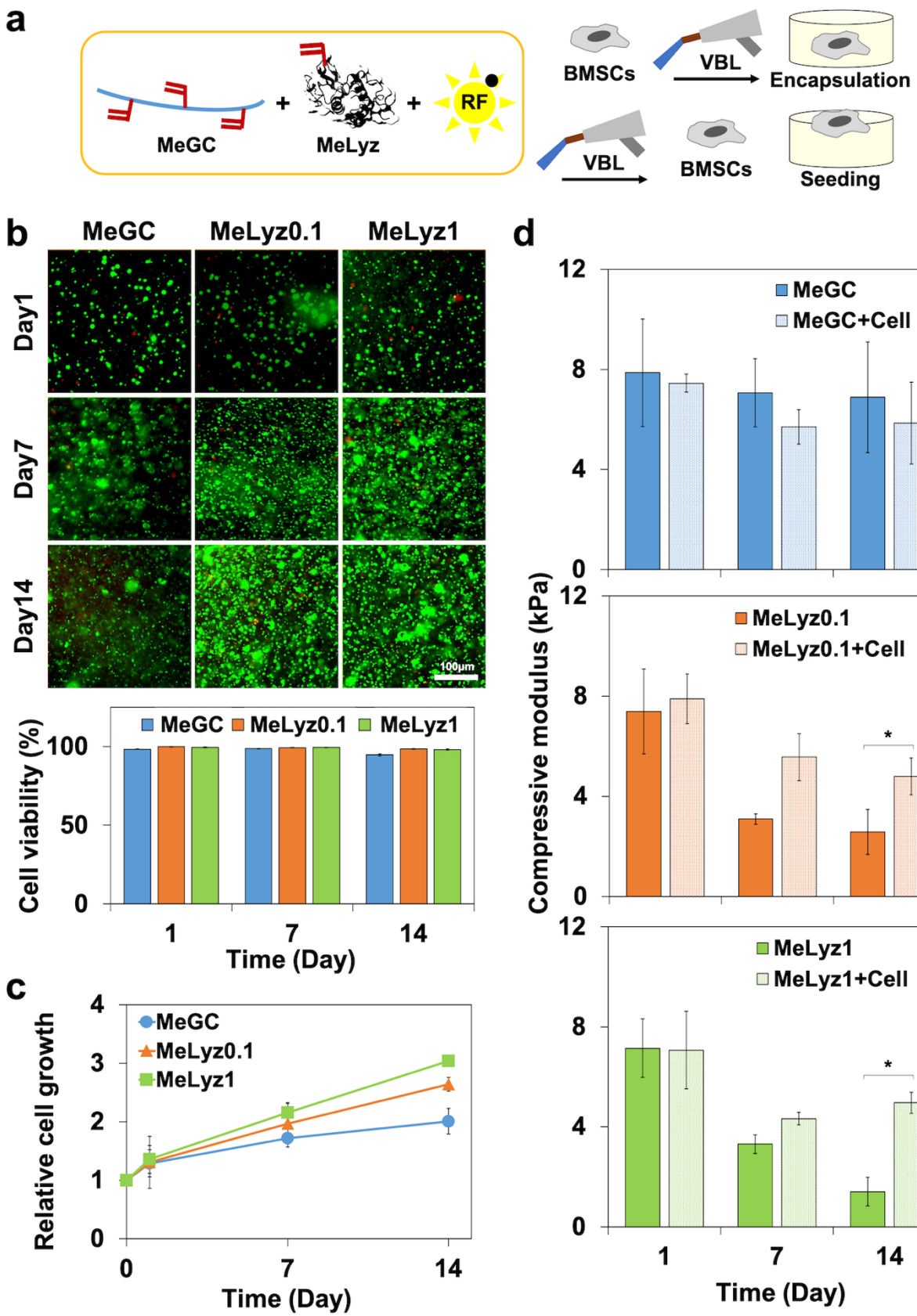
a
MeGC
MeLyz
RF
BMSCs
VBL
Encapsulation
VBL
BMSCs
Seeding
b
MeGC
MeLyz0.1
MeLyz1
Day1
Day7
Day14
100μm
Cell viability (%)
MeGC MeLyz0.1 MeLyz1
Time (Day)
c
Relative cell growth
MeGC
MeLyz0.1
MeLyz1
Time (Day)
d
Compressive modulus (kPa)
MeGC
MeGC+Cell
MeLyz0.1
MeLyz0.1+Cell
MeLyz1
MeLyz1+Cell
Time (Day)

Figure 3-4. a) The scheme of BMSCs encapsulation and seeding to hydrogels. b) Live/Dead staining images of BMSCs encapsulated in MeGC, MeLyz0.1, and MeLyz1 for 14 days and quantified cell viability. c) Relative cell growth of BMSCs encapsulated in hydrogels evaluated by alamarBlue assay. d) Compressive modulus of MeGC, MeLyz0.1, and MeLyz1 hydrogels compared with hydrogels with BMSCs encapsulation for 14 days (*$p < 0.05$).

3.3.5. *In vitro* Cell Migration on Hydrogels

The BMSCs were seeded on the surface of VBL-crosslinked hydrogels (Figure 3-4a), and migration from the upper surface to the inside of hydrogels was monitored by the confocal microscope for two weeks. Cells were observed only on the surface of MeGC hydrogels, instead spread throughout the hydrogel bulk in MeLyz1 over time (Figure 3-5a). To further investigate the migrated cells on the hydrogels, histological analysis was processed (Figure 3-5b). For MeGC, cells seeded on the surface of hydrogels did not penetrate inside of hydrogels. On the other hand, cells seeded on MeLyz1 permeated into hydrogels over two weeks. The surface of both hydrogels changed from smooth to rough structure, possibly due to contractile force on the surface with the proliferation of cells[10]. Specifically, the surface of MeLyz1 at day 14 was entangled with the migrated cells and exhibited more uneven structure than that of MeGC.

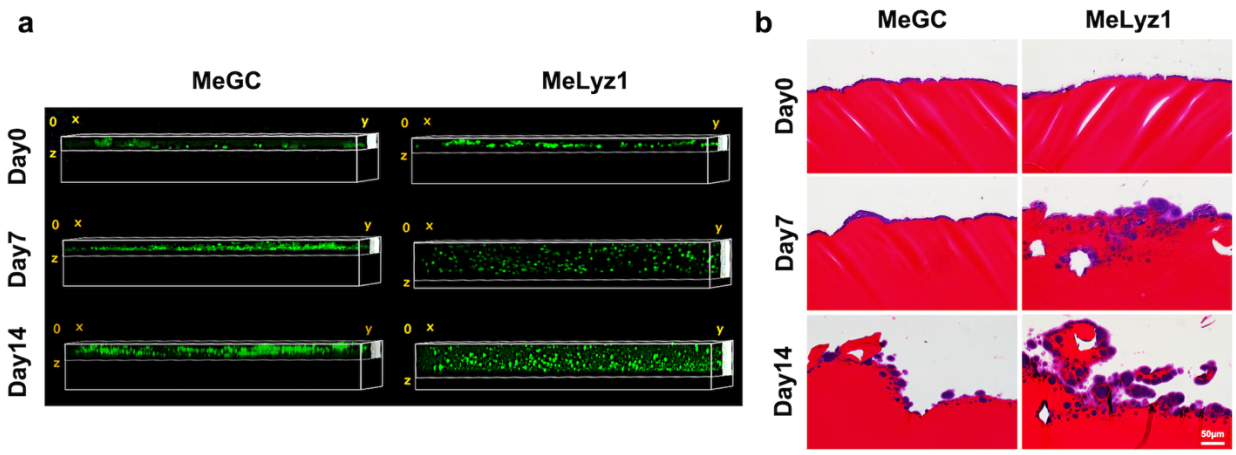

Figure 3-5. *In vitro* cell migration on hydrogels. a) BMSCs seeded on hydrogel surface at day 0 and monitored cell movement for 14 days. b) Histological evaluation (H&E staining) of cell migration from hydrogel surface for 14 days.

3.3.6. *In vitro* Osteogenesis of Cells in Hydrogels

The BMSCs were encapsulated in hydrogels (Figure 3-4a) and osteogenic differentiation of cells was evaluated. The alkaline phosphatase (ALP) expression, an early stage osteogenic marker, was assessed by staining and the activity test (Figure 3-6a). The intensified staining and increment of ALP activity normalized by total protein expression was observed in MeLyz incorporated hydrogels in a dose dependent manner. Next, mineral expression, a late osteogenic marker, was examined by alizarin red S staining and the calcium production assay (Figure 3-6b). Similar with ALP expression, darker staining and elevated calcium production were shown in MeLyz incorporated hydrogels with higher dosage compared with those in MeGC. The early osteogenic genes, *Runx2*, an essential controller of osteogenesis, and *Col1a*, a gene for type I procollagen, were upregulated at day 4 with the incorporation of MeLyz (Figure 3-6c). In addition, the late

osteogenic gene, *OCN*, expression was also enhanced at day 21 in MeLyz incorporated hydrogels. All three osteogenic genes were highly produced in a MeLyz dose dependent manner.

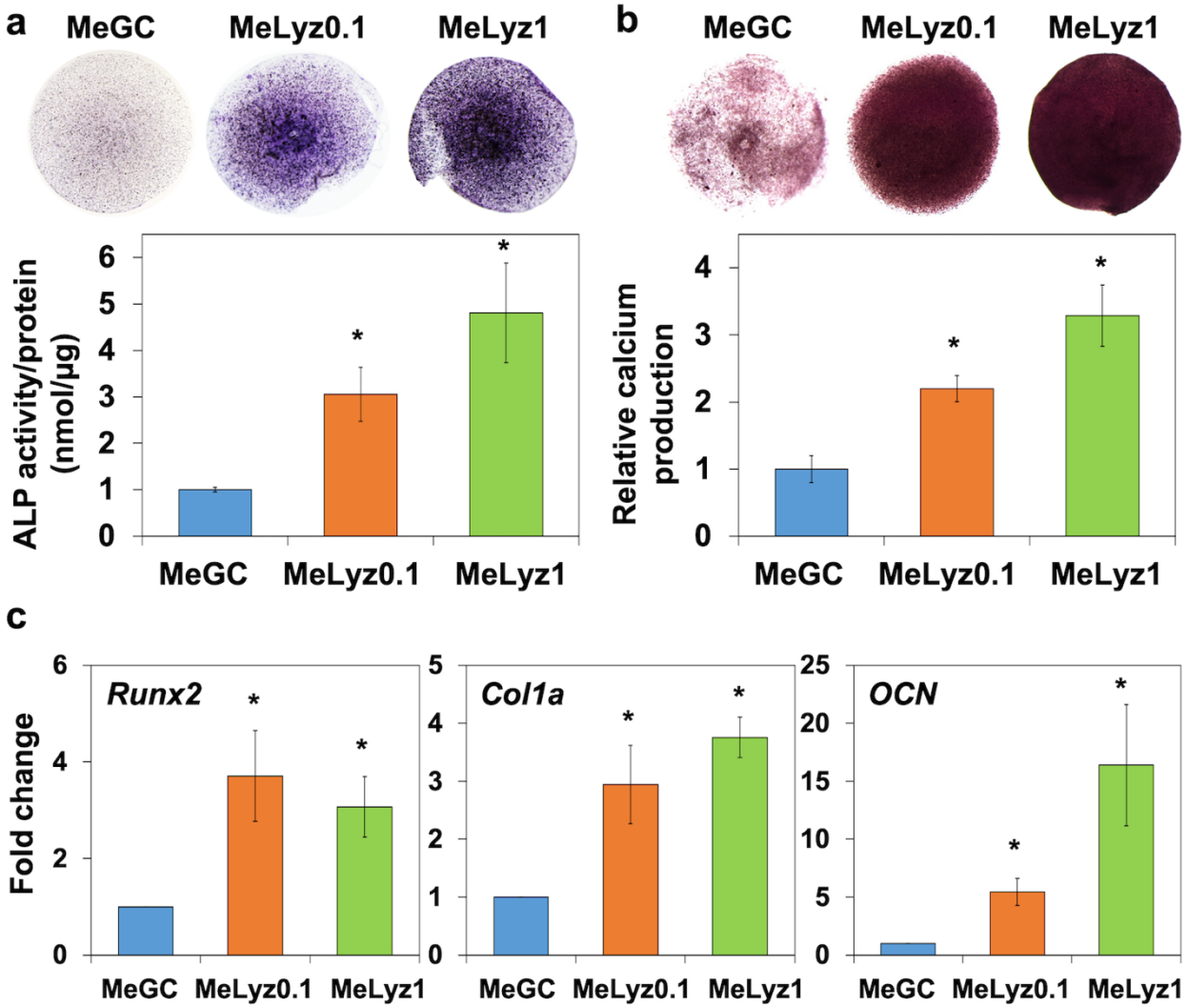

Figure 3-6. *In vitro* osteogenesis of cells in hydrogels. a) ALP staining images of BMSCs in hydrogels and quantified ALP activity normalized by total protein production at day 4. b) Alizarin red S staining images of BMSCs in hydrogels and its quantified calcium production at day 21. c) Osteogenic gene expression of BMSCs analyzed by qRT- PCR at day 4 (*Runx2*, *Col1a*) and day 21 (*OCN*) (*$p < 0.05$).

3.3.7. *In vivo* Bone Forming Ability of Hydrogels

The benefit of MeLyz incorporated hydrogels for *in vivo* bone formation was studied after six weeks of hydrogel implantation. The microCT images revealed that the defect area was filled more with the incorporation MeLyz, specifically there was more bone formation near the edge of the defect (Figure 3-7a). The bone growth area was quantified, 9, 37, and 52% for blank, MeGC, and MeLyz1 respectively, and this result demonstrated that MeLyz incorporated hydrogels promoted significant new bone formation (Figure 3-7b). The quantified percent bone volume (BV TV^{-1}) of hydrogels were 8, 19, and 50% for blank, MeGC, and MeLyz1 respectively, which indicated the significantly enhanced bone volume with MeLyz incorporation (Figure 3-7c). The trabecular number was also significantly increased up to 1.8 and 5.3 mm^{-1} for MeGC and MeLyz1 from 0.06 mm^{-1} for blank (Figure 3-7d). The microCT results were further supported by histological examinations of H&E and Masson-goldner trichrome staining. The development of osteoid near the boundary of the defect was observed more in MeLyz1 compared to that in the blank and MeGC samples as well as the size of defect was decreased (Figure 3-7e).

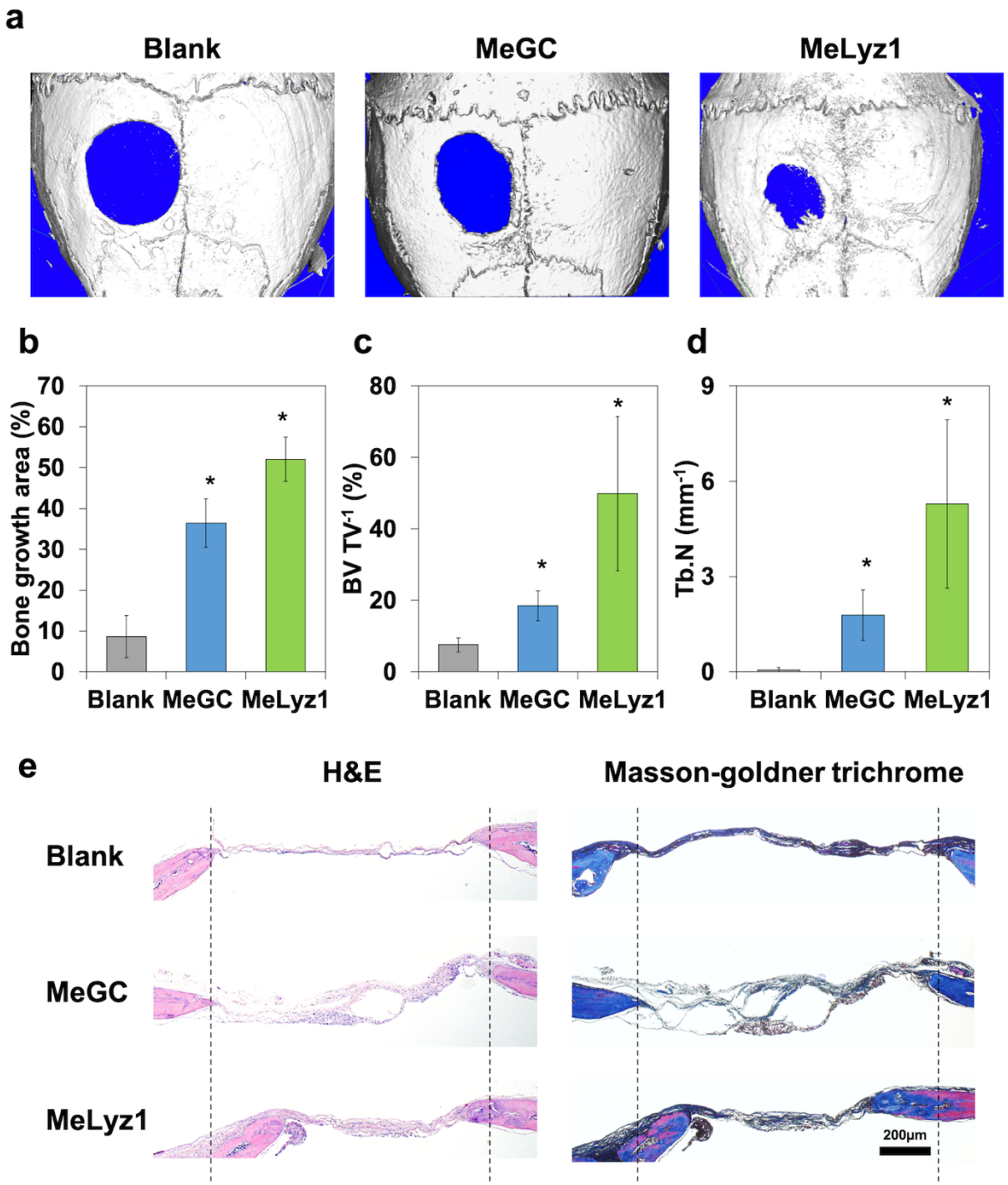

Figure 3-7. *In vivo* bone formation. a) MicroCT images of calvarial defects treated with hydrogels after 6 weeks. b) Quantification of percent bone growth area. c) Quantification of percent bone volume over tissue volume (BV TV^{-1}). d) Quantification of trabecular number (Tb. N, mm^{-1}). e)

Histological evaluation of regenerated bone in calvarial defects. H&E (left) and masson-goldner trichrome (right) staining of calvarial defects. Two vertical lines were drawn for easy observation (*$p < 0.05$).

3.4. Discussion

Lysozyme-induced degradation of chitosan was well studied[52, 152], but the potential of a lysozyme-chitosan construct as a degradable tissue engineering scaffold was not fully explored yet. First, we investigated whether lysozyme can influence growth or differentiation of BMSCs at various lysozyme concentrations. The viability of BMSCs was well maintained over a wide range of lysozyme concentrations up to 100 mg mL^{-1}, which is well above the highest lysozyme concentration (10 mg mL^{-1}) used in this study (Figure 3-8a). In addition, the minimal osteogenic effect was observed with lysozyme as confirmed by *ALP* and *Runx2* gene expression at various lysozyme concentrations (Figure 3-8b). These results indicated the minimal toxicity and unwanted adverse effects of lysozyme.

Next, the fine-tuned degradation profiles were successfully achieved by varying MeLyz concentrations (Figure 3-1c). The rate of degradation was observed to be in proportion to the concentration of lysozyme in the hydrogels. However, hydrogels underwent significant mass loss with high MeLys incorporation such as MeLys10, which provided an inadequate structure for scaffold applications. An increase in lysozyme concentration from 1 to 10 mg mL^{-1} led to significant reduction in cell growth due to early loss of mechanical integrity of the fast degrading hydrogels (Figure 3-9). For this reason, MeLys10 was excluded for further investigation.

The tissue-engineered hydrogels are replaced by host tissues with multicellular invasion following degradation[26]. The hydrogel swelling ratio correlated with degradation, is a key

parameter to calculate theoretical mesh size[148]. For example, the theoretical initial mesh size of polyethylene glycol (PEG) hydrogels is about 25 nm, which is 2-3 orders smaller than MSCs and potentially restricted cell migration[46]. The internal network structure of hydrogels started to cleave with degradation, potentially increasing water uptake (Figure 3-2a) as well as swelling ratio (Figure 3-2b). The computed theoretical hydrogel mesh sizes of MeGC, MeLyz0.1, and MeLyz1 based on swelling ratio were 49, 52, and 77 nm respectively at day 0. These values increased up to 64, 389, and 592 nm at day 14, respectively (Figure 3-2). From cryo-SEM image analysis, the average pore size of hydrogels was comparable to theoretical mesh sizes at day 0. The calculation of theoretical mesh size was hypothesized with a uniform distribution[153], however, it hardly matched with the non-homogeneously cleaved network observed in our hydrogels. Therefore, the distribution of pore diameters was much broader in actual hydrogel samples. This corresponds to our observation using cryo-SEM that the attenuated and cleaved network with a wide range of pore sizes was detected from MeLyz1 at day 10 (Figure 3-3a and b). In addition, the interconnectivity of pore structure was increased with the incorporation of MeLys, and exhibited disconnected and attenuated polymer network, which was different with homogenously enlarged networks from MeGC. Although the increased pore size with a more open structure is desired, the inhomogeneous porous hydrogels with a large variation of pore size may limit uniform nutrient diffusion and homogeneous cell distribution throughout the hydrogel. Future studies will need to create more homogeneous structure.

Hydrogel degradation could provide room for cell migration and deposition of ECM molecules which can interact with cells to induce specific signaling pathways for cell binding, migration, and differentiation[14, 154]. We noticed higher proliferation of encapsulated MSCs and longer migration of seeded MSCs with enhanced hydrogel degradability (Figure 3-4c, and Figure

3-5a, b). The ECM production and accumulation were enhanced with the elevated cell proliferation, and increased compressive modulus of MeLyz incorporated hydrogels (Figure 3-4d)[12]. The stored ECM not only improved physical properties of hydrogels, but also enhanced osteogenic differentiation. Elevated *Col1a* gene expression was observed, which produced a component of type I collagen, a bone specific ECM and an essential factor for osteogenesis[13]. During the ossification process, type I collagen secreted by osteoblasts could initiate mineral deposition, and this was further confirmed by high mineral accumulation (Figure 3-6b)[16].

We also evaluated the osteogenic potency of MeLyz incorporated hydrogel using a mouse calvarial critical-sized defect model. We verified promoted cell migration in MeLyz incorporated hydrogel *in vitro* (Figure 3-5a, b), and reflected this study *in vivo* by observing cell infiltration. Our MeLyz incorporated hydrogel system showed great efficacy to recruit surrounding cells into the defect area at an early time point, week 1 (Figure 3-10). The bone healing efficacy of encapsulated cells in MeLyz incorporated hydrogel was confirmed by bone ingrowth from the edge as well as osteoid matrix formation at week 6 (Figure 3-7a, e). The observed improvement of bone formation in the MeLyz incorporated hydrogel may be due to increased proliferation and osteogenic differentiation of encapsulated cells in the fast degrading hydrogels as demonstrated by *in vitro* characterization as well as accelerated endogenous cell infiltration as confirmed in calvarial defects.

The lysozyme incorporated hydrogel system developed in this study showed that it is promising to be used as bone regeneration biomaterial platform. Moreover, this hydrogel platform could be applied in different areas of tissue engineering such as wound healing. Lysozyme is a well-known antimicrobial enzyme, which cleaves the peptidoglycan in gram positive bacteria cell wall[155]. The bacterial infection is one of the main issues from the surgical practice, which can

be potentially solved by our lysozyme incorporated hydrogel system. In addition, this system can be used as a drug release carrier in a sustained manner based on tunable degradation[156, 157]. Lastly, it has favorable features for blood vessel regeneration, which can create an enlarged network from degradation to induce angiogenesis[158].

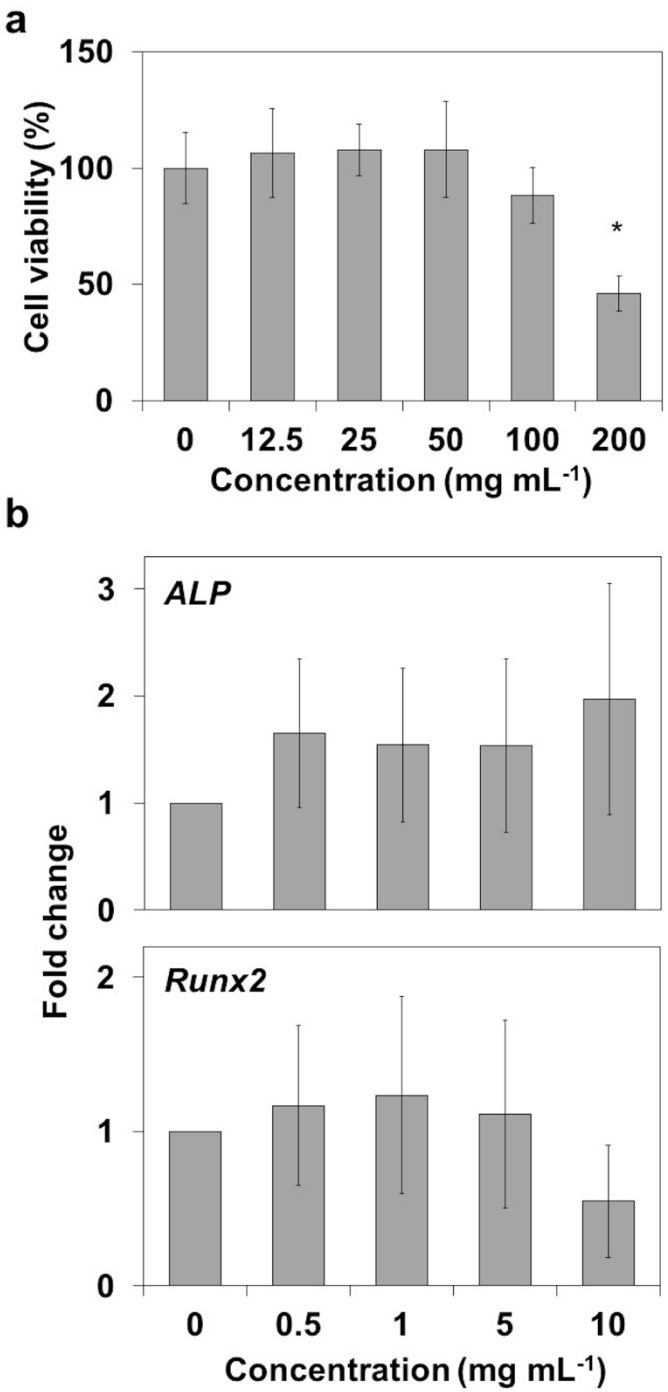

Figure 3-8. a) Viability of BMSCs after 24 h culture at various lysozyme concentrations (0, 12.5, 25, 50, 100, and 200 mg mL^{-1}). b) Osteogenic effect of lysozyme on BMSCs by measuring *ALP* and *Runx2* gene expression at day 4 (*$p < 0.05$, *N.S* not significant).

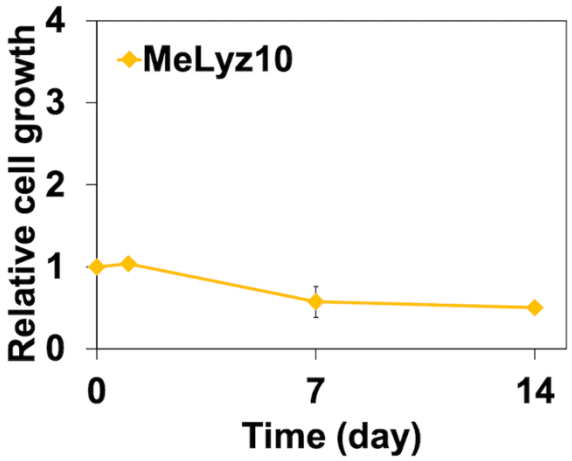

Figure 3-9. Relative cell growth of BMSCs encapsulated in MeLyz10 hydrogel evaluated by alamarBlue assay for 14 days.

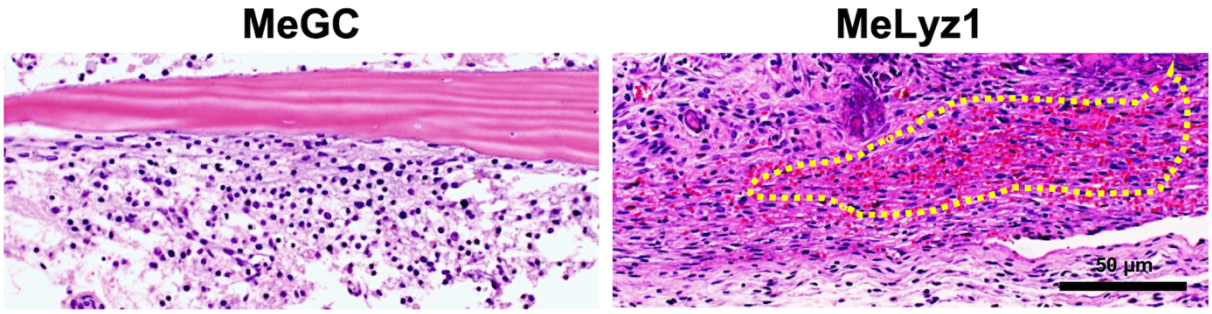

Figure 3-10. *In vivo* cell recruitment. H&E staining images of mouse calvarial defects after 7 days post hydrogel implantation.

3.5. Conclusions

In this work, enzymatically degradable hydrogel systems were designed to allow hydrogel degradation in a cell-independent manner. We have selected a unique enzyme-substrate pair as a hydrogel where the hydrogel is designed with photocrosslinkable chitosan and lysozyme. Our study demonstrated that the enzyme-functionalized hydrogel successfully modulated the

degradation rates of the hydrogel and aspects of cell behavior and supported functional tissue formation. The findings demonstrate that the strategy of combining lysozyme with chitosan is a promising approach to increase the efficacy of current material-based therapeutics for tissue repair.

3.6. Acknowledgement

This work has been published in *ACS Applied Materials and Interfaces*, 2018, S. Kim, Z.-K. Cui, B. Koo, J. Zheng, T. Aghaloo, and M. Lee. "Chitosan-Lysozyme Conjugates for Enzyme-Triggered Hydrogel Degradation in Tissue Engineering Applications."

Chapter 4. Dual Functions of a Lysozyme-Chitosan Conjugate: Tunable Degradation and Anti-Infection

4.1. Introduction

Hydrogel plays a key role in tissue engineering and regenerative medicine fields with a proper delivery ability of cells and drugs[1]. It also provides three-dimensional structure mimicking native extracellular matrix (ECM) that can support the growth and differentiation of the encapsulated cells[10]. For wound healing application, injectable hydrogel can fill irregular wound site and stick to wound to protect from outside environment such as pathogenic infection[159].

Bacterial infection during surgical process leads to serious complications with inflammatory reactions, and continuously results in unsuccessful wound repair[160-162]. It is important to minimize microbial infection to accelerate wound regeneration, and the most common treatment is the use of synthetic antibiotics. However, due to bacterial resistance derived from the overused antibiotics, it is required to investigate a novel approach to effectively administer an antibacterial agent.

Lysozyme, a glycoside hydrolase or also called as a muramidase, presents naturally in diverse human tissues and secretions as part of an innate protection system[141, 163]. It has distinctive roles of antiviral, antiseptic, anti-inflammatory properties which allows to utilize in pharmaceutical science[164] or food preservatives[165]. It attacks beta-1, 4 glycosidic linkage of *N*-acetylglucosamine and *N*-acetylmuramic acid, existed in chitosan[166] or peptidoglycan wall of gram-positive bacteria. Gram-negative bacteria are more resistant to and their lipopolysaccharide cellular membranes also hinder the access of lysozyme[167]. Although

lysozyme is less susceptible to gram-negative bacteria, antimicrobial activity of lysozyme could be intensified with the association of other materials[168, 169].

Biopolymer is a great candidate to integrate lysozyme and enhance its antibacterial power. Chitosan, a biocompatible polysaccharide, has abundant amines which make it easy to modify with functional groups such as photocrosslinkable moieties[149] and/or cell adhesion motifs[8]. Chitosan hydrogel have been applied in many tissue engineering applications including wound[159], bone[170], cartilage[118, 130, 171] regenerations. In addition, its cationic nature shows broad antimicrobial features[172, 173] including cell membrane damage or bacterial cell disintegration conducting cell lysis[174, 175].

Recently, we have developed a unique photocrosslinkable lysozyme-chitosan pair with a tunable degradability which could enhance ECM depositions secreted from the encapsulated mesenchymal stem cells[176]. This hydrogel platform employed methacrylated glycol chitosan, methacrylated lysozyme, riboflavin as a photoinitiator, and visible blue light[176, 177]. However, chitosan itself presents a minimal cell attachment site which could potentially hinder further cell spreading, proliferation, and ECM accumulation resulting in insufficient tissue repair. Therefore, a new design of integrating lysozyme into chitosan hydrogel modified with a cell adhesion motif containing Arg–Gly–Asp (RGD) residues should be studied.

This research demonstrates that a novel lysozyme-chitosan conjugate with dual functions of tunable degradation and anti-infection. RGD-conjugated chitosan and lysozyme were modified with methacrylate group to form secure binding under visible light irradiation. The hydrogels with various lysozyme concentrations were characterized with degradation kinetics, swelling ratio, and compressive modulus. The effects of degradation on cell morphological change, proliferation, migration, and ECM depositions were studied after encapsulation or seeding of mouse fibroblasts

(NIH/3T3s). In addition, we evaluated the antibacterial properties of hydrogels which confirmed the dual functions of lysozyme. This new lysozyme-chitosan pair with dual functions provides a great potential in tissue engineering application.

4.2. Materials and Methods

4.2.1. Materials

Glycol chitosan (~100 kDa) was obtained from Wako Chemicals USA, Inc. (Richmond, VA). Glycidyl methacrylate, lysozyme from chicken egg white, and riboflavin were supplied by Sigma-Aldrich (St. Louis, MO). The mouse embryonic fibroblast (NIH/3T3, ATCC® CRL-1658™) was provided from American Type Culture Collection (ATCC, Manassas, VA). High glucose Dulbecco's Modified Eagle's Medium (DMEM), Antibiotic-Antimycotic (AA, 100X), Fetal Bovine Serum (FBS), trypsin, Luria-Bertani (LB) powder, LB-agar, calcein-AM, ethidium homodimer-1, TRIzol, cDNA transcription kit, Succinimidyl-4-(N-Maleimido-methyl)Cyclohexane-1-Carboxylate (SMCC), and Pierce BCA protein assay kit were purchased from Thermo Scientific (Rockford, IL, USA). RNeasy mini kit was supplied by Qiagen (Valencia, CA, USA). The Ac-GCGYGRGDSPG-NH_2 peptide (RGD peptide) was obtained from Anaspec, Inc. (Fremont, CA). All the products were used as received.

4.2.2. Preparation of Chitosan Hydrogels

RGD peptide conjugated chitosan hydrogel[8] and methacrylated lysozyme (Lyz)[176] were prepared by the previously published method. Briefly, 2% glycol chitosan solution and 10% lysozyme solution in distilled water were reacted with glycidyl methacrylate at 1 to 1 molar ratio. The methacrylated glycol chitosan (MeGC) was further modified with 7.4 mg mL^{-1} SMCC

solution for 16 h, purified, conjugated with 1 mg mL^{-1} RGD peptide for 16 h, and purified. All hydrogels solutions were dissolved in 1x PBS or distilled water at 2%.

4.2.3. Characterization of Hydrogels

The 100 uL hydrogel solution with various Lyz concentrations (0, 0.1, and 1 mg mL^{-1}) was mixed with 0.0125% riboflavin 0.5 uL and irradiated under visible blue light (VBL, 400–500 nm, 300 mW cm^{-2}, Bisco Inc., Schaumburg, IL) for 80 s for hydrogel fabrication.

The degradation of hydrogel with various Lyz concentration (0, 0.1, and 1 mg mL^{-1}) was calculated by the following equation 1 measuring the dry weight change for two weeks after incubation in distilled water.

$$Hydrogel\ degradation\ (\%) = \left(\frac{W_i - W_t}{W_t}\right) \times 100 \qquad (1)$$

where W_i and W_t indicate the dry weight at initial and each respective time points.

The swelling ratio of hydrogel was quantified by the following equation 2.

$$Swelling\ ratio\ (\%) = \left(\frac{W_s}{W_d}\right) \times 100 \qquad (2)$$

where W_s and W_d indicate the swollen and dry weight at each time points.

The compressive modulus of hydrogels was evaluated by the indentation test with a 1.6 mm diameter indenter using Instron electromechanical testing machine (Instron, Model 5564, Norwood, MA)[149, 177].

4.2.4. *In Vitro* Cell Proliferation and Morphological Observation of the Encapsulated Cells

The hydrogels encapsulated with cells were cultured for two weeks and the alamarBlue assay was performed at the predetermined time points. The relative cell growth was computed by the following equation 3.

$$Cell\ growth\ (\%) = \left(\frac{F_e - F_b}{F_c - F_b}\right) \times 100 \qquad (3)$$

where F_e, F_c, and F_b indicate the fluorescence value at 585 nm after excitation at 570 nm of experimental, control, and blank groups.

The NIH/3T3s were cultured in culture media (DMEM, 10% FBS, and 1% AA) at 37 °C under 5% CO_2 humidified atmosphere. The cells were encapsulated in hydrogels at 2 x 10^6 cells mL^{-1} concentration and incubated in media for two weeks at 37 °C. The incubated hydrogels were collected at day 1, 7, and 14 to stain with calcein-AM to visualize the morphology of the encapsulated cells by a confocal multiphoton STED microscope (Leica TCS-SP5 AOBS, Buffalo, IL). All images were analyzed by ImageJ Analyze Particles tool (NIH, Bethesda, Maryland) to quantify the circularity and the aspect ratio of the cells.

4.2.5. Extracellular Matrix Deposition in Hydrogels

The particular gene expressions during cell proliferation were studied by quantitative real-time polymerase chain reaction (qRT-PCR). The total RNA from the collected hydrogels at day 4 and 14 were extracted by TRIzol and RNeasy mini kit. The reverse transcription of the total RNA was executed by cDNA transcription kit. Then, qRT-PCR was performed in a LightCycler 480 PCR (Indianapolis, IN) with SYBR Green under 45 cycles of amplification, and *GAPDH* expression was used for normalization. The primer sequences were given as following. *GAPDH*: AGGTCGGTGTGAACGGATTTG (forward) and TGTAGACCATGTAGTTGAGGTCA (reverse); *FGF2*: GCGACCCACACGTCAAACTA (forward) and TCCCTTGATAGACACAACTCCTC (reverse); *COL1A1*: AACCCGAGGTATGCTTGATCT (forward), CCAGTTCTTC ATTGCATTGC (reverse); *COL3A1*:

CTGTAACATGGAAACTGGGGAAA (forward) and CCATAGCTGAACTGAAAACCACC (reverse). All experimental runs were triplicated.

Furthermore, hydrogels after two weeks of culture were fixed in 10% neutral buffered formalin for 16 h and total collagen accumulation in hydrogels was examined by Picrosirius red (Polysciences, Inc.) staining.

4.2.6. *In Vitro* Cell Migration

The hydrogels were fabricated in 48-well plate as 300 uL, and 2 x 10^4 number of NIH/3T3s were seeded on the surface of each hydrogels. For two weeks, hydrogels were stained with calcein-AM and cell migration through Z-direction was observed by a confocal multiphoton STED microscope.

4.2.7. Bacteria Culture

Fresh culture of gram-positive bacteria, vancomycin-resistant *Staphylococcus aureus* Mu50 (*S. aureus*), and gram-negative bacteria, *Escherichia coli* K-12 (*E. coli*) were prepared by suspending a single colony from LB-agar culture in 5 mL of sterile LB medium. The counts of bacteria were quantified by reading the optical density of medium at 600 nm (OD_{600}) by UV/Vis spectrophotometer (Beckman Coulter). Based on the OD_{600} value, bacterial colony-forming units (CFU) mL^{-1} was calculated.

4.2.8. Antibacterial Characterization of Hydrogels

The bacteria suspension was diluted to 5 x 10^7 CFU mL^{-1} in sterile LB. Lysozyme solution was prepared as 0, 0.01, 0.1, 0.5, 1, and 5 mg mL^{-1} in sterile LB. The bacteria solution (500 uL) was added to lysozyme solution (500 uL) and cultured for 5 h at 37 ^oC. The OD_{600} of bacteria and

lysozyme mixture was measured at 0, 0.5, 1, 3 and 5 h. The bacterial survival rate was calculated by the following equation 4.

$$Bacterial\ survival\ rate\ (\%) = \left(1 - \frac{CFU_{exp}}{CFU_{cont}}\right) \times 100 \qquad (4)$$

where CFU_{exp} and CFU_{cont} indicate CFU mL^{-1} of an experimental and control group, respectively.

The measurements of inhibition zones of hydrogels were employed by the disc diffusion. The 100 uL of bacteria suspension of 10^6 CFU mL^{-1} was spread on LB-agar plate, 100 uL of hydrogels were placed on, and incubated at 37 ^oC for 16 h.

The morphological changes of *E. coli* and *S. aureus* after the contact with hydrogel was observed using Scanning Electron Microscopy (SEM, FEI Nova NanoSEM 230, Hillsboro, OR). The bacteria solution was encapsulated in hydrogel at 10^8 CFU mL^{-1} concentration and incubated for 24 h at 37 ^oC. After incubation, hydrogels were fixed with 2.5% glutaraldehyde for 2 h, dehydrated sequentially with 30, 50, 75, and 90% ethanol for 10 min respectively, and air-dried for 30 min. All samples were gold-coated with a sputter coater at 20 mA under 70 mTorr for 1 min.

4.3. Results

4.3.1. Characterization of Hydrogels

The fabrication of lysozyme-chitosan conjugated hydrogels with different concentrations of lysozyme (0, 0.1, 1 mg mL^{-1}) was illustrated in Figure 4-1a. The incorporation of lysozyme significantly accelerated the degradation rate regardless of RGD modification (Figure 4-1b). Without lysozyme modification, hydrogels maintained its weight around 85% till day 14. However, as lysozyme concentration increased from 0.1 to 1 mg mL^{-1}, the remaining gel weight

at day 14 decreased to 50%. In addition, swelling ratio of hydrogels also enhanced in a lysozyme dose dependent manner over time (Figure 4-1c) which potentially correlated with increased hydrogel network mesh size after degradation[176]. Degradation also influenced the mechanical strength of hydrogels that the compressive modulus decreased over time with higher lysozyme concentration (Figure 4-1d). These results indicated that physical characteristics of hydrogels were mainly governed by lysozyme incorporation, not RGD modification.

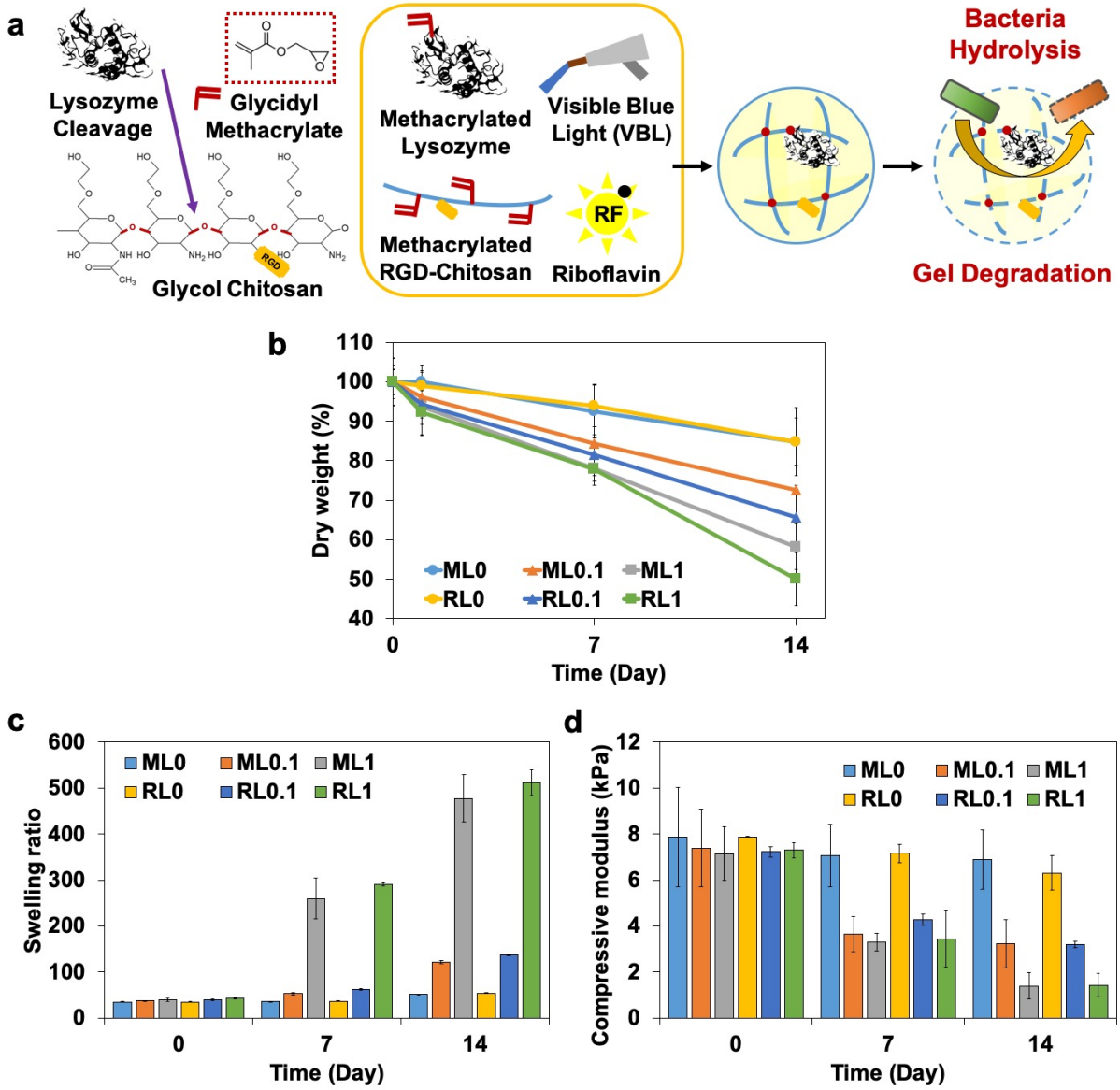

Figure 4-1. Characterization of lysozyme-chitosan conjugate hydrogel. (a) Reaction scheme of lysozyme-chitosan conjugate and hydrogel fabrication under visible blue light curing in the presence of a photoinitiator, riboflavin. This hydrogel presenting dual functions to induce degradation and prevent bacterial infection. (b) Degradation profile measured by dry weight change of hydrogels for two weeks. (c) Swelling ratio of hydrogels calculated by the ratio of wet weight and dry weight of hydrogels for two weeks. (d) Compressive modulus of hydrogels with RGD and lysozyme modification for two weeks.

4.3.2. *In Vitro* Cell Proliferation and Morphological Observation of the Encapsulated Cells

The morphology of encapsulated NIH/3T3s in different hydrogels showed significant change over 14 days of culture (Figure 4-2a). Although cells in MeGC groups (ML0, ML0.1, and ML1) kept spherical shapes over time, cells in RGD groups (RL0, RL0.1, and RL1) started to change to oval shape individually at day 1 and become more polarized and stretched out at the later time points. Especially, the effects of lysozyme were clearly observed in RGD groups with the broader area of spreading. The circularity of individual cells decreased with RGD modification as well as lysozyme incorporation (Figure 4-2b). A circularity value of 1.0 stated a perfect round shape, and a value approaching 0.0 stated an elongated shape. The aspect ratio also increased with RGD modification and lysozyme incorporation (Figure 4-2c). Even though there are no morphological changes of cells with lysozyme incorporation in MeGC groups, the cell growth result showed that the lysozyme enhanced cell proliferation about 1.6 times higher at day 14 compared with day 0 (Figure 4-2d). The enhancement of cell proliferation with lysozyme incorporation was also observed in RGD groups. At this point, we could notice the distinctive additive effects of RGD conjugation as well as lysozyme incorporation on cell growth, which indicated both modifications did not hinder each other.

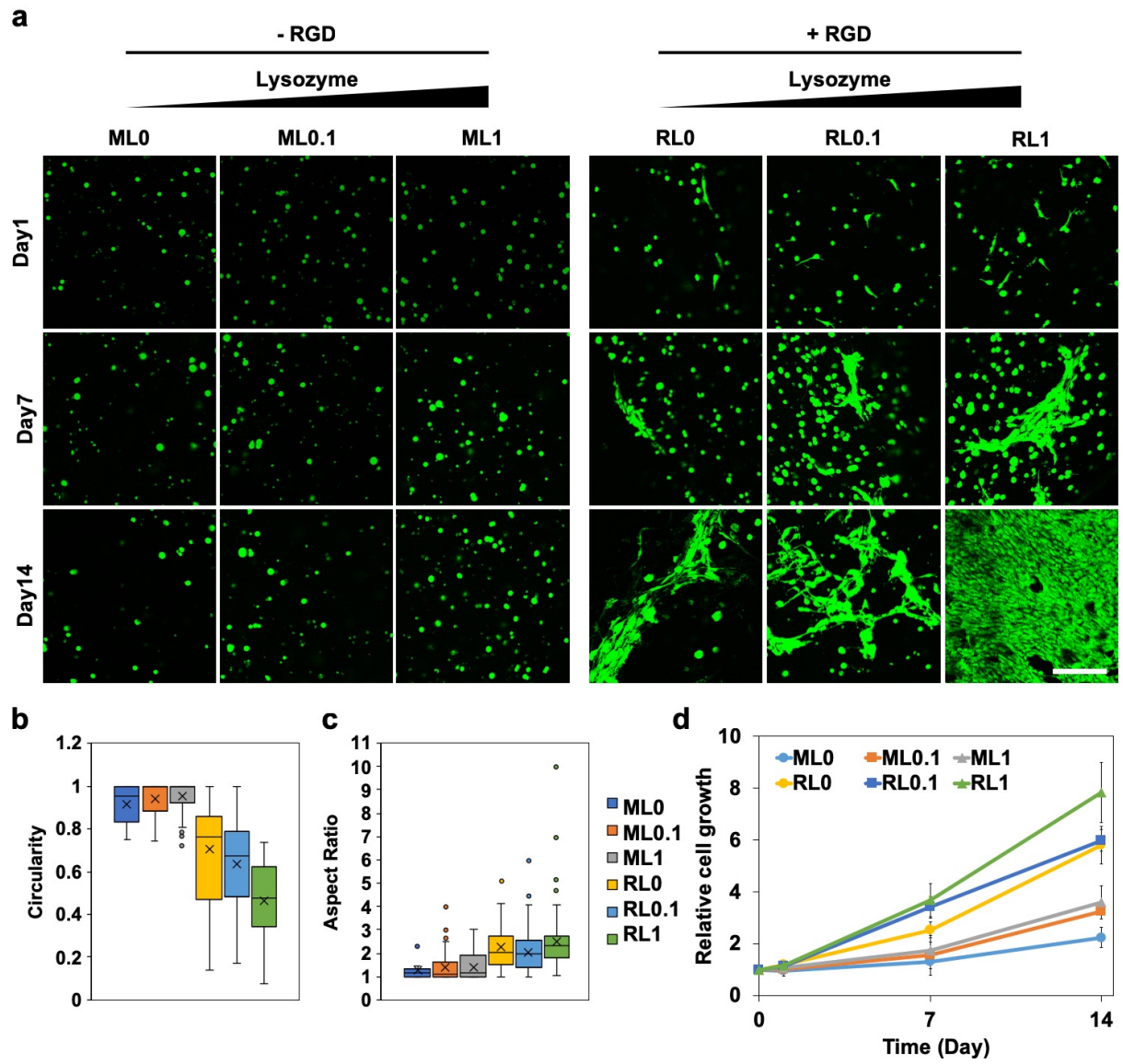

Figure 4-2. *In vitro* studies of encapsulated NIH/3T3s in hydrogels with RGD and lysozyme modification for two weeks. (a) Representative confocal images to show morphological change of cells (green). Scale bar is 100 μm. (b) Circularity and (c) Aspect ratio of cells at day 14 quantified by ImageJ. (d) Relative cell growth analyzed by alamarBlue assay.

4.3.3. Extracellular Matrix Deposition in Hydrogels

Various gene expression guiding ECM deposition were evaluated by qRT-PCR results. First of all, *FGF2*, fibroblast growth factor 2, expression at day 4 was upregulated with lysozyme incorporation in both MeGC and RGD groups (Figure 4-3a). In addition, all RGD groups have higher expression compared with MeGC groups which also correlated with cell proliferation result (Figure 4-1b). The expression of *Col3a*, type III collagen, at day 4 also exhibited similar pattern with *FGF2*. However, at day 14, *Col3a* expression was downregulated which indicated that both *FGF2* and *Col3a* genes upregulated in early proliferative phase (Figure 4-3b). At day 14, *Col1a*, type I collagen, expression was upregulated, and the ratio of *Col1a* to *Col3a* increased with RGD and lysozyme co-modification (Figure 4-3c). Total collagen deposited in hydrogels were examined by picrosirius staining that stronger red color showed higher buildup of collagen (Figure 4-3d). These results demonstrated that the synergistic effect of RGD and lysozyme on collagen expression.

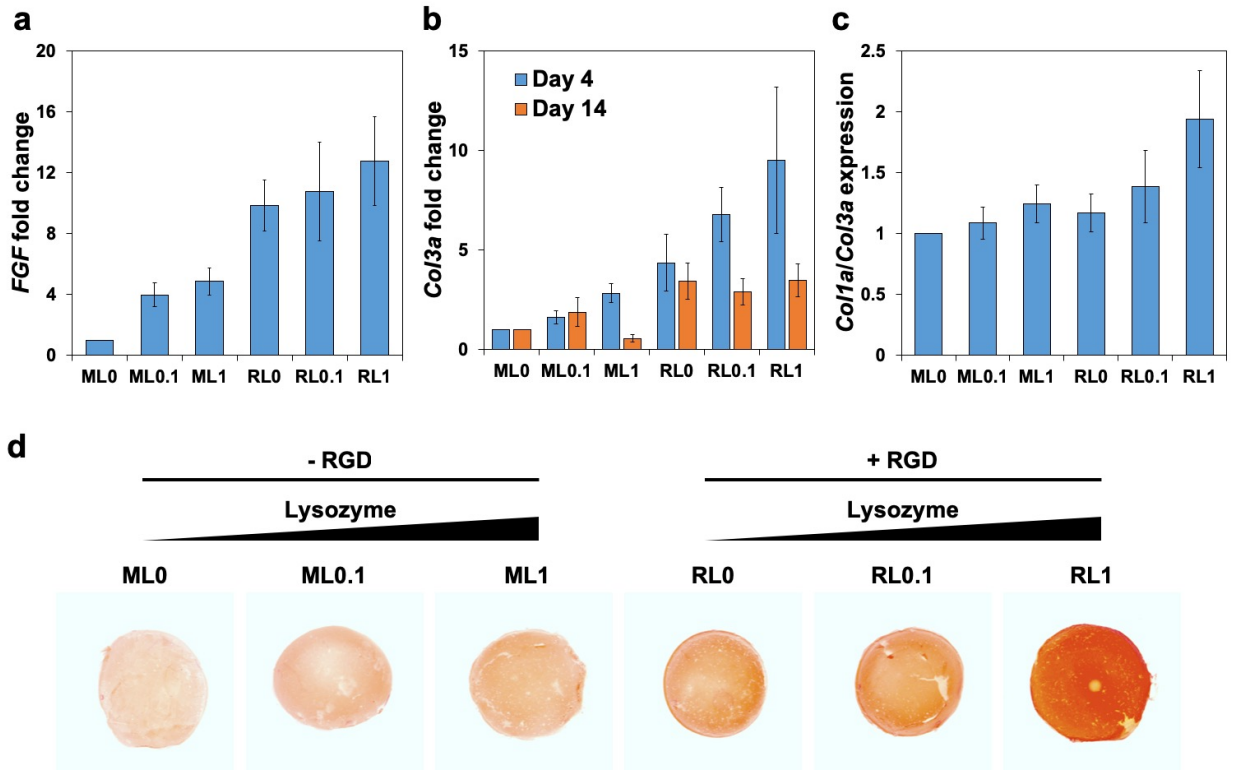

Figure 4-3. *In vitro* extracellular matrix deposition in hydrogels with the encapsulation of NIH/3T3s over two weeks. Fibroblast related gene expression. (a) *FGF* at day 4, (b) *Col3a* at day 4 and 14, and (c) The ratio of *Col1a* to *Col3a* at day 14. (d) Picrosirius staining images representing total collagen deposition in hydrogels.

4.3.4. *In Vitro* Cell Migration

The NIH/3T3s seeded on hydrogels surface were monitored for two weeks in both vertical (xz) and horizontal (xy) direction (Figure 4-4). At day 1, cells only stayed on the top of hydrogels (xz) and scattered individually (xy). Although cell migration along vertical direction was barely noticed at day 7, cells started to spread throughout the surface of hydrogels along horizontal direction. In addition, spreading area on hydrogel surface increased with lysozyme incorporation. However, cells started to spread throughout the hydrogel mass (xz) at day 14, and especially lysozyme

incorporated groups (RL0.1 and RL1) showed deeper depth compared with nonmodified group. This implied that lysozyme incorporation induced cell migration not only on surface level but also in an invasive manner.

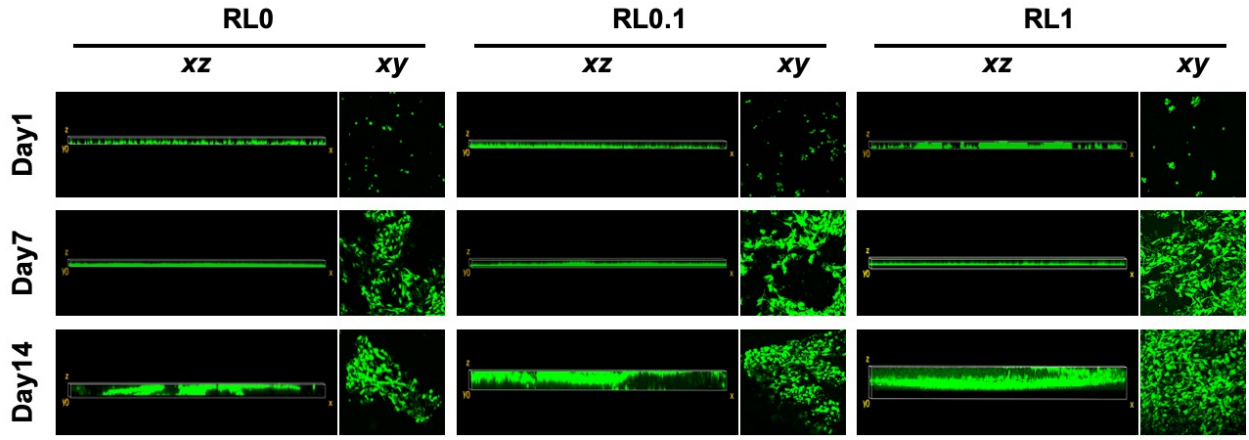

Figure 4-4. *In vitro* monitor of NIH/3T3s migration on hydrogels in both vertical (xz) and horizontal (xy) directions for two weeks. Cells seeded on the surface of hydrogels at day 0 and started to spread throughout the hydrogel bulk over time.

4.3.5. Antibacterial Characterization of Hydrogels

The survival rates of two bacterial strains, *S. aureus* and *E. coli,* the most prevalent gram-positive, and negative bacteria in human body[178], were studied by exposing bacterial strains to various concentrations of free methacrylated lysozyme, 0, 0.01, 0.1, 0.5, 1, and 5 mg mL^{-1} (Figure 4-5a and b). Antibacterial properties of lysozyme started to show at 0.1 mg mL^{-1} for both strains, but it was more effective to *S. aureus* compared with *E. coli*. However, 5 mg mL^{-1} treatment exhibited the lowest survival rate which can be considered as the most efficacious concentration for both strains.

Antimicrobial activities of lysozyme incorporated hydrogels were investigated with various approaches. Control hydrogel without lysozyme did not prevent bacterial proliferation, while lysozyme modified hydrogel showed antibacterial effect for both strains (Figure 4-6a). Lysozyme incorporation in hydrogels delayed initial bacterial growth and reduced the number at the final phase. Antibacterial properties were more effective to *S. aureus* compared with *E. coli* that the initial holdup of bacterial growth was longer for *S. aureus*. This holdup time became longer by decreasing the initial bacterial inocula from 10^7 to 10^6 CFU per hydrogel. The growth of two bacterial strains on the agar plates were visualized to show antibacterial activity of lysozyme incorporated hydrogels (Figure 4-6b). It was observed that the bacterial strains totally covered the plates with nonmodified hydrogel after 24 h incubation. However, inhibition occurred for both strains near the lysozyme modified group at the same time point. The bacterial morphology observed by SEM also confirmed the antimicrobial effect of lysozyme (Figure 4-6c). After 24h culture of bacterial seeding, bacteria clustered together on the surface of hydrogel. Both bacterial strains exposed to nonmodified hydrogel showed regular and smooth surface, while lysozyme exposed groups showed cell lysis and membrane disruption. The arrows indicated the damaged bacterial membranes or intracellular efflux after contact with lysozyme modified hydrogel.

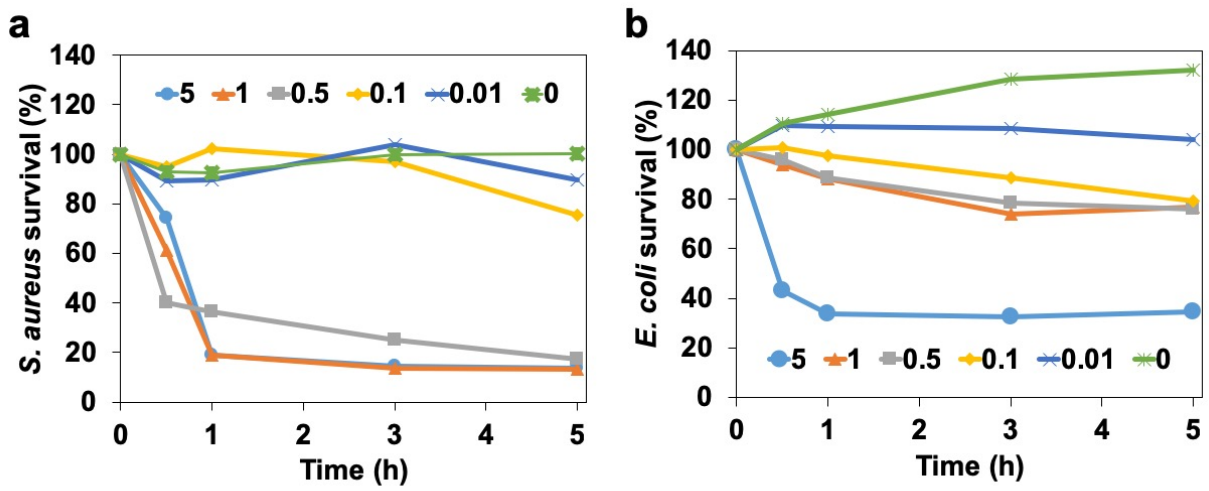

Figure 4-5. *In vitro* antibacterial effects of free lysozyme with various concentration, 0, 0.01, 0.1, 0.5, 1, and 5 mg mL^{-1} for five hours. Studies against (a) gram positive species, *S. aureus* and (b) gram negative species, *E. coli*.

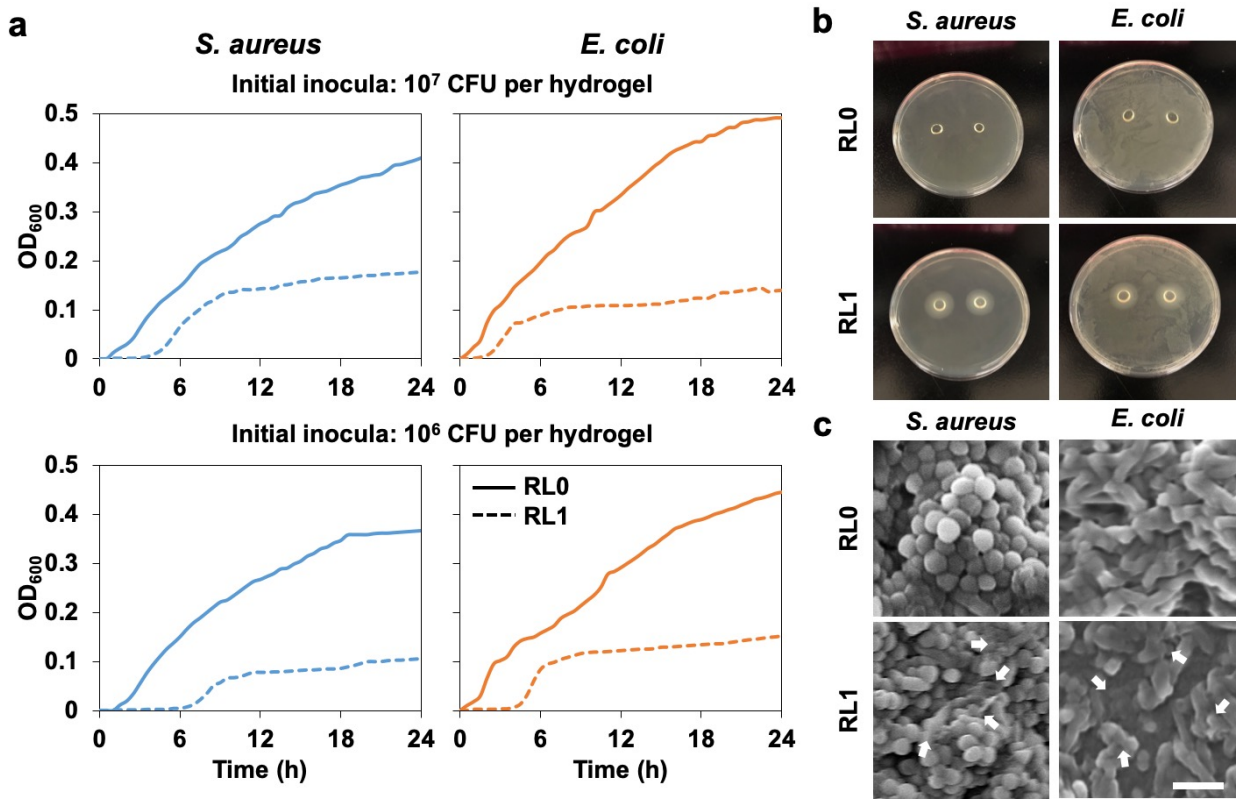

Figure 4-6. *In vitro* antibacterial characterization of lysozyme incorporated hydrogels. (a) Antibacterial activity of hydrogels with different inocula (10^7 and 10^6 CFU per hydrogels) of *S. aureus* and *E. coli* tested by microplate proliferation assay. (b) Agar petri dish cultured with *S. aureus* and *E. coli* with hydrogel samples placed on the center of dish for one day to analyze inhibition zone. (c) SEM micrographs of *S. aureus* and *E. coli* in hydrogels following one day incubation. Scale bar is 2 μm.

4.4. Discussion

The concept of lysozyme-chitosan conjugate as a tissue engineering scaffold with a tunable degradability was proved in our previous study[176]. However, the additional function of lysozyme to provide antimicrobial environment in RGD modified chitosan hydrogel was not fully

investigated. From overall material characterization result, RGD conjugation to chitosan hydrogel did not significantly changed its swelling ratio, compressive modulus which may alter the effect of lysozyme to the construct. The successful fine-tuned degradation, swelling ratio, and compressive modulus were accomplished by changing lysozyme concentrations regardless of RGD modification (Figure 4-1).

RGD peptide was well-studied peptide existing abundantly in various extracellular matrix proteins, thereby RGD modified polymers showed promising features as biomaterials to support cell attachment, spreading, proliferation as well as differentiation[8, 19, 20, 179-181]. In addition, recent studies demonstrated the importance of degradable local environment to induce the encapsulated cell spreading[176, 182-184]. The increment of swelling ratio with hydrogel degradation was closely associated the enlargement of theoretical pore sizes which could influence cell migration in hydrogels[148, 185]. Therefore, the significant change of cell morphology due to high spreading and enhanced proliferation were observed with the incorporation of RGD and lysozyme (Figure 4-2). From the former study, it was investigated that hydrogel degradation also induced ECM depositions which could support mechanical properties as well as growth and differentiation of the encapsulated cells[176].

The wound healing process followed several critical steps, hemostasis, inflammation, proliferation, and remodeling, which were orchestrated by critical molecular, cellular, and physiologic incidents[186]. Multiple growth factors including fibroblast growth factors (FGFs), vascular endothelial growth factors (VEGFs), and transforming growth factors (TGFs) were secreted at the proliferative phase which induced cell proliferation, migration, and ECM formation[187]. Type III collagen, a thin fiber, secretion was predominantly increased at the early remodeling phase, and replaced by type I collagen, a thick fiber[188]. Therefore, the increment of

Col1a to *Col3a* ratio at the late remodeling phase showed the substitution of thin collagen to thick one (Figure 4-3c). In addition, total accumulation of collagen at the late remodeling phase also supported the granulation tissue formation[189] appearing at the healed wound (Figure 4-3d). RGD and lysozyme co-modification synergistically upregulated growth factors and extracellular matrix protein expressions which assisted better wound healing.

Degradation of hydrogel led by lysozyme incorporation produced a space for cell migration and ECM accumulation[176, 190, 191]. The synergistic effect of RGD to lysozyme modification allowed increased cell proliferation and elevated ECM depositions which trigger cell movement throughout hydrogel bulk (Figure 4-4).

Infection control during wound regeneration is a desired condition, but major hurdle to construct an antibacterial scaffold is a difficulty to select specific antibiotics usually accompanying toxicity or multi-drug resistance[192]. However, general antiseptics such as lysozyme are less likely to affect cell growth[176] or induce microbial resistance[193, 194]. Lysozyme is a well-known lytic enzyme with stable three-dimensional structure over a broad range of pH and temperature[195] which made it easy to modify with different functional groups. Also, antimicrobial scope of lysozyme could be enhanced with the combination of other material such as hydrogen peroxide and ascorbic acid[196] or chitosan[173]. Especially, the limited efficacy to gram negative bacteria could be complemented[197] which was also verified in our antibacterial studies of lysozyme-chitosan conjugate to both *S. aureus* and *E. coli* (Figure 4-6).

4.5. Conclusions

In this work, we demonstrated that the incorporation of lysozyme into chitosan hydrogel successfully promoted its degradability and antibacterial property. These findings suggest a promising hydrogel with dual effects for tissue engineering application.

Chapter 5. Design of Hydrogels to Stabilize and Enhance Bone Morphogenetic Protein Activity by Heparin Mimetics

5.1. Introduction

Bone formation requires a proper commitment of mesenchymal stem cells (MSCs) to an osteoprogenitor lineage mediated by various osteoinductive factors, particularly bone morphogenetic protein-2 (BMP) signaling[198, 199]. Recombinant human BMP-2 (rhBMP-2) demonstrated extraordinary potential in bone formation and has been widely employed for bone repair[200, 201]. However, clinical applications of rhBMP-2 require supraphysiological milligram-level dosages due to its intrinsic instability and fast enzymatic degradation *in vivo*[202-208]. The premature release of such high dose rhBMP-2 from conventional collagen carriers may lead to unwanted ectopic bone formation and numerous unpredictable side effects such as well-documented soft tissue swelling, osteoclastic bone resorption, and inappropriate adipogenesis [209-215].

The extracellular matrix (ECM) is a natural reservoir of many growth factors and potentiates their bioactivities[11, 216, 217]. In particular, sulfated polysaccharides such as heparin possess structural domains exhibiting affinity to various growth factors including BMPs and have been shown to form stable complexes with rhBMP-2[81, 85, 218]. Therefore, heparin is often used to immobilize rhBMP-2 onto biomaterials for a controlled protein delivery with prolonged bioactivity[219-221]. However, heparin itself suffers from natural variability in structure, difficulty in modification, non-targeting bioactivities, anticoagulant activity, and unknown physiological roles[222-227]. Thus, the direct use of native heparin in tissue engineering is not desirable. Similar biological activities to heparin have been observed in small compounds that

contain groups similar to those in the heparin, in particular, sulfates or sulfonates[105, 106].

We have previously developed an injectable hydrogel system composed of visible light crosslinkable chitosan (methacrylated glycol chitosan, MeGC) and riboflavin as a photoinitiator [6-8]. The MeGC hydrogel well supported proliferation of encapsulated MSCs and their commitment to an osteo- and chondroprogenitor lineage[8, 125, 171]. However, the hydrogel system was not efficient to deliver growth factor proteins and the majority of the initially loaded protein was released in one day from the hydrogel [118].

Here, we report a hydrogel surface that can mimic a natural protector of BMPs, heparin, to stabilize rhBMP-2 and enhance osteogenesis by incorporating heparin-mimicking polysulfonates, poly-vinylsulfonic acid (PVSA) or poly-4-styrenesulfonic acid (PSS), into MeGC hydrogel. The protective effect of PVSA or PSS on BMP stability was evaluated in various therapeutically relevant environments in comparison to that of natural heparin. The ability of the sulfonated hydrogels to bind or deliver rhBMP-2 was evaluated by incubating the hydrogels in a rhBMP-2 solution or loading rhBMP-2 into the hydrogels during photocrosslinking. We also determined the ability of the developed hydrogels to enhance BMP signaling and osteoinductive activity by encapsulating bone marrow stromal cells (BMSCs) into the hydrogels with or without the addition of exogenous rhBMP-2.

5.2. Materials and Methods

5.2.1. Materials

Glycol chitosan (GC, ~ 100 kDa) was supplied from Wako Chemical USA, Inc. (Richmond, VA). Glycidyl methacrylate, poly-vinylsulfonic acid (PVSA, ~ 2 kDa), poly-4-styrenesulfonic acid (PSS, ~ 75 kDa), heparin sodium salt from porcine intestinal mucosa (heparin, ~ 18 kDa), Tween-20, *p*-

nitrophenol phosphate, β-glycerophosphate, dexamethasone, nitro blue tetrazolium (NBT) and alizarin red S were purchased from Sigma-Aldrich (St. Louis, MO). Recombinant human bone morphogenetic protein-2 (rhBMP-2) was purchased from R&D Systems (Minneapolis, MN). Mouse bone marrow stromal cells (BMSCs, D1 ORL UVA, CRL-12424) and mouse myoblast (C2C12, CRL-1772) cells were obtained from American Type Culture Collection (ATCC, Manassas, VA).

5.2.2. Polysulfonates cytotoxicity

Each polysulfonate was dissolved in phosphate buffered saline (PBS) at final concentrations of 65, 2.6, and 29 μM for PVSA, PSS, and Hep, respectively (This will be referred to as 1× polysulfonate solution), to present the same number of sulfonate groups per polysulfonate molecule. BMSCs were cultured in culture medium (CM) with high glucose Dulbecco's Modified Eagle's Medium (DMEM, Life Technologies, Grand Island, NY), 10% (v/v) Fetal Bovine Serum (FBS, Mediatech Inc, Manassas, VA) and 1% (v/v) antibiotic-antimycotic (AA, Life Technologies) at 37 ^{o}C with a 5% CO_2 humidified atmosphere. BMSCs at passages 3-6 were used and stemness of early passage cells were confirmed by monitoring cell morphology and/or expression of MSC surface markers as previously described[228]. Then, BMSCs were seeded in a 96-well culture plate at 2×10^4 cells per well. After 24 h, the medium was replaced with the mixture of CM (180 μL) and 1× polysulfonate solution (20 μL). The polysulfonates were tested in various concentrations ranging from 0.1× (6.5, 0.26, and 2.9 μM for PVSA, PSS, and Hep, respectively) to 10× (655, 26, and 290 μM for PVSA, PSS, and Hep, respectively) The cell viability was measured by following equation (1) after alamarBlue (Thermo Fisher Scientific, CA) assay as previously described[229]. In brief, BMSCs were cultured in CM containing polysulfonate 1× solution for 24 h and the medium was

replaced with 10% (v/v) alamarBlue reagent in CM. Following 3 h incubation, alamarBlue fluorescence was measured.

$$Cell\ viability\ (\%) = \frac{F_e - F_b}{F_c - F_b} \times 100 \qquad (1)$$

where F_e, F_c, and F_b refers fluorescence value read at 585 nm and excited at 570 nm of experimental, control and blank groups, respectively.

5.2.3. BMP-2 stabilizing effect of polysulfonates

rhBMP-2 (1 μg) and 100 μL of polysulfonate 1× solution was dissolved in 1 mL of PBS. The rhBMP-2 and polysulfonate mixture was incubated in PBS at 37 °C for 7 days, 0.5% trypsin at 37 °C for 24 h, or pH 4.5 buffer at 37 °C for 24 h. Then, 20 μL of the treated mixture was combined with at 180 μL of osteogenic media (OM) including DMEM, 10% (v/v) FBS, 1% (v/v) AA, 10 mM β-glycerophosphate, 50 mg/mL L-ascorbic acid, and 100 nM dexamethasone. The bioactivity of rhBMP-2 in the treated mixture was determined by assessing its ability to enhance expression of alkaline phosphatase (ALP) in BMSCs. After incubation for 4 days, cells were fixed with 10% neutral buffered formalin (NBF) and incubated in a solution consisting of NBT and 5-bromo-4-chloro-3-indoxylphosphate solutions in AP buffer (100 mM Tris pH 8.5, 50 mM $MgCl_2$, and 100 mM NaCl) for 3 h. In addition, ALP activity was measured by *p*-nitrophenol phosphate test with the same method from a previous study[8].

5.2.4. Preparation of heparin-mimicking sulfonated hydrogels

Photo-crosslinkable methacrylated glycol chitosan (MeGC) was prepared by following the

previously developed methods[5, 6]. Briefly, GC was dissolved in distilled water (DW) (2% w/v) and functionalized with GMA (1:1.1 molar ratio) at pH 9.0 for 40 h. After the purification and lyophilization step, MeGC was rehydrated at 2% (w/v) in PBS solution. The sulfonated hydrogels were formed by 40 s irradiation of a mixture of MeGC, 1× polysulfonates solution, and 6 μM riboflavin initiator (100:10:0.5 volume ratio) with visible blue light (VBL, 400-500 nm, 300 mW/cm^2, Bisco Inc., Schaumburg, IL).

5.2.5. Characterization of the sulfonated hydrogels

Sulfonated hydrogels were incubated in PBS for 21 days and collected at predetermined time points (0 h, 24 h, 7 days, 14 days, and 21 days). The incubating solution was used for 1,9-dimethyl-methylene blue (DMB, Sigma-Aldrich) assay to quantify polysulfonate released in PBS[118, 125, 171]. The collected hydrogels were stained with 1% (w/v) toluidine blue (Sigma-Aldrich, MO) solution in PBS for 5 min and washed with PBS for 1 h. Mechanical strength was assessed by measuring compressive modulus with an indentation experiment setting using Instron Electro-Mechanical Testing Machines (Instron, Model 5564, Norwood, MA). The compressive modulus was calculated using a Poisson's ratio of 0.25 as described from the previous protocol[5, 6]. The water contents of hydrogels were calculated by the following equation (2).

$$Water\ content\ (\%) = \frac{W_w - W_d}{W_d} \times 100 \qquad (2)$$

where W_w and W_d, refers wet weight of a hydrogel and dry weight of the same hydrogel after lyophilization, respectively. The morphology of hydrogels was observed using scanning electron microscopy (SEM, FEI Nova NanoSEM 230, Hillsboro, OR). All hydrogels were frozen in liquid

nitrogen for 5 min, lyophilized overnight, and gold-coated with a sputter coater at 20 mA under 70 mTorr for 1 min.

5.2.6. Cell proliferation in the sulfonated hydrogels

BMSCs were encapsulated in the sulfonated hydrogels at 2×10^6 cells/mL concentration and cultured in CM for 14 days. The live/dead staining image was obtained on an Olympus IX71 fluorescence microscope (Olympus, Tokyo, Japan) after calcein/ethidium homodimer staining for 15 min. The viability of cells was quantified by ImageJ software (NIH, Bethesda, Maryland) analysis measuring the ratio of live cells (green) to total cells (green + red). BMSCs proliferation was measured using alamarBlue assay following the manufacturer's protocol.

5.2.7. BMP-2 release from sulfonated hydrogels

rhBMP-2 was encapsulated as 10 μg/mL in the mixture of MeGC, 1× polysulfonates, and 6 μM riboflavin initiator (100:10:0.5 volume ratio) and crosslinked under 40 s VBL irradiation. rhBMP-2 encapsulated hydrogels were incubated in 1 mL PBS for 21 days at 37 ^{o}C. The incubating solution was replaced with fresh PBS twice a week. At predetermined time points, the released rhBMP-2 in supernatant was quantified using BMP-2 ELISA kit (R&D Systems, MN) as per manufacturer's protocol. The released rhBMP-2 was collected at day 7, 14, and 21 and its bioactivity was assessed by monitoring ALP expression in C2C12 cells.

5.2.8. Zeta potential of sulfonated hydrogels

The electrostatic potential on the hydrogel surface was evaluated by measuring the zeta potential measurement of the hydrogel. Briefly, samples were prepared according to the previous

protocol[153]. Briefly, freeze-dried powders of the sulfonated hydrogels were suspended in DW to generate 5% (w/w) stock solution and centrifuged at 12,000 *g* for 2 min. The supernatant was used for the zeta potential measurement at 25 ºC using a Malvern Zetasizer (Worcestershire, UK).

5.2.9. BMP-2 binding of sulfonated hydrogels

The sulfonated hydrogels were incubated in PBS with 1 μg/mL rhBMP-2 for 7 days. Then, the hydrogels were placed in optimal cutting temperature (OCT, Thermo Fisher Scientific, CA) medium and frozen at -80 ºC. The frozen samples were cryosectioned at a thickness of 20 μm and mounted on glass slides. The sections were incubated with primary antibody against rhBMP-2 (R&D Systems, MN) and Alexa Flour 633-tagged secondary antibody (Invitrogen, CA). Images were obtained using an Olympus IX71 microscope (Olympus, Tokyo, Japan). The amounts of rhBMP-2 in the hydrogel and incubating supernatant were quantified by ELISA. The absorbed rhBMP-2 was collected by digesting the hydrogel in 10 mg/mL lysozyme solution at 37 ºC for 16 h.

5.2.10. Osteogenic differentiation of BMSCs in the sulfonated hydrogels

BMSCs were encapsulated in sulfonated hydrogels loaded with PBS or rhBMP-2 (1 μg/mL) and cultured in OM for 21 days. Osteogenic ability of BMSCs in sulfonated hydrogels was determined using real-time polymerase chain reaction (qRT-PCR) of different osteogenic gene markers along with ALP and alizarin red S staining. Samples were collected at day 4 for measuring *Runx2* expression and day 21 for *Osteocalcin (OCN)* expression. Total RNAs inside hydrogels were extracted by TRIzol (Invitrogen, CA) and RNeasy Mini kit (Qiagen, CA). The RNAs were reversely transcribed to cDNAs using cDNA transcription kit (Invitrogen) and the products were

carried out in a LightCycler 480 PCR system (Indianapolis, IN) with 20 μL SYBR Green. The cDNAs were amplified for 45 cycles and the *GAPDH* expression was used for normalization. The primer sequence of *GAPDH*, *Runx2*, and *OCN* were listed in Table 5-1. All experiments were run in multiplicate (n=6). Hydrogels were collected at day 4 for ALP staining and at day 21 for alizarin red S staining. The collected hydrogel samples were fixed in NBF for 16 h. For alizarin red S staining, the fixed samples were incubated in 2% alizarin red S staining solution for 5 min and washed in PBS for 16 h. The stained samples were imaged with the Olympus SZX16 Stereomicroscope (Olympus, Tokyo, Japan).

Table 5-1. Primer sequence for qRT-PCR

Gene		Sequence
GAPDH	Forward	AGGTCGGTGTGAACGGATTTG
	Reverse	TGTAGACCATGTAGTTGAGGTCA
Runx2	Forward	CGGTCTCCTT CCAGGATGGT
	Reverse	GCTTCCGTCAGCGTCAACA
OCN	Forward	GGGAGACAACAGGGAGGAAAC
	Reverse	CAGGCTTCCTGCCAGTACCT

5.2.11. BMP-2 stabilizing effect of sulfonated hydrogels

For BMP-2 stabilizing test in a hydrogel system, rhBMP-2 was encapsulated into sulfonated hydrogels during hydrogel crosslinking at 10 μg/mL. The hydrogel loaded with rhBMP-2 was incubated in PBS at 37 ºC for 3 days, 0.5% trypsin at 37 ºC for 5 h, or at pH 4.5, 37 ºC for 5 h. Then, the treated hydrogel was digested with lysozyme (10 mg/mL in PBS) at 37 ºC for 16 h. After enzymatic degradation, the hydrogel digest was centrifuged for 2 min at 10,000 *g* and the supernatant was collected. rhBMP-2 concentration in the supernatant was quantified using BMP-

2 ELISA and the final concentration of 100 ng/mL was used for ALP activity test using BMSCs.

5.2.12. Statistical analysis

All experiments were performed in triplicate unless otherwise stated. The values represent the average and the error bars are the standard deviation. Statistical analysis was performed using one-way analysis of variance (ANOVA) with Tukey's post hoc test. A value of $p < 0.05$ was considered as significant.

5.3. Results

5.3.1. Polysulfonates cytotoxicity

Since polysulfonates may be potentially toxic to cells, the cytotoxicity of polysulfonates was evaluated in BMSCs culture at various polysulfonate concentrations of 0, 0.1, 0.5, 1, 5, and 10× (Figure 5-1). The addition of polysulfonates supported high cell viability over 90% up to 1× (65, 2.6, and 29 μM for PVSA, PSS, and Hep, respectively) polysulfonate. Increasing the polysulfonate concentration from 1× to 5× (325, 18, and 145 μM for PVSA, PSS, and Hep, respectively) led to a decrease in BMSCs viability to approximately 80%. Significantly decreased cell viability (< 70%) was observed with 10× (650, 26, and 290 μM for PVSA, PSS, and Hep, respectively) polysulfonate and PSS led to the lowest cell viability among the experiment groups with values lower than 60%.

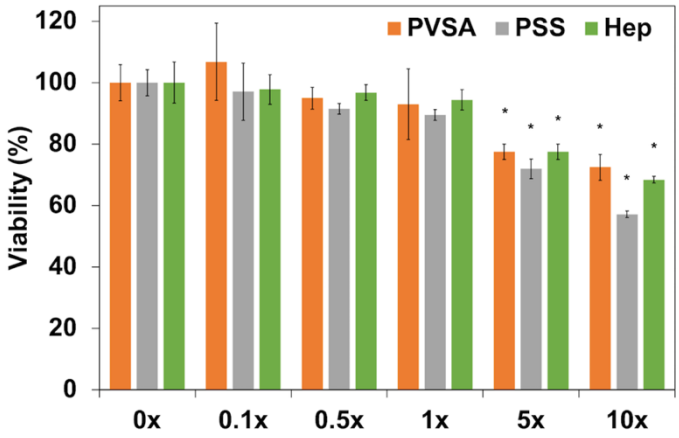

Figure 5-1. Viability of BMSCs after 24 h culture at various polysulfonate concentrations (0, 0.1, 0.5, 1, 5, and 10×) measured by alamarBlue assay (1× polysulfonate: 65, 2.6, and 29 μM for PVSA, PSS, and Hep, respectively) (*: $p < 0.05$ compared with 0×).

5.3.2. BMP-2 stabilizing effect of polysulfonates

In order to evaluate the ability of heparin mimicking polysulfonate molecules to protect the bioactivity of rhBMP-2, rhBMP-2 was incubated with various concentrations of PVSA, PSS or natural heparin in various therapeutically relevant environments (Figure 5-3A). rhBMP-2 was incubated with 0.5% trypsin or pH 4.5 buffer for 16 h to mimic the proteolytic or mild acidic conditions present in bone fracture healing. The bioactivity of treated rhBMP-2 was determined by monitoring its ability to increase ALP expression in BMSCs at day 4 post stimulation. Freshly thawed rhBMP-2 served as a positive control. rhBMP-2 in the treatment with trypsin or pH 4.5 buffer as well as in the incubation for 7 days in PBS at 37 ºC did not significantly increase ALP activity of BMSCs, indicating that rhBMP-2 lost its bioactivity during the stressor treatments. In contrast, rhBMP-2 exposed to the stressors in the presence of polysulfonates, especially with PSS, significantly enhanced ALP expression as shown by ALP staining (Figure 5-2). In particular, 1×

PSS exhibited higher protective effects compared to heparin as quantified by ALP colorimetric assay (Figure 5-3B). Further increase in PSS concentration to 10×, however, greatly reduced ALP activity in comparison to heparin. This is mostly due to high cytotoxicity of 10× PSS as shown in cell viability study (Figure 5-1).

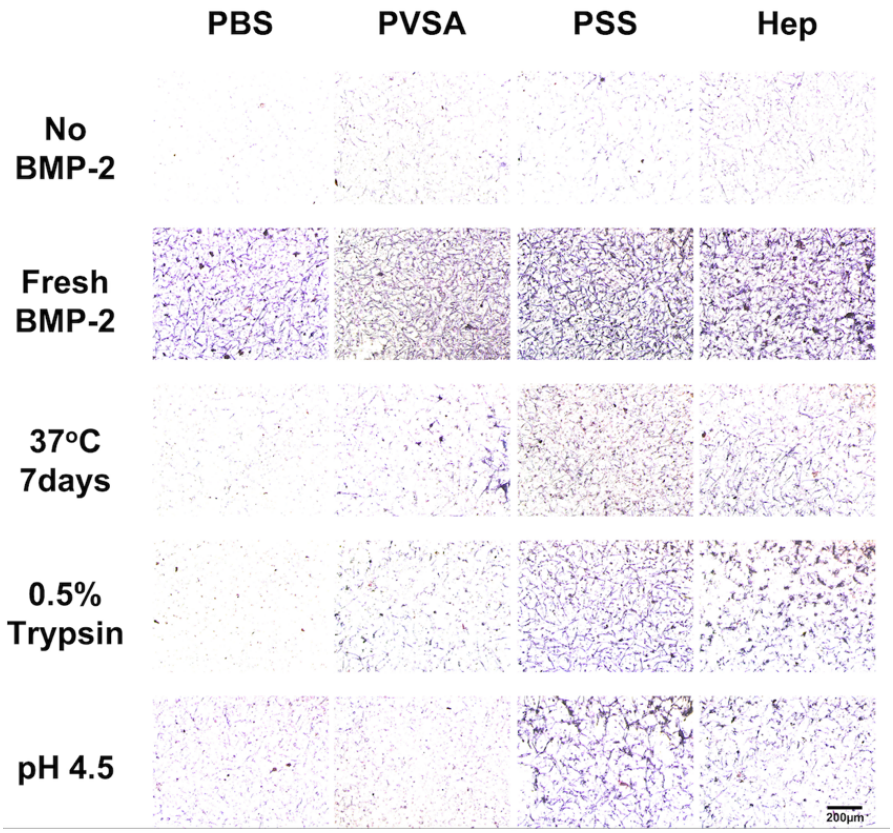

Figure 5-2. ALP staining of BMSCs after 4 days of culture with BMP-2 treated in various stressor conditions in the presence of 1× polysulfonates.

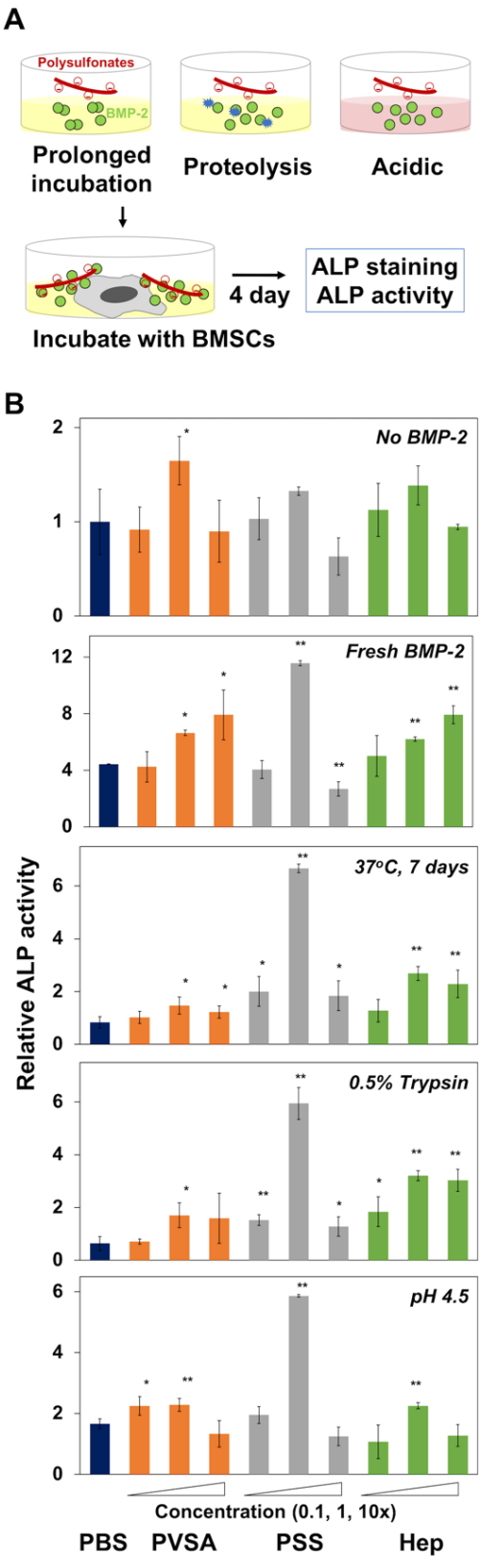
A
Polysulfonates
BMP-2
Prolonged incubation
Proteolysis
Acidic
4 day
ALP staining
ALP activity
Incubate with BMSCs
B
No BMP-2
Fresh BMP-2
37°C, 7 days
0.5% Trypsin
pH 4.5
Relative ALP activity
Concentration (0.1, 1, 10x)
PBS
PVSA
PSS
Hep

Figure 5-3. BMP-2 stabilizing effect of polysulfonates. (A) The scheme of BMP-2 stabilizing test. BMP-2 was incubated in various therapeutically relevant environments (37 ^{o}C for 7 days, 0.5% trypsin for 16 h, and pH 4.5 for 16 h) in the presence of PVSA, PSS or heparin (Hep). BMSCs were cultured with the treated BMP-2 for 4 days and ALP production was measured by ALP staining and ALP activity test. (B) ALP activity of BMSCs measured by a colorimetric assay after 4 days of culture with BMP-2 samples treated in the presence of various concentrations of polysulfonates (0.1, 1, and 10×) (*: $p < 0.05$, **: $p < 0.01$).

5.3.3. Preparation and characterization of heparin-mimicking sulfonated hydrogels

In order to prepare heparin-mimicking sulfonated hydrogels, MeGC solution was mixed with 1× polysulfonates and polymerized with a riboflavin (RF) initiator under visible blue light (VBL) irradiation (Figure 5-4A). The homogenous distribution and stable incorporation of polysulfonates in hydrogels was verified using toluidine blue staining and DMB assay during a 21-day incubation. Blue color indicated incorporation of negatively charged polysulfonates in hydrogels and no significant color change or indication of polysulfonates release for three weeks was observed (Figure 5-4B). High polysulfonate loading efficiency (>98%) was observed. DMB assay was performed to quantify the amount of polysulfonates released from hydrogels, and negligible quantity was detected for 21 days (Figure 5-5). The mechanical strength of the sulfonated hydrogels was characterized by indentation measurements. The addition of polysulfonates or heparin did not significantly change the modulus of the hydrogel (Figure 5-4C). No significant difference was observed in the equilibrium water content (>97%) among all four experimental groups (Figure 5-6). The morphology of the hydrogels was characterized by SEM (Figure 5-4D).

Interpenetrating network was observed in sulfonated hydrogels, indicating the retention of polysulfonates or heparin added.

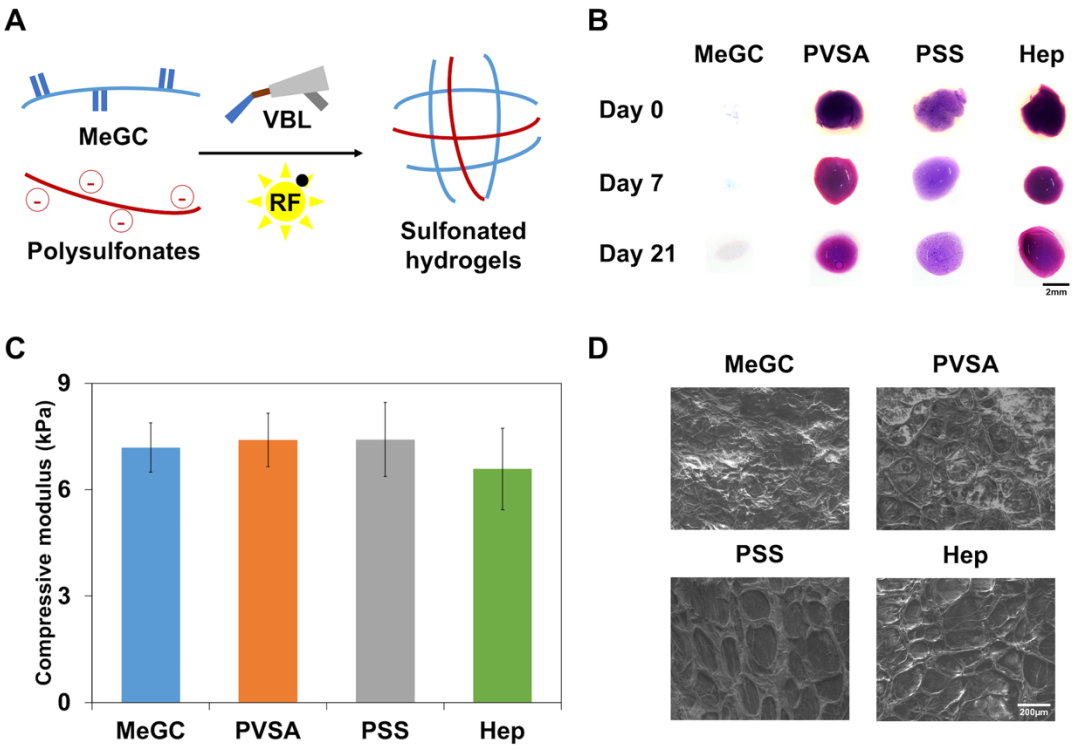

Figure 5-4. Characterization of the sulfonated hydrogels. (A) The scheme of sulfonated hydrogels preparation. The mixture of MeGC, 1× polysulfonates, and riboflavin (RF) was crosslinked under 40 s VBL irradiation. (B) Toluidine blue staining of MeGC and sulfonated hydrogels after incubation up to 21 days. (C) Compressive modulus of hydrogels. (D) Morphological characterization of sulfonated hydrogels using SEM.

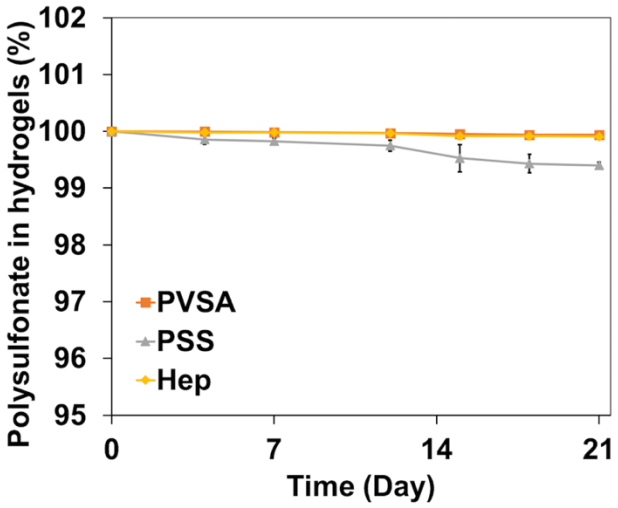

Figure 5-5. DMB assay result of released polysulfonates from sulfonated hydrogels in PBS at 37 °C for 21 days.

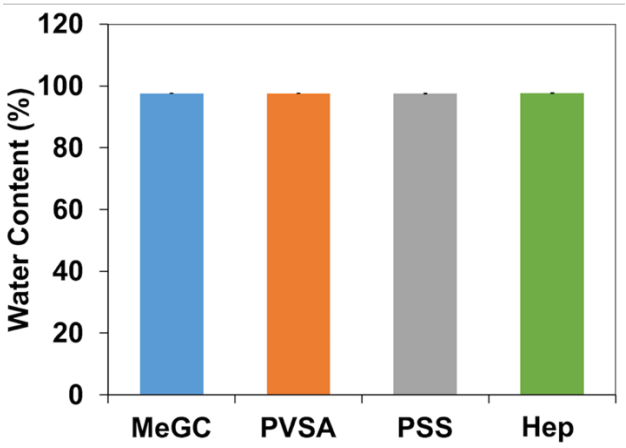

Figure 5-6 .Water contents of sulfonated hydrogels.

5.3.4. Cell viability and proliferative potential in sulfonated hydrogels

BMSCs were encapsulated in sulfonated hydrogels and viability of BMSCs was characterized during a 14-day culture. Live/dead fluorescence staining demonstrated that BMSCs in sulfonated hydrogels maintained cell viability above 90% over the 14 days culture period, indicating

biocompatible nature of the hydrogel system (Figure 5-7A and Figure 5-8). The alamarBlue assay was employed to evaluate the proliferative potential of encapsulated cells in sulfonated hydrogels. The alamarBlue fluorescence intensity increased over time up to day 14, reflecting proliferative capacity of BMSCs, and there was no significant difference in fluorescence intensity among the hydrogels (Figure 5-7B).

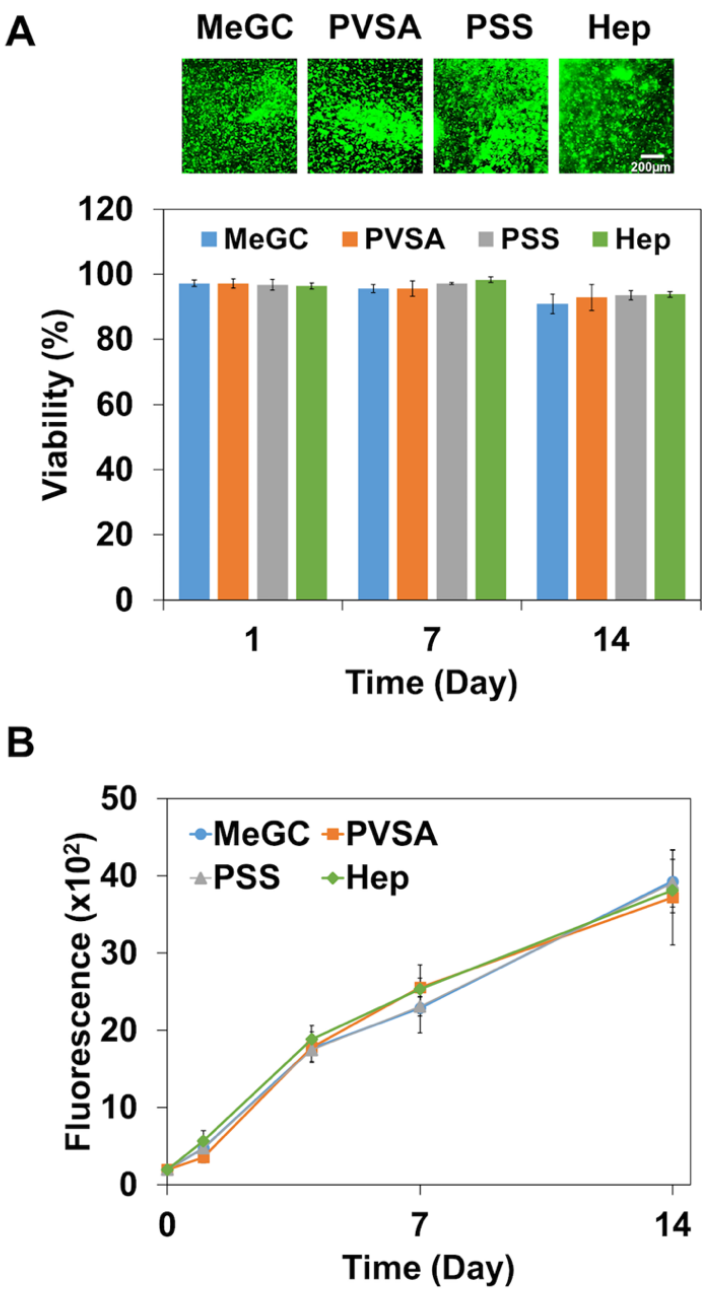

Figure 5-7. Viability and proliferative potential of BMSCs encapsulated in MeGC and sulfonated hydrogels for 14 days. (A) Live/dead staining images were obtained and cell viability was quantified by ImageJ analysis. (B) Proliferative potential of BMSCs was evaluated by alamarBlue assay.

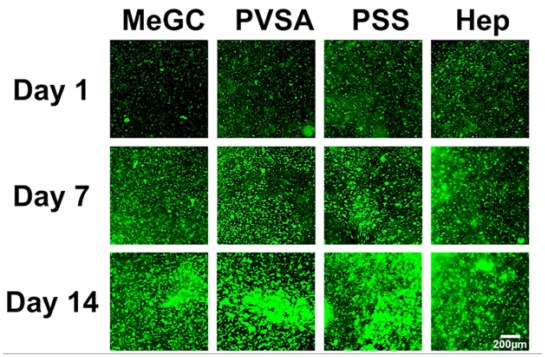

Figure 5-8. Live/dead staining images of BMSCs encapsulated in the sulfonated hydrogels at day 1, 7, and 14.

5.3.5. BMP-2 release from sulfonated hydrogels

In order to investigate the ability of sulfonated hydrogels to deliver growth factors, we determined the effective concentration range of polysulfonates to reduce initial burst release using avidin, a basic glycoprotein that binds heparin[230], as a model protein. Fluorescently labeled avidin was mixed with MeGC solutions and various concentrations of polysulfonates (0.1, 1 and 10×) and polymerized under VBL irradiation with RF (Figure 5-9A). The release profile of avidin encapsulated in MeGC hydrogels demonstrated a rapid burst release of 60% within one day (Figure 5-9B). The addition of PVSA or PSS into hydrogels reduced the release rate of avidin in a dose-dependent manner. Similar trend of reduced burst release was observed with the addition of heparin. Since there was no significant difference in release profile between 1× and 10× polyfulsulfontes, rhBMP-2 was encapsulated in MeGC hydrogels modified with 1× polysulfonates and rhBMP-2 release was observed by BMP-2 ELISA (Figure 5-9C and Figure 5-10). The high loading efficiency of rhBMP-2 was observed in all hydrogels (MeGC 95%, PVSA 97%, PSS 98%, and Hep 97%). The addition of polysulfonates or heparin into MeGC hydrogels significantly reduced the burst release of loaded rhBMP-2, consistent with the model protein observations. In

particular, PSS was the most effective one to lower rhBMP-2 burst release. The zeta potential of MeGC hydrogels was 6 ± 1 mV, while the modification of the hydrogels with PVSA, PSS, and heparin greatly reduced to the negative zeta potentials of -2, -8, and -3 mV respectively (Figure 5-9D). This result indicates that negatively charged sulfonate groups incorporated in MeGC led to hydrogel surfaces providing stronger interactions with rhBMP-2. The bioactivity of released rhBMP-2 was evaluated by examining ALP expression in C2C12 cells (Figure 5-9E). The rhBMP-2 release media collected from sulfonated hydrogels at day 14 and 21 significantly increased ALP activity compared to that of MeGC.

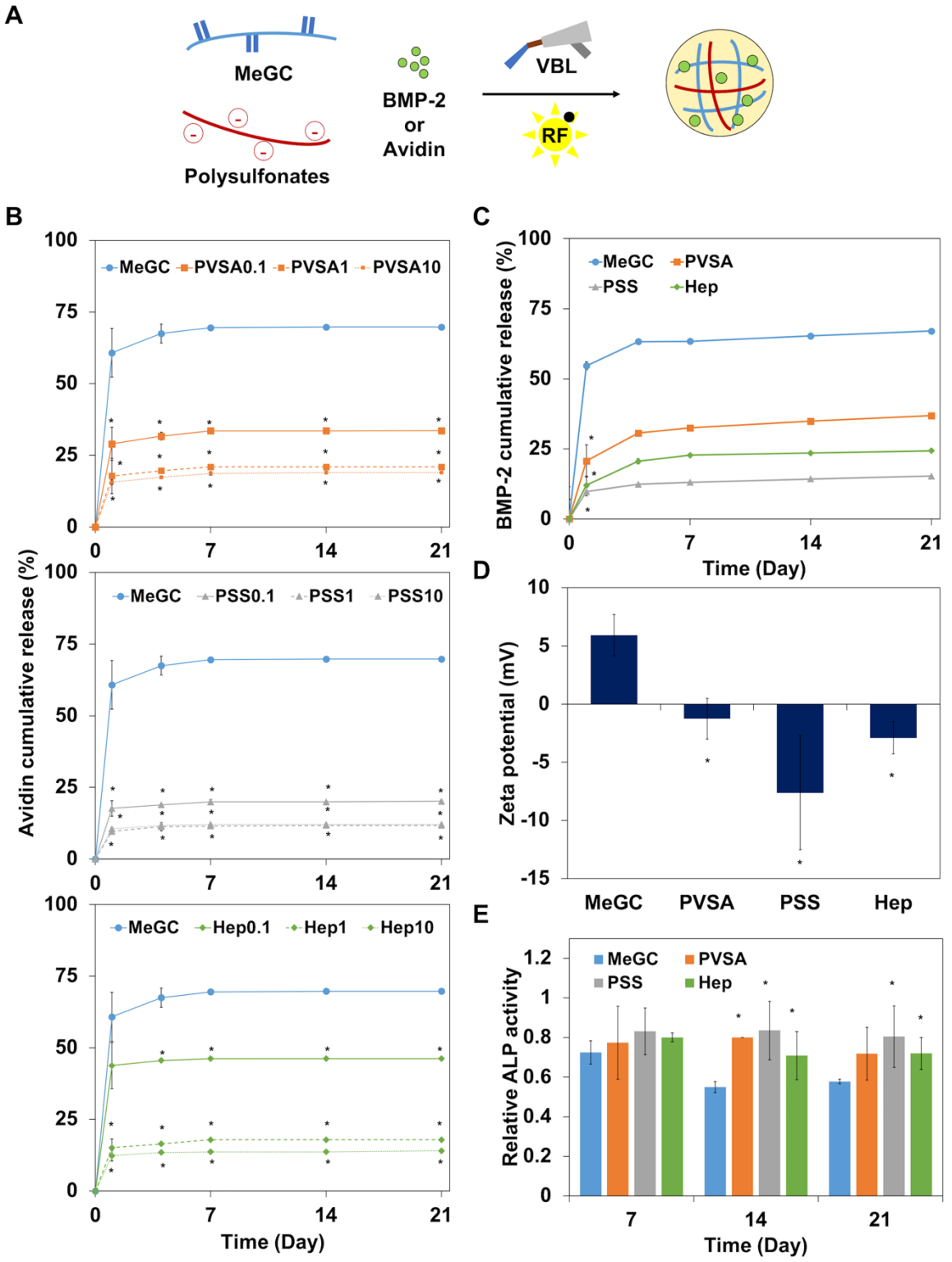

Figure 5-9. (A) The scheme of protein (BMP-2 or avidin) encapsulation during photocrosslinking of hydrogels. (B) The release profile of a model protein, avidin, from MeGC hydrogels containing

various concentrations (0.1, 1, and 10×) of PVSA, PSS or heparin (Hep) in PBS at 37 ºC. (C) BMP-2 release profile from MeGC hydrogels containing 1x polysulfonates in PBS at 37 ºC for 21 days. (D) Zeta potential of MeGC and sulfonated hydrogels. (E) Bioactivity of BMP-2 released from sulfonated hydrogels as assessed by measuring ALP activity in C2C12 cells (*: $p < 0.05$).

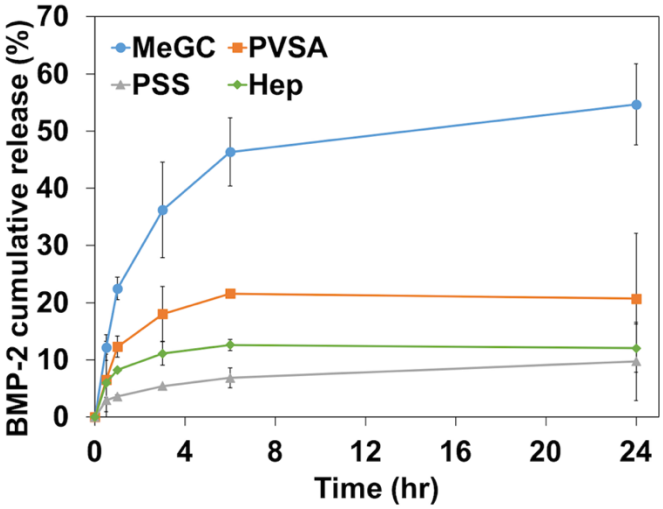

Figure 5-10. BMP-2 release profile from MeGC hydrogels containing 1x polysulfonates in PBS at 37 ºC at 0.5, 1, 3, 6, and 24 hr.

5.3.6. BMP-2 binding ability of sulfonated hydrogels

In order to evaluate the ability of rhBMP-2 binding to sulfonated hydrogels, hydrogels were incubated in a rhBMP-2 solution for a week and bound rhBMP-2 was observed after immunofluorescent staining (Figure 5-11A). PSS modified hydrogels were found to bind BMP-2 while MeGC showed no significant staining of the protein, indicating successful sequestering of rhBMP-2 in sulfonated hydrogels through polysulfonates functionalization. Higher amount of rhBMP-2 was detected in the sulfonated hydrogels, especially in the PSS modified hydrogels,

compared with unmodified MeGC hydrogels as measured by ELISA (Figure 5-11B). To investigate the ability of sulfonated hydrogels to bind with endogenous BMP-2 produced by cells, BMSCs were encapsulated in sulfonated hydrogels and cultured in OM without rhBMP-2 supplementation (Figure 5-11C). At day 7, highly intense rhBMP-2 staining was observed in PSS or heparin modified hydrogels compared to unmodified MeGC groups.

In order to test the intrinsic effects of sulfonated hydrogels on osteogenesis, BMSCs were encapsulated in sulfonated hydrogels in the absence of rhBMP-2 and expression of ALP was monitored. The addition of polysulfonates into MeGC hydrogels significantly increased the expression of ALP as observed by ALP staining and quantified by ALP colorimetric assay (Figure 5-11D). The findings are consistent with the observation that sulfonated hydrogels bind more exogenous (Figure 5-11A and B) or cell-secreted BMP-2 (Figure 5-11C).

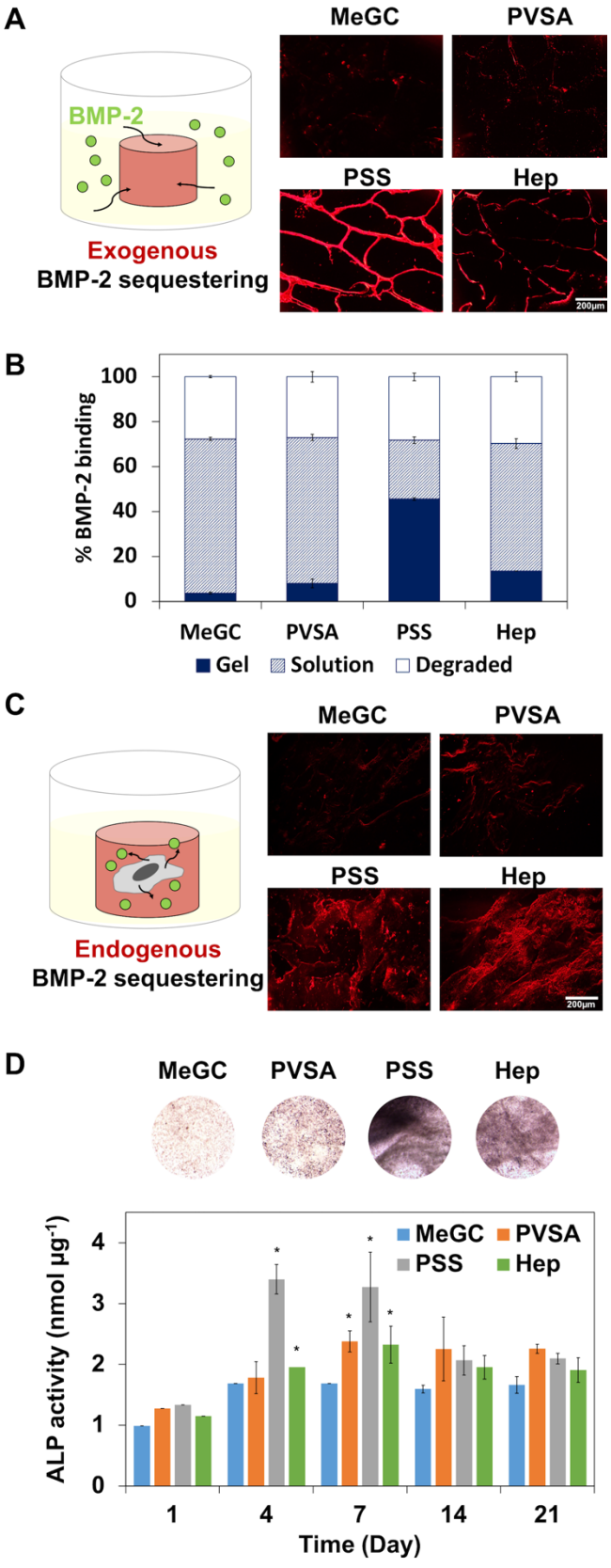
A
MeGC
PVSA
BMP-2
PSS
Hep
200μm
Exogenous
BMP-2 sequestering
B
% BMP-2 binding
100
80
60
40
20
0
MeGC
PVSA
PSS
Hep
Gel
Solution
Degraded
C
MeGC
PVSA
PSS
Hep
200μm
Endogenous
BMP-2 sequestering
D
MeGC
PVSA
PSS
Hep
ALP activity (nmol μg-1)
4
3
2
1
0
MeGC
PVSA
PSS
Hep
1
4
7
14
21
Time (Day)

Figure 5-11. BMP-2 binding to sulfonated hydrogels. (A) BMP-2 immunostaining of hydrogels after 7-day incubation in BMP-2 solution. (B) Amount of BMP-2 in sulfonated hydrogels and incubating supernatant quantified by ELISA. (C) BMP-2 immunostaining of hydrogels encapsulated with BMSCs after 7-day culture in OM. (D) ALP staining of hydrogels encapsulated with BMSCs after 4-day culture in OM. ALP activity was measured by ALP colorimetric assay (*: $p < 0.05$).

5.3.7. Osteogenic efficacy of BMP-2 in sulfonated hydrogels

In order to evaluate the efficacy of sulfonated hydrogels delivering rhBMP-2 to enhance osteogenesis, BMSCs and rhBMP-2 were co-encapsulated in the hydrogels and osteogenic differentiation of BMSCs was evaluated by both ALP and alizarin red S staining (Figure 5-12A). The rhBMP-2 loaded hydrogels modified with polysulfonates showed highly intense positive ALP and alizarin red S staining, suggesting strong ALP expression and mineral deposition compared to unmodified MeGC hydrogels. The sulfonated hydrogels also significantly increased osteogenic differentiation of encapsulated BMSCs as observed by upregulation of *Runx2*, a key regulator of osteogenesis as well as *OCN*, a late osteogenic marker (Figure 5-12B). To evaluate the maintenance of BMP-2 bioactivity in the sulfonated hydrogels during exposure to stressors, hydrogels loaded with rhBMP-2 were treated under various stress conditions first and the bioactivity of the rhBMP-2 extracted from the hydrogels was assessed in BMSCs by ALP assay (Figure 5-12C and Figure 5-13). Significantly increased ALP expression was observed in BMSCs cultured with rhBMP-2 recovered from MeGC or polysulfonates modified hydrogels with no stressor treatment. After exposure to stressors, MeGC hydrogels without polysulfonates exhibited

low rhBMP-2 bioactivity. In contrast, sulfonated hydrogels provided better stabilizing effect during the treatment.

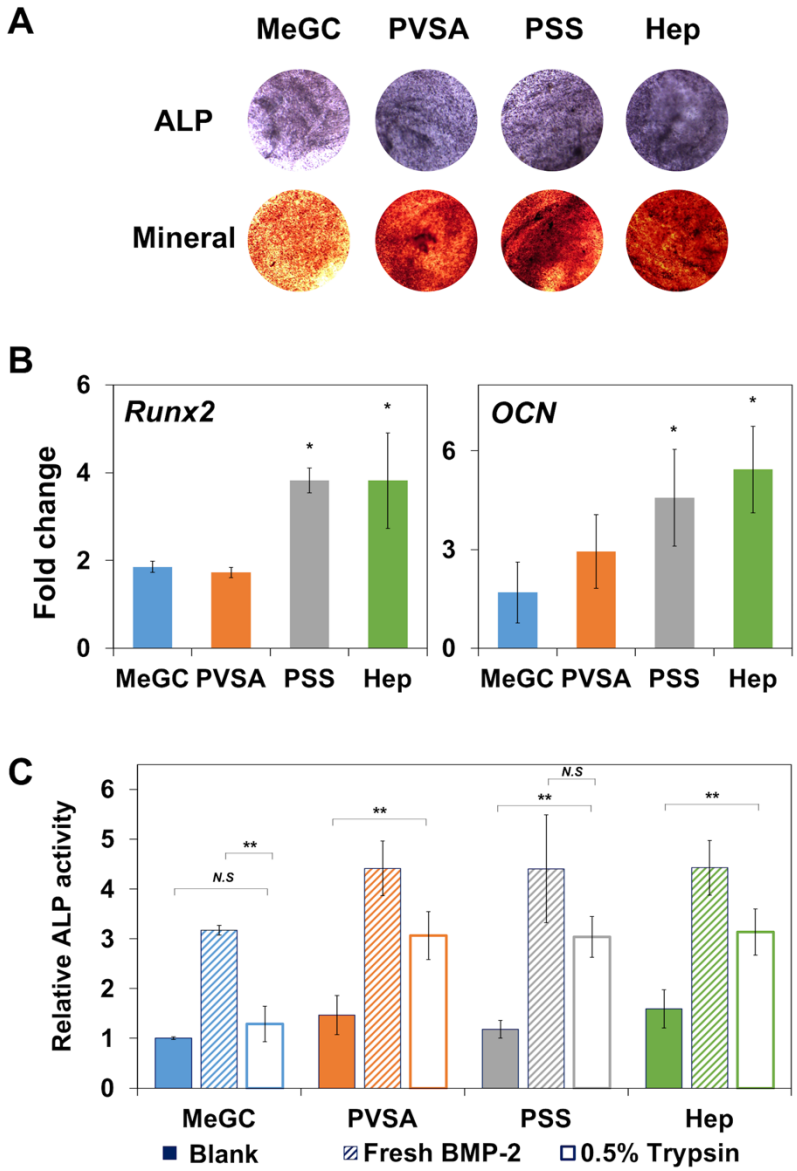

Figure 5-12. Osteogenic differentiation of encapsulated BMSCs in sulfonated hydrogels loaded with BMP-2. (A) ALP (top) and mineral deposition (bottom) of BMSCs in hydrogels at day 4 (ALP) or day 21 (mineral) after culture. (B) Osteogenic gene expression of BMSCs analyzed by qRT-PCR at day 4 (*Runx2*) or day 21 (*OCN*) after culture. (C) BMP-2 stabilizing effect of

sulfonated hydrogels. BMP-2 was loaded into sulfonated hydrogels and incubated in 0.5% trypsin for 5 h. Solution obtained after hydrogel degradation was collected and its bioactivity was determined by measuring ALP activity of BMSCs compared with hydrogels loaded with BMP-2 without trypsin treatment (Fresh BMP-2) or hydrogels loaded with PBS (Blank). (*: $p < 0.05$, **: $p < 0.01$, *N.S*: not significant).

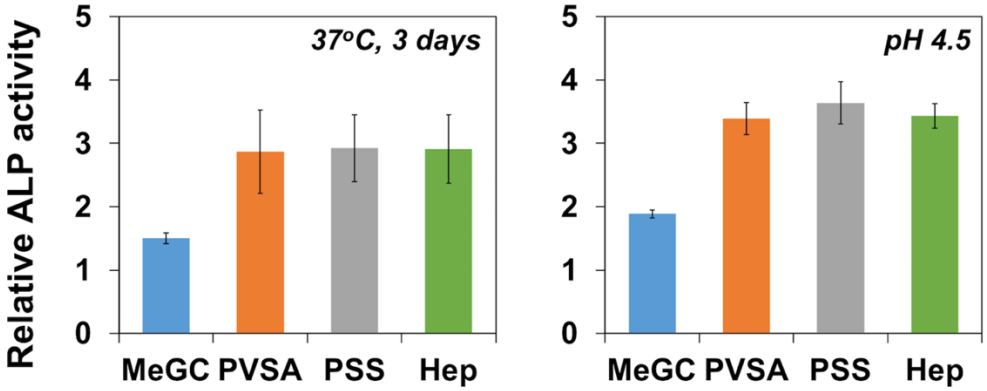

Figure 5-13. BMP-2 stabilizing effect in sulfonated hydrogels after incubation at 37 oC for 3 days and with pH 4.5 buffer for 5 h.

5.4. Discussion

In this study, we seek to increase biological activity of BMP-2 for osteogenesis by binding with heparin-mimicking molecules in MeGC hydrogels. Heparin is a polysaccharide with a highly negatively charged density and is being widely used in tissue engineering scaffolds and controlled release systems for many growth factors including BMP-2 due to its strong binding property and protective effect for the proteins from degradation[80, 231]. We investigated here whether the heparin-mimicking sulfonated polymers could stabilize rhBMP-2 and enhance MSCs osteogenic differentiation induced by rhBMP-2.

We evaluated the protective effect of polysulfonates under various physiological stressors found in bone fracture healing. Fracture healing is a cascade of osteoblastic new bone formation and osteoclastic resorption events. The bone remodeling process is related to proteolytic degradation of organic extracellular compartment through enzyme activity such as matrix metalloproteinase (MMPs), cathepsin K, and trypsin[232, 233]. Osteoclasts created mild acidic extracellular environment (pH 4-5) by secreting acid to dissolve bone mineral. Our results showed that the bioactivity of rhBMP-2 was well maintained with the addition of polysulfonates during exposure to enzyme or acidic stress conditions, especially with PSS. The acidic condition decreased the rhBMP-2 bioactivity to a lesser extent probably due to increased protein solubility at the experimental pH 4.5[207, 234]. Incubation of rhBMP-2 at physiological pH for 7 days greatly reduced the protein bioactivity. Given that rhBMP-2 reduces solubility at pH above 6.5, the increase in test pH might cause protein aggregation which could affect the bioactivity of rhBMP-2[78, 235]. Interestingly, the bioactivity of freshly reconstituted rhBMP-2 was significantly increased in the presence of polysulfonates or heparin. It is demonstrated that the BMP-2 dimer contains two heparin binding sites on N-terminal domains which modulate its bioactivity[81]. The cell surface heparan sulfate played a direct and stimulatory role in BMP-2 signaling. Specifically, heparan sulfate serves as a catalyst to form signaling complexes by enhancing the recruitment of type II receptor although it does not directly affect BMP binding to type I receptor[94]. Heparin also reduced BMP-2 interaction with its antagonist noggin by modulating its distribution on the cell surface with prolonged half-life[92]. Extracellular regulation of BMP activity by other ECM proteins was also studied that BMP-7 underwent conformational change from bioactive open V-shape to latent closed ring shape upon binding to fibrillin-1[236].

rhBMP-2 binding ability of sulfonated hydrogels was explored after incorporation of the

polysulfonates into MeGC. The sulfonated hydrogels were found to bind higher amount of rhBMP-2 compared with unmodified MeGC hydrogels as shown by rhBMP-2 ELISA assay. This may be attributed to strong electrostatic interactions between sulfonate residues on the hydrogel surface and positively charged rhBMP-2 (isoelectric point: 8.5) [237, 238]. Specifically, PSS-functionalized hydrogels exhibited the highest sequestering ability. This may be due to decreased (more negative) zeta potential with PSS which created higher affinity binding of rhBMP-2. Moreover, the observed low levels of protein release in sulfonated hydrogels may be associated with high levels of protein absorption.

Sulfonated hydrogels significantly increased osteogenic differentiation of encapsulated BMSCs without addition of exogenous rhBMP-2 compared with unmodified MeGC hydrogels as observed by increased ALP expression (Figure 5-11D). Matrix mechanical properties such as elastic modulus and stress relaxation are known to regulate osteogenic differentiation of MSCs[34, 239]. The addition of polysulfonates into MeGC did not have significant effect on hydrogel mechanical properties as well as cell viability and proliferation. Thus, the observed increase in osteogenesis is likely due to sulfonated hydrogel surfaces that may sequester BMPs secreted by entrapped BMSCs as validated by immunostaining for BMP-2. BMP-2 stabilizing effects of sulfonated hydrogels were verified after stress exposures (Figure 5-12C). These findings suggest a promising hydrogel surface that could augment endogenous BMP activity by localizing the cell-produced BMPs. Moreover, the addition of polysulfonates reduced initial burst and further increased rhBMP-2 induced osteogenesis differentiation of encapsulated BMSCs, suggesting efficient protein delivery systems. In addition, the therapeutic efficacy of using large amount of heparin in tissue engineering scaffolds or drug delivery microparticles is limited due to its cytotoxicity and high charge density limiting BMP-2 release. Our study here incorporated heparin-

mimicking sulfonated molecules into biodegradable bulk hydrogels to sequester, stabilize and release BMP-2 as the hydrogel degrades *in vivo*. Future study will modulate hydrogel degradation properties for tunable BMP-2 release kinetics and *in vivo* performance will be evaluated in a more challenging bone fracture healing model for clinical translation.

5.5. Conclusions

We developed a heparin-mimicking hydrogel surface that can stabilize BMP activity to enhance osteogenesis by incorporating sulfonated molecules into photocrosslinkable MeGC hydrogel. The sulfonated molecules exhibited protecting effects on BMP-2 bioactivity against various therapeutically relevant stressors. The sulfonated hydrogel was not only effective in delivering exogenous BMP-2, but also potentiated endogenous BMP signaling mediated by cells. This work suggests a promising hydrogel system to improve clinical efficacy of BMP-2 and other heparin-binding growth factors and also provides basis for future development of material-based therapeutics for tissue engineering.

5.6. Acknowledgement

This study has been published in *Acta Biomaterialia*, 2018, S. Kim, Z.-K. Cui, P. Kim, L. Jung, and M. Lee: Design of hydrogels to stabilize and enhance bone morphogenetic protein activity by heparin mimetics.

5.7. Future Directions

Although heparin mimetic sulfonated molecules enhanced BMP-2 bioactivity by protecting the protein from therapeutically relevant stressors, the role of sulfonated molecules in BMP-2

bioactivity was not fully explored. Heparin is known to enhance BMP-2 signaling by enhancing binding of BMP-2 to its receptors and also inhibiting its natural antagonist such as noggin (Figure 5-14). Further study will investigate whether the sulfonated molecules are able to enhance BMP-2 signaling as heparin does.

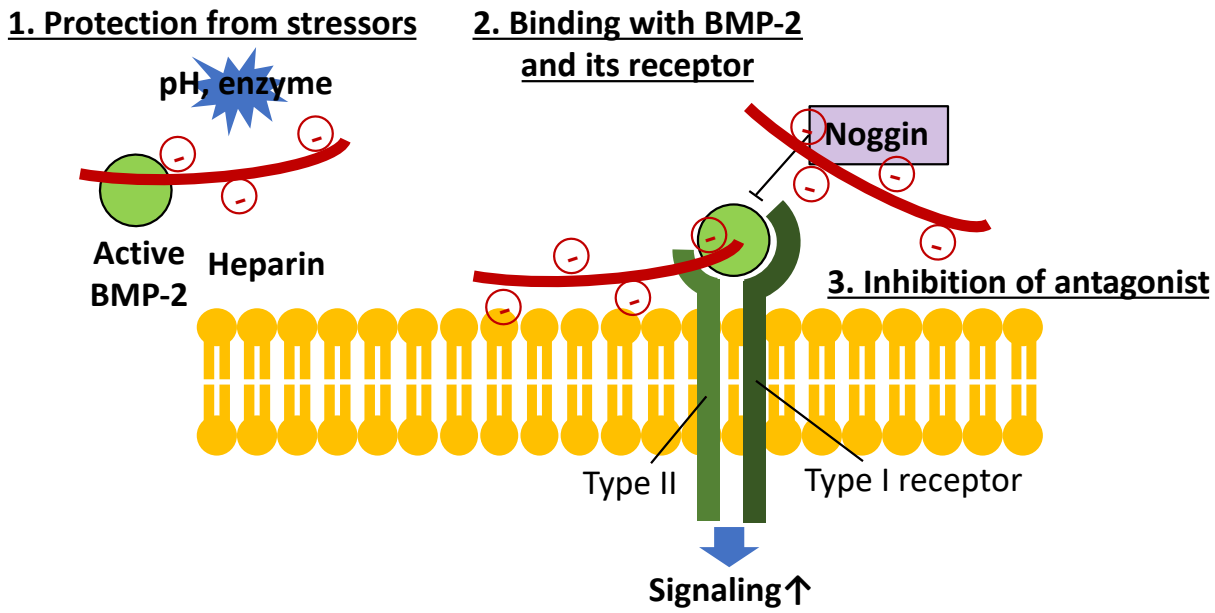

Figure 5-14. Mechanism of heparin enhancing BMP-2 bioactivity. 1. Protecting effect from stressed environment. 2. Affinity binding with BMP-2 and its receptors. 3. Inhibition of BMP-2 antagonist, noggin, by binding with it.

Aim 1: To investigate whether synthetic heparin mimetic enhances BMP-2 bioactivity.

Rationale: Heparin has a high binding affinity to growth factors such as BMP-2[80, 81] or basic fibroblast growth factor-2 (FGF-2) and controls those bioactivities. Stabilization of growth factor–receptor interactions were primarily studied with FGF-2. Heparin builds a stable trimolecular complex with FGF-2 and its receptors to stabilize FGF dimers as well as promote receptor dimers[101-103]. Also, heparin has a stimulatory role to form BMP-2 signaling complexes by

recruiting type II receptor subunits[94]. In this aim, it will be studied whether synthetic heparin mimetic enhances BMP-2 bioactivity through stimulating its binding with receptors.

Hypothesis: Synthetic heparin mimetic will enhance BMP-2 signaling by increasing its binding with receptors.

A. To investigate the effect of sulfonated molecules on BMP-2 receptor expression.
B. To investigate the effect of sulfonated molecules on binding of BMP-2 and its receptors complex.

Aim 2: To investigate whether synthetic heparin mimetic suppresses noggin bioactivity.

Rationale: Heparin also binds to noggin, a well-known BMP-2 antagonist, and manages its activity[90, 240]. In this aim, it will be investigated whether synthetic heparin mimetic will enhance BMP-2 signaling through binding with noggin.

Hypothesis: Synthetic heparin mimetics will enhance BMP-2 signaling by binding with noggin.

A. To investigate the effect of sulfonated molecules on noggin bioactivity.
B. To investigate the effect of sulfonated molecules in noggin suppressed model.

Chapter 6. Conclusions

We developed a new chitosan-based hydrogel system which can support proliferation and differentiation of the encapsulated cells by mimicking native extracellular microenvironments, providing tunable degradation, and stabilizing bioactivity of growth factors. The studies in Chapter 2-5 suggest the great potentials of a newly developed hydrogel platform for tissue engineering application. Further investigation is required to develop more reliable system to support prolonged release of growth factors or deliver other similar recombinant or native proteins.

Although the incorporation of heparin mimetic sulfonated molecules into chitosan hydrogel could successfully decrease the burst release of BMP-2 loaded in the hydrogel, the release profile reached a plateau after 24h. We already developed a chitosan hydrogel platform with tunable degradability via lysozyme functionalization. Future study will test whether this system can continue to release the loaded BMP-2 as hydrogel degraded. Sulfonated molecules were physically incorporated in the hydrogel by simple mixing, but the molecules can be easily affected and dissociated in an *in vivo* environment. Further study of stable incorporation by chemical conjugation will be needed to achieve more reliable prolonged system.

Heparin mimetic sulfonated molecules were effective to deliver recombinant BMP-2 in chitosan hydrogel. Further study will investigate the ability of this system to deliver other heparin-binding proteins such as transforming growth factor beta (TGF-β) or vascular endothelial growth factor (VEGF). The heparin mimicking hydrogel surface was also effective to sequester and stabilize endogenous BMP-2 secreted by the encapsulated cells. This system may be useful as a hydrogel carrier for currently available bone graft materials and enhance bioactivity of native

BMPs presented in bone matrix. Successful completion of this study will identify a new strategy to improve clinical efficacy of current bone therapeutics for accelerated bone repair.

BIBLIOGRAPHY

[1] J. Elisseeff, C. Puleo, F. Yang, B. Sharma, Advances in skeletal tissue engineering with hydrogels, Orthod Craniofac Res 8(3) (2005) 150-61.

[2] J.-B. Park, The use of hydrogels in bone-tissue engineering, Medicina Oral Patologia Oral Y Cirugia Bucal 16(1) (2011) E115-E118.

[3] A.S. Hoffman, Hydrogels for biomedical applications, Adv Drug Deliv Rev 54(1) (2002) 3-12.

[4] M.S. Bae, J.Y. Ohe, J.B. Lee, D.N. Heo, W. Byun, H. Bae, Y.D. Kwon, I.K. Kwon, Photo-cured hyaluronic acid-based hydrogels containing growth and differentiation factor 5 (GDF-5) for bone tissue regeneration, Bone 59 (2014) 189-98.

[5] B.G. Amsden, A. Sukarto, D.K. Knight, S.N. Shapka, Methacrylated glycol chitosan as a photopolymerizable biomaterial, Biomacromolecules 8(12) (2007) 3758-66.

[6] J. Hu, Y. Hou, H. Park, B. Choi, S. Hou, A. Chung, M. Lee, Visible light crosslinkable chitosan hydrogels for tissue engineering, Acta Biomater 8(5) (2012) 1730-8.

[7] P. Hyejin, C. Bogyu, H. Junli, L. Min, Injectable chitosan hyaluronic acid hydrogels for cartilage tissue engineering, Acta Biomaterialia 9(1) (2013) 4779-86.

[8] S. Kim, Z.K. Cui, J.B. Fan, A. Fartash, T.L. Aghaloo, M. Lee, Photocrosslinkable Chitosan Hydrogels Functionalized with the RGD Peptide and Phosphoserine to Enhance Osteogenesis, Journal of Materials Chemistry B 4(31) (2016) 5289-5298.

[9] Z.-K. Cui, J. Fan, S. Kim, O. Bezouglaia, A. Fartash, B.M. Wu, T. Aghaloo, M. Lee, Delivery of siRNA via cationic Sterosomes to enhance osteogenic differentiation of mesenchymal stem cells, Journal of Controlled Release 217 (2015) 42-52.

[10] C. Arakawa, R. Ng, S. Tan, S. Kim, B. Wu, M. Lee, Photopolymerizable Chitosan-Collagen Hydrogels for Bone Tissue Engineering, J Tissue Eng Regen Med 11(1) (2017) 164-174.

[11] J. Taipale, J. Keski-Oja, Growth factors in the extracellular matrix, FASEB J 11(1) (1997) 51-9.

[12] T.E. Hardingham, A.J. Fosang, Proteoglycans: many forms and many functions, FASEB J 6(3) (1992) 861-70.

[13] M. Mizuno, M. Shindo, D. Kobayashi, E. Tsuruga, A. Amemiya, Y. Kuboki, Osteogenesis by bone marrow stromal cells maintained on type I collagen matrix gels in vivo, Bone 20(2) (1997) 101-7.
[14] S.L. Schor, Cell proliferation and migration on collagen substrata in vitro, J Cell Sci 41 (1980) 159-75.
[15] T.E. Kruger, A.H. Miller, J. Wang, Collagen Scaffolds in Bone Sialoprotein-Mediated Bone Regeneration, Scientific World Journal (2013).
[16] A.M. Ferreira, P. Gentile, V. Chiono, G. Ciardelli, Collagen for bone tissue regeneration, Acta Biomaterialia 8(9) (2012) 3191-3200.
[17] S. Ibusuki, G.J. Halbesma, M.A. Randolph, R.W. Redmond, I.E. Kochevar, T.J. Gill, Photochemically cross-linked collagen gels as three-dimensional scaffolds for tissue engineering, Tissue Engineering 13(8) (2007) 1995-2001.
[18] H. Hosseinkhani, M. Hosseinkhani, F. Tian, H. Kobayashi, Y. Tabata, Bone regeneration on a collagen sponge self-assembled peptide-amphiphile nanofiber hybrid scaffold (Retracted article. See vol. 21, pg. 2777, 2015), Tissue Engineering 13(1) (2007) 11-19.
[19] P. Schaffner, M.M. Dard, Structure and function of RGD peptides involved in bone biology, Cellular and Molecular Life Sciences 60(1) (2003) 119-132.
[20] R. Visser, P.M. Arrabal, L. Santos-Ruiz, R. Fernandez-Barranco, J. Becerra, M. Cifuentes, A Collagen-Targeted Biomimetic RGD Peptide to Promote Osteogenesis, Tissue Engineering Part A 20(1-2) (2014) 34-44.
[21] N.R. Gandavarapu, P.D. Mariner, M.P. Schwartz, K.S. Anseth, Extracellular matrix protein adsorption to phosphate-functionalized gels from serum promotes osteogenic differentiation of human mesenchymal stem cells, Acta Biomaterialia 9(1) (2013) 4525-4534.
[22] M.C. Porte-Durrieu, F. Guillemot, S. Pallu, C. Labrugere, B. Brouillaud, R. Bareille, J. Amedee, N. Barthe, M. Dard, C. Baquey, Cyclo-(DfKRG) peptide grafting onto Ti-6Al-4V: physical characterization and interest towards human osteoprogenitor cells adhesion, Biomaterials 25(19) (2004) 4837-4846.
[23] Y. Bala, D. Farlay, G. Boivin, Bone mineralization: from tissue to crystal in normal and pathological contexts, Osteoporosis International 24(8) (2013) 2153-2166.

[24] D.S.W. Benoit, M.P. Schwartz, A.R. Durney, K.S. Anseth, Small functional groups for controlled differentiation of hydrogel-encapsulated human mesenchymal stem cells, Nature Materials 7(10) (2008) 816-823.
[25] D.S.W. Benoit, S.D. Collins, K.S. Anseth, Multifunctional hydrogels that promote osteogenic human mesenchymal stem cell differentiation through stimulation and sequestering of bone morphogenic protein 2, Advanced Functional Materials 17(13) (2007) 2085-2093.
[26] B.M. Watson, T.N. Vo, A.M. Tatara, S.R. Shah, D.W. Scott, P.S. Engel, A.G. Mikos, Biodegradable, phosphate-containing, dual-gelling macromers for cellular delivery in bone tissue engineering, Biomaterials 67 (2015) 286-96.
[27] Y. Wang, T. Azaïs, M. Robin, A. Vallée, C. Catania, P. Legriel, G. Pehau-Arnaudet, F. Babonneau, M.M. Giraud-Guille, N. Nassif, The predominant role of collagen in the nucleation, growth, structure and orientation of bone apatite, Nat Mater 11(8) (2012) 724-33.
[28] M. Guvendiren, J.A. Burdick, Engineering synthetic hydrogel microenvironments to instruct stem cells, Curr Opin Biotechnol 24(5) (2013) 841-6.
[29] B. Trappmann, B.M. Baker, W.J. Polacheck, C.K. Choi, J.A. Burdick, C.S. Chen, Matrix degradability controls multicellularity of 3D cell migration, Nat Commun 8(1) (2017) 371.
[30] N. Huebsch, P.R. Arany, A.S. Mao, D. Shvartsman, O.A. Ali, S.A. Bencherif, J. Rivera-Feliciano, D.J. Mooney, Harnessing traction-mediated manipulation of the cell/matrix interface to control stem-cell fate, Nat Mater 9(6) (2010) 518-26.
[31] A.J. Engler, S. Sen, H.L. Sweeney, D.E. Discher, Matrix elasticity directs stem cell lineage specification, Cell 126(4) (2006) 677-89.
[32] R.J. Pelham, Y. Wang, Cell locomotion and focal adhesions are regulated by substrate flexibility, Proc Natl Acad Sci U S A 94(25) (1997) 13661-5.
[33] S. Khetan, M. Guvendiren, W.R. Legant, D.M. Cohen, C.S. Chen, J.A. Burdick, Degradation-mediated cellular traction directs stem cell fate in covalently crosslinked three-dimensional hydrogels, Nat Mater 12(5) (2013) 458-65.
[34] N. Huebsch, E. Lippens, K. Lee, M. Mehta, S.T. Koshy, M.C. Darnell, R.M. Desai, C.M. Madl, M. Xu, X. Zhao, O. Chaudhuri, C. Verbeke, W.S. Kim, K. Alim, A. Mammoto, D.E. Ingber, G.N. Duda, D.J. Mooney, Matrix elasticity of void-forming hydrogels controls transplanted-stem-cell-mediated bone formation, Nat Mater 14(12) (2015) 1269-77.

[35] T. Mammoto, A. Mammoto, Y.S. Torisawa, T. Tat, A. Gibbs, R. Derda, R. Mannix, M. de Bruijn, C.W. Yung, D. Huh, D.E. Ingber, Mechanochemical control of mesenchymal condensation and embryonic tooth organ formation, Dev Cell 21(4) (2011) 758-69.
[36] M.W. Tibbitt, C.B. Rodell, J.A. Burdick, K.S. Anseth, Progress in material design for biomedical applications, Proc Natl Acad Sci U S A 112(47) (2015) 14444-51.
[37] S.R. Caliari, J.A. Burdick, A practical guide to hydrogels for cell culture, Nat Methods 13(5) (2016) 405-14.
[38] A.T. Metters, K.S. Anseth, C.N. Bowman, Fundamental studies of biodegradable hydrogels as cartilage replacement materials, Biomed Sci Instrum 35 (1999) 33-8.
[39] K.S. Anseth, A.T. Metters, S.J. Bryant, P.J. Martens, J.H. Elisseeff, C.N. Bowman, In situ forming degradable networks and their application in tissue engineering and drug delivery, J Control Release 78(1-3) (2002) 199-209.
[40] S. Jo, H. Shin, A.G. Mikos, Modification of oligo(poly(ethylene glycol) fumarate) macromer with a GRGD peptide for the preparation of functionalized polymer networks, Biomacromolecules 2(1) (2001) 255-61.
[41] S. Sahoo, C. Chung, S. Khetan, J.A. Burdick, Hydrolytically degradable hyaluronic acid hydrogels with controlled temporal structures, Biomacromolecules 9(4) (2008) 1088-92.
[42] B.V. Sridhar, J.L. Brock, J.S. Silver, J.L. Leight, M.A. Randolph, K.S. Anseth, Development of a cellularly degradable PEG hydrogel to promote articular cartilage extracellular matrix deposition, Adv Healthc Mater 4(5) (2015) 702-13.
[43] C.B. Forsyth, A. Cole, G. Murphy, J.L. Bienias, H.J. Im, R.F. Loeser, Increased matrix metalloproteinase-13 production with aging by human articular chondrocytes in response to catabolic stimuli, J Gerontol A Biol Sci Med Sci 60(9) (2005) 1118-24.
[44] J. Hu, Y. Quan, Y. Lai, Z. Zheng, Z. Hu, X. Wang, T. Dai, Q. Zhang, Y. Cheng, A smart aminoglycoside hydrogel with tunable gel degradation, on-demand drug release, and high antibacterial activity, J Control Release 247 (2017) 145-152.
[45] O. Veiseh, J.C. Doloff, M. Ma, A.J. Vegas, H.H. Tam, A.R. Bader, J. Li, E. Langan, J. Wyckoff, W.S. Loo, S. Jhunjhunwala, A. Chiu, S. Siebert, K. Tang, J. Hollister-Lock, S. Aresta-Dasilva, M. Bochenek, J. Mendoza-Elias, Y. Wang, M. Qi, D.M. Lavin, M. Chen, N. Dholakia, R. Thakrar, I. Lacík, G.C. Weir, J. Oberholzer, D.L. Greiner, R. Langer, D.G. Anderson, Size- and

shape-dependent foreign body immune response to materials implanted in rodents and non-human primates, Nat Mater 14(6) (2015) 643-51.
[46] M.D. Hoffman, A.H. Van Hove, D.S. Benoit, Degradable hydrogels for spatiotemporal control of mesenchymal stem cells localized at decellularized bone allografts, Acta Biomater 10(8) (2014) 3431-41.
[47] D.S. Benoit, A.R. Durney, K.S. Anseth, Manipulations in hydrogel degradation behavior enhance osteoblast function and mineralized tissue formation, Tissue Eng 12(6) (2006) 1663-73.
[48] S.C. Skaalure, S. Chu, S.J. Bryant, An enzyme-sensitive PEG hydrogel based on aggrecan catabolism for cartilage tissue engineering, Adv Healthc Mater 4(3) (2015) 420-31.
[49] A.S. Gobin, J.L. West, Cell migration through defined, synthetic ECM analogs, FASEB J 16(7) (2002) 751-3.
[50] R.J. Wade, E.J. Bassin, C.B. Rodell, J.A. Burdick, Protease-degradable electrospun fibrous hydrogels, Nat Commun 6 (2015) 6639.
[51] J.L. Leight, E.Y. Tokuda, C.E. Jones, A.J. Lin, K.S. Anseth, Multifunctional bioscaffolds for 3D culture of melanoma cells reveal increased MMP activity and migration with BRAF kinase inhibition, Proc Natl Acad Sci U S A 112(17) (2015) 5366-71.
[52] K. Tomihata, Y. Ikada, In vitro and in vivo degradation of films of chitin and its deacetylated derivatives, Biomaterials 18(7) (1997) 567-75.
[53] H.S. Chou, M. Larsson, M.H. Hsiao, Y.C. Chen, M. Röding, M. Nydén, D.M. Liu, Injectable insulin-lysozyme-loaded nanogels with enzymatically-controlled degradation and release for basal insulin treatment: In vitro characterization and in vivo observation, J Control Release 224 (2016) 33-42.
[54] A.W. James, G. LaChaud, J. Shen, G. Asatrian, V. Nguyen, X. Zhang, K. Ting, C. Soo, A Review of the Clinical Side Effects of Bone Morphogenetic Protein-2, Tissue Eng Part B Rev 22(4) (2016) 284-97.
[55] J.O. Hollinger, J.M. Schmitt, D.C. Buck, R. Shannon, S.P. Joh, H.D. Zegzula, J. Wozney, Recombinant human bone morphogenetic protein-2 and collagen for bone regeneration, Journal of Biomedical Materials Research 43(4) (1998) 356-364.
[56] J.A. Rihn, R. Patel, J. Makda, J. Hong, D.G. Anderson, A.R. Vaccaro, A.S. Hilibrand, T.J. Albert, Complications associated with single-level transforaminal lumbar interbody fusion, Spine Journal 9(8) (2009) 623-629.

[57] J.K. Burkus, E.E. Transfeldt, S.H. Kitchel, R.G. Watkins, R.A. Balderston, Clinical and radiographic outcomes of anterior lumbar interbody fusion using recombinant human bone morphogenetic protein-2, Spine 27(21) (2002) 2396-2408.
[58] M. Yamazaki, H. Fukushima, M. Shin, T. Katagiri, T. Doi, T. Takahashi, E. Jimi, Tumor Necrosis Factor alpha Represses Bone Morphogenetic Protein (BMP) Signaling by Interfering with the DNA Binding of Smads through the Activation of NF-kappa B, Journal of Biological Chemistry 284(51) (2009) 35987-35995.
[59] Q. Kang, W.-X. Song, Q. Luo, N. Tang, J. Luo, X. Luo, J. Chen, Y. Bi, B.-C. He, J.K. Park, W. Jiang, Y. Tang, J. Huang, Y. Su, G.-H. Zhu, Y. He, H. Yin, Z. Hu, Y. Wang, L. Chen, G.-W. Zuo, X. Pan, J. Shen, T. Vokes, R.R. Reid, R.C. Haydon, H.H. Luu, T.-C. He, A Comprehensive Analysis of the Dual Roles of BMPs in Regulating Adipogenic and Osteogenic Differentiation of Mesenchymal Progenitor Cells, Stem Cells and Development 18(4) (2009) 545-U33.
[60] S.D. Boden, T.A. Zdeblick, H.S. Sandhu, S.E. Heim, The use of rhBMP-2 in interbody fusion cages - Definitive evidence of osteoinduction in humans: A preliminary report, Spine 25(3) (2000) 376-381.
[61] S.D. Boden, J. Kang, H. Sandhu, J.G. Heller, Use of recombinant human bone morphogenetic protein-2 to achieve posterolateral lumbar spine fusion in humans - A prospective, randomized clinical pilot trial - 2002 Volvo Award in clinical studies, Spine 27(23) (2002) 2662-2673.
[62] W.F. McKay, S.M. Peckham, J.M. Badura, A comprehensive clinical review of recombinant human bone morphogenetic protein-2 (INFUSE (R) Bone Graft), International Orthopaedics 31(6) (2007) 729-734.
[63] K. Itoh, N. Udagawa, T. Katagiri, S. Iemura, N. Ueno, H. Yasuda, K. Higashio, J.M.W. Quinn, M.T. Gillespie, T.J. Martin, T. Suda, N. Takahashi, Bone morphogenetic protein 2 stimulates osteoclast differentiation and survival supported by receptor activator of nuclear factor-kappa B ligand, Endocrinology 142(8) (2001) 3656-3662.
[64] M. Hori, H. Sawai, Y. Tsuji, H. Okamura, K. Koyama, Bone morphogenetic protein-2 counterregulates interleukin-18 mRNA and protein in MC3T3-E1 mouse osteoblastic cells, Connective Tissue Research 47(3) (2006) 124-132.
[65] E.J. Carragee, E.L. Hurwitz, B.K. Weiner, A critical review of recombinant human bone morphogenetic protein-2 trials in spinal surgery: emerging safety concerns and lessons learned, Spine Journal 11(6) (2011) 471-491.

[66] R. Aryal, X.-p. Chen, C. Fang, Y.-c. Hu, Bone Morphogenetic Protein-2 and Vascular Endothelial Growth Factor in Bone Tissue Regeneration: New Insight and Perspectives, Orthopaedic Surgery 6(3) (2014) 171-178.
[67] W.R. Michael, W.R. King, M.D. Francis, EFFECTIVENESS OF DIPHOSPHONATES IN PREVENTING OSTEOPOROSIS OF DISUSE IN RAT, Clinical Orthopaedics and Related Research (78) (1971) 271-&.
[68] P.D. Saville, R. Heaney, TREATMENT OF OSTEO POROSIS WITH DI PHOSPHONATES, Seminars in Drug Treatment 2(1) (1972) 47-50.
[69] K.-B. Lee, C.E. Taghavi, K.-J. Song, C. Sintuu, J.H. Yoo, G. Keorochana, S.-T. Tzeng, Z. Fei, J.-C. Liao, J.C. Wang, Inflammatory Characteristics of rhBMP-2 In Vitro and in an In Vivo Rodent Model, Spine 36(3) (2011) E149-E154.
[70] C. Xiong, M.D. Daubs, S.R. Montgomery, B. Aghdasi, H. Inoue, H. Tian, A. Suzuki, Y. Tan, T. Hayashi, M. Ruangchainikom, T. Chai, M. Corey, J.C. Wang, BMP-2 Adverse Reactions Treated With Human Dose Equivalent Dexamethasone in a Rodent Model of Soft-Tissue Inflammation, Spine 38(19) (2013) 1640-1647.
[71] R.R. Chen, D.J. Mooney, Polymeric growth factor delivery strategies for tissue engineering, Pharmaceutical Research 20(8) (2003) 1103-1112.
[72] K. Saito, I. Konishi, M. Nishiguchi, T. Hoshino, T. Fujiwara, Amelogenin binds to both heparan sulfate and bone morphogenetic protein 2 and pharmacologically suppresses the effect of noggin, Bone 43(2) (2008) 371-376.
[73] M. Geiger, R.H. Li, W. Friess, Collagen sponges for bone regeneration with rhBMP-2, Advanced Drug Delivery Reviews 55(12) (2003) 1613-1629.
[74] Z.S. Haidar, R.C. Hamdy, M. Tabrizian, Delivery of recombinant bone morphogenetic proteins for bone regeneration and repair. Part B: Delivery systems for BMPs in orthopaedic and craniofacial tissue engineering, Biotechnology Letters 31(12) (2009) 1825-1835.
[75] B. Kwon, L.G. Jenis, Carrier materials for spinal fusion, The spine journal : official journal of the North American Spine Society 5(6 Suppl) (2005) 224S-230S.
[76] H. Seeherman, J.M. Wozney, Delivery of bone morphogenetic proteins for orthopedic tissue regeneration, Cytokine & Growth Factor Reviews 16(3) (2005) 329-345.

[77] W.G. De Long, Jr., T.A. Einhorn, K. Koval, M. McKee, W. Smith, R. Sanders, T. Watson, Bone, grafts and bone graft substitutes in orthopedic trauma surgery - A critical analysis, Journal of Bone and Joint Surgery-American Volume 89A(3) (2007) 649-658.
[78] R.J. Sola, K. Griebenow, Effects of Glycosylation on the Stability of Protein Pharmaceuticals, Journal of Pharmaceutical Sciences 98(4) (2009) 1223-1245.
[79] W.H. Burgess, T. Maciag, THE HEPARIN-BINDING (FIBROBLAST) GROWTH-FACTOR FAMILY OF PROTEINS, Annual Review of Biochemistry 58 (1989) 575-606.
[80] C.C. Rider, Heparin/heparan sulphate binding in the TGF-beta cytokine superfamily, Biochemical Society Transactions 34 (2006) 458-460.
[81] R. Ruppert, E. Hoffmann, W. Sebald, Human bone morphogenetic protein 2 contains a heparin-binding site which modifies its biological activity, European Journal of Biochemistry 237(1) (1996) 295-302.
[82] K. Miyazono, K. Kusanagi, H. Inoue, Divergence and convergence of TGF-beta/BMP signaling, J Cell Physiol 187(3) (2001) 265-76.
[83] K. Miyazono, Signal transduction by bone morphogenetic protein receptors: functional roles of Smad proteins, Bone 25(1) (1999) 91-3.
[84] J. Schlessinger, I. Lax, M. Lemmon, Regulation of growth factor activation by proteoglycans: what is the role of the low affinity receptors?, Cell 83(3) (1995) 357-60.
[85] T. Takada, T. Katagiri, M. Ifuku, N. Morimura, M. Kobayashi, K. Hasegawa, A. Ogamo, R. Kamijo, Sulfated polysaccharides enhance the biological activities of bone morphogenetic proteins, J Biol Chem 278(44) (2003) 43229-35.
[86] A. Yayon, M. Klagsbrun, J.D. Esko, P. Leder, D.M. Ornitz, Cell surface, heparin-like molecules are required for binding of basic fibroblast growth factor to its high affinity receptor, Cell 64(4) (1991) 841-8.
[87] A.C. Rapraeger, A. Krufka, B.B. Olwin, Requirement of heparan sulfate for bFGF-mediated fibroblast growth and myoblast differentiation, Science 252(5013) (1991) 1705-8.
[88] B. Ohkawara, S. Iemura, P. ten Dijke, N. Ueno, Action range of BMP is defined by its N-terminal basic amino acid core, Curr Biol 12(3) (2002) 205-9.
[89] N.S. Gandhi, R.L. Mancera, The structure of glycosaminoglycans and their interactions with proteins, Chem Biol Drug Des 72(6) (2008) 455-82.

[90] J. Groppe, J. Greenwald, E. Wiater, J. Rodriguez-Leon, A.N. Economides, W. Kwiatkowski, M. Affolter, W.W. Vale, J.C. Izpisua Belmonte, S. Choe, Structural basis of BMP signalling inhibition by the cystine knot protein Noggin, Nature 420(6916) (2002) 636-42.
[91] S.A. Khan, M.S. Nelson, C. Pan, P.M. Gaffney, P. Gupta, Endogenous heparan sulfate and heparin modulate bone morphogenetic protein-4 signaling and activity, Am J Physiol Cell Physiol 294(6) (2008) C1387-97.
[92] D.S. Bramono, S. Murali, B. Rai, L. Ling, W.T. Poh, Z.X. Lim, G.S. Stein, V. Nurcombe, A.J. van Wijnen, S.M. Cool, Bone marrow-derived heparan sulfate potentiates the osteogenic activity of bone morphogenetic protein-2 (BMP-2), Bone 50(4) (2012) 954-64.
[93] X. Jiao, P.C. Billings, M.P. O'Connell, F.S. Kaplan, E.M. Shore, D.L. Glaser, Heparan sulfate proteoglycans (HSPGs) modulate BMP2 osteogenic bioactivity in C2C12 cells, J Biol Chem 282(2) (2007) 1080-6.
[94] W.J. Kuo, M.A. Digman, A.D. Lander, Heparan sulfate acts as a bone morphogenetic protein coreceptor by facilitating ligand-induced receptor hetero-oligomerization, Mol Biol Cell 21(22) (2010) 4028-41.
[95] J. Folkman, M. Klagsbrun, Vascular physiology. A family of angiogenic peptides, Nature 329(6141) (1987) 671-2.
[96] Y. Shing, J. Folkman, R. Sullivan, C. Butterfield, J. Murray, M. Klagsbrun, Heparin affinity: purification of a tumor-derived capillary endothelial cell growth factor, Science 223(4642) (1984) 1296-9.
[97] D. Gospodarowicz, J. Cheng, Heparin protects basic and acidic FGF from inactivation, J Cell Physiol 128(3) (1986) 475-84.
[98] S.R. Coughlin, P.J. Barr, L.S. Cousens, L.J. Fretto, L.T. Williams, Acidic and basic fibroblast growth factors stimulate tyrosine kinase activity in vivo, J Biol Chem 263(2) (1988) 988-93.
[99] D. Moscatelli, Metabolism of receptor-bound and matrix-bound basic fibroblast growth factor by bovine capillary endothelial cells, J Cell Biol 107(2) (1988) 753-9.
[100] D. Moscatelli, High and low affinity binding sites for basic fibroblast growth factor on cultured cells: absence of a role for low affinity binding in the stimulation of plasminogen activator production by bovine capillary endothelial cells, J Cell Physiol 131(1) (1987) 123-30.

[101] D.M. Ornitz, A. Yayon, J.G. Flanagan, C.M. Svahn, E. Levi, P. Leder, Heparin is required for cell-free binding of basic fibroblast growth factor to a soluble receptor and for mitogenesis in whole cells, Mol Cell Biol 12(1) (1992) 240-7.
[102] B.M. Loo, J. Kreuger, M. Jalkanen, U. Lindahl, M. Salmivirta, Binding of heparin/heparan sulfate to fibroblast growth factor receptor 4, J Biol Chem 276(20) (2001) 16868-76.
[103] A. Baird, D. Schubert, N. Ling, R. Guillemin, Receptor- and heparin-binding domains of basic fibroblast growth factor, Proc Natl Acad Sci U S A 85(7) (1988) 2324-8.
[104] G. Gao, M. Goldfarb, Heparin can activate a receptor tyrosine kinase, EMBO J 14(10) (1995) 2183-90.
[105] T.H. Nguyen, S.H. Kim, C.G. Decker, D.Y. Wong, J.A. Loo, H.D. Maynard, A heparin-mimicking polymer conjugate stabilizes basic fibroblast growth factor, Nature Chemistry 5(3) (2013) 221-227.
[106] S.J. Paluck, T.H. Nguyen, J.P. Lee, H.D. Maynard, A Heparin-Mimicking Block Copolymer Both Stabilizes and Increases the Activity of Fibroblast Growth Factor 2 (FGF2), Biomacromolecules 17(10) (2016) 3386-3395.
[107] S. Liekens, D. Leali, J. Neyts, R. Esnouf, M. Rusnati, P. Dell'Era, P.C. Maudgal, E. De Clercq, M. Presta, Modulation of fibroblast growth factor-2 receptor binding, signaling, and mitogenic activity by heparin-mimicking polysulfonated compounds, Molecular Pharmacology 56(1) (1999) 204-213.
[108] L. Yu, J. Ding, Injectable hydrogels as unique biomedical materials, Chemical Society Reviews 37(8) (2008) 1473-1481.
[109] S.R. Van Tomme, G. Storm, W.E. Hennink, In situ gelling hydrogels for pharmaceutical and biomedical applications, International Journal of Pharmaceutics 355(1-2) (2008) 1-18.
[110] H. Junli, H. Yaping, P. Hyejin, C. Bogyu, H. Siying, A. Chung, L. Min, Visible light crosslinkable chitosan hydrogels for tissue engineering, Acta Biomaterialia 8(5) (2012) 1730-8.
[111] K.T. Nguyen, J.L. West, Photopolymerizable hydrogels for tissue engineering applications, Biomaterials 23(22) (2002) 4307-4314.
[112] R. Censi, T. Vermonden, M.J. van Steenbergen, H. Deschout, K. Braeckmans, S.C. De Smedt, C.F. van Nostrum, P. di Martino, W.E. Hennink, Photopolymerized thermosensitive hydrogels for tailorable diffusion-controlled protein delivery, Journal of Controlled Release 140(3) (2009) 230-236.

[113] A. Hoshikawa, Y. Nakayama, T. Matsuda, H. Oda, K. Nakamura, K. Mabuchi, Encapsulation of chondrocytes in photopolymerizable styrenated gelatin for cartilage tissue engineering, Tissue Engineering 12(8) (2006) 2333-2341.
[114] C.S. Bahney, T.J. Lujan, C.W. Hsu, M. Bottlang, J.L. West, B. Johnstone, VISIBLE LIGHT PHOTOINITIATION OF MESENCHYMAL STEM CELL-LADEN BIORESPONSIVE HYDROGELS, European Cells & Materials 22 (2011) 43-55.
[115] S.B. Anderson, C.-C. Lin, D.V. Kuntzler, K.S. Anseth, The performance of human mesenchymal stem cells encapsulated in cell-degradable polymer-peptide hydrogels, Biomaterials 32(14) (2011) 3564-3574.
[116] C. Bogyu, K. Soyon, B. Lin, L. Kevin, O. Bezouglaia, K. Jinku, D. Evseenko, T. Aghaloo, L. Min, Visible-light-initiated hydrogels preserving cartilage extracellular signaling for inducing chondrogenesis of mesenchymal stem cells, Acta Biomaterialia 12 (2015) 30-41.
[117] J.R. Xavier, T. Thakur, P. Desai, M.K. Jaiswal, N. Sears, E. Cosgriff-Hernandez, R. Kaunas, A.K. Gaharwar, Bioactive nanoengineered hydrogels for bone tissue engineering: a growth-factor-free approach, ACS Nano 9(3) (2015) 3109-18.
[118] B. Choi, S. Kim, J. Fan, T. Kowalski, F. Petrigliano, D. Evseenko, M. Lee, Covalently conjugated transforming growth factor-beta 1 in modular chitosan hydrogels for the effective treatment of articular cartilage defects, Biomaterials Science 3(5) (2015) 742-752.
[119] J. Kim, B. Lin, S. Kim, B. Choi, D. Evseenko, M. Lee, TGF-beta 1 conjugated chitosan collagen hydrogels induce chondrogenic differentiation of human synovium-derived stem cells, Journal of Biological Engineering 9 (2015).
[120] J.L. Holloway, H. Ma, R. Rai, J.A. Burdick, Modulating hydrogel crosslink density and degradation to control bone morphogenetic protein delivery and in vivo bone formation, J Control Release 191 (2014) 63-70.
[121] B. Choi, Z.-K. Cui, S. Kim, J. Fan, B.M. Wu, M. Lee, Glutamine-chitosan modified calcium phosphate nanoparticles for efficient siRNA delivery and osteogenic differentiation, Journal of Materials Chemistry B 3(31) (2015) 6448-6455.
[122] Z. Lu, B.Z. Doulabi, C. Huang, R.A. Bank, M.N. Helder, Collagen type II enhances chondrogenesis in adipose tissue-derived stem cells by affecting cell shape, Tissue Eng Part A 16(1) (2010) 81-90.

[123] A.Y. Wang, S. Leong, Y.C. Liang, R.C. Huang, C.S. Chen, S.M. Yu, Immobilization of growth factors on collagen scaffolds mediated by polyanionic collagen mimetic peptides and its effect on endothelial cell morphogenesis, Biomacromolecules 9(10) (2008) 2929-36.
[124] C. Arakawa, R. Ng, S. Tan, S. Kim, B. Wu, M. Lee, Photopolymerizable chitosan-collagen hydrogels for bone tissue engineering, J Tissue Eng Regen Med (2014).
[125] B. Choi, S. Kim, B. Lin, B.M. Wu, M. Lee, Cartilaginous Extracellular Matrix-Modified Chitosan Hydrogels for Cartilage Tissue Engineering, ACS Appl Mater Interfaces (2014).
[126] L.W. Fisher, N.S. Fedarko, Six genes expressed in bones and teeth encode the current members of the SIBLING family of proteins, Connective Tissue Research 44 (2003) 33-40.
[127] L. Masi, M.L. Brandi, P.G. Robey, C. Crescioli, J.C. Calvo, P. Bernabei, J.M. Kerr, M. Yanagishita, BIOSYNTHESIS OF BONE SIALOPROTEIN BY A HUMAN OSTEOCLAST-LIKE CELL-LINE (FLG-29.1), Journal of Bone and Mineral Research 10(2) (1995) 187-196.
[128] C.E. Tye, G.K. Hunter, H.A. Goldberg, Identification of the type I collagen-binding domain of bone sialoprotein and characterization of the mechanism of interaction, Journal of Biological Chemistry 280(14) (2005) 13487-13492.
[129] M. Kantlehner, P. Schaffner, D. Finsinger, J. Meyer, A. Jonczyk, B. Diefenbach, B. Nies, G. Holzemann, S.L. Goodman, H. Kessler, Surface coating with cyclic RGD peptides stimulates osteoblast adhesion and proliferation as well as bone formation, Chembiochem 1(2) (2000) 107-114.
[130] B. Choi, S. Kim, B. Lin, B.M. Wu, M. Lee, Cartilaginous Extracellular Matrix-Modified Chitosan Hydrogels for Cartilage Tissue Engineering, ACS Appl Mater Interfaces 6(22) (2014) 20110-20121.
[131] L.C. Baxter, V. Frauchiger, M. Textor, I. ap Gwynn, R.G. Richards, Fibroblast and osteoblast adhesion and morphology on calcium phosphate surfaces, European Cells & Materials 4(Cited March 7, 2003) (2002) 1-17.
[132] J. Lian, CELL BIOLOGY OF MINERALIZED TISSUES - OSTEOBLASTS, Connective Tissue Research 27(2-3) (1992) 135-146.
[133] J.G. Steele, G. Johnson, K.M. McLean, G.J. Beumer, H.J. Griesser, Effect of porosity and surface hydrophilicity on migration of epithelial tissue over synthetic polymer, J Biomed Mater Res 50(4) (2000) 475-82.

[134] R.J. Wade, J.A. Burdick, Engineering ECM signals into biomaterials, Materials Today 15(10) (2012) 454-459.
[135] S.P. Zustiak, J.B. Leach, Hydrolytically degradable poly(ethylene glycol) hydrogel scaffolds with tunable degradation and mechanical properties, Biomacromolecules 11(5) (2010) 1348-57.
[136] A.M. Kloxin, M.W. Tibbitt, K.S. Anseth, Synthesis of photodegradable hydrogels as dynamically tunable cell culture platforms, Nat Protoc 5(12) (2010) 1867-87.
[137] R. Visse, H. Nagase, Matrix metalloproteinases and tissue inhibitors of metalloproteinases: structure, function, and biochemistry, Circ Res 92(8) (2003) 827-39.
[138] J. Hu, G. Zhang, S. Liu, Enzyme-responsive polymeric assemblies, nanoparticles and hydrogels, Chem Soc Rev 41(18) (2012) 5933-49.
[139] S. Wang, S. Guan, J. Xu, W. Li, D. Ge, C. Sun, T. Liu, X. Ma, Neural stem cell proliferation and differentiation in the conductive PEDOT-HA/Cs/Gel scaffold for neural tissue engineering, Biomater Sci 5(10) (2017) 2024-2034.
[140] S.H. Pangburn, P.V. Trescony, J. Heller, Lysozyme degradation of partially deacetylated chitin, its films and hydrogels, Biomaterials 3(2) (1982) 105-8.
[141] V.A. Proctor, F.E. Cunningham, The Chemistry of Lysozyme and Its Use as a Food Preservative and a Pharmaceutical, Crit Rev Food Sci Nutr 26(4) (1988) 359-395.
[142] V.A. Proctor, F.E. Cunningham, The chemistry of lysozyme and its use as a food preservative and a pharmaceutical, Crit Rev Food Sci Nutr 26(4) (1988) 359-95.
[143] A.M. Martins, C.M. Alves, F. Kurtis Kasper, A.G. Mikos, R.L. Reis, Responsive and in situ-forming chitosan scaffolds for bone tissue engineering applications: an overview of the last decade, Journal of Materials Chemistry 20(9) (2010) 1638-1645.
[144] A.M. Martins, R.C. Pereira, I.B. Leonor, H.S. Azevedo, R.L. Reis, Chitosan scaffolds incorporating lysozyme into CaP coatings produced by a biomimetic route: a novel concept for tissue engineering combining a self-regulated degradation system with in situ pore formation, Acta Biomater 5(9) (2009) 3328-36.
[145] A.M. Martins, Q.P. Pham, P.B. Malafaya, R.M. Raphael, F.K. Kasper, R.L. Reis, A.G. Mikos, Natural stimulus responsive scaffolds/cells for bone tissue engineering: influence of lysozyme upon scaffold degradation and osteogenic differentiation of cultured marrow stromal cells induced by CaP coatings, Tissue Eng Part A 15(8) (2009) 1953-63.

[146] Z. Zheng, W. Yin, J.N. Zara, W. Li, J. Kwak, R. Mamidi, M. Lee, R.K. Siu, R. Ngo, J. Wang, D. Carpenter, X. Zhang, B. Wu, K. Ting, C. Soo, The use of BMP-2 coupled - Nanosilver-PLGA composite grafts to induce bone repair in grossly infected segmental defects, Biomaterials 31(35) (2010) 9293-300.
[147] N.M. Ranjha, G. Ayub, S. Naseem, M.T. Ansari, Preparation and characterization of hybrid pH-sensitive hydrogels of chitosan-co-acrylic acid for controlled release of verapamil, J Mater Sci Mater Med 21(10) (2010) 2805-16.
[148] N.A. Peppas, J.Z. Hilt, A. Khademhosseini, R. Langer, Hydrogels in Biology and Medicine: From Molecular Principles to Bionanotechnology, Advanced Materials 18(11) (2006) 1345-1360.
[149] B.G. Amsden, A. Sukarto, D.K. Knight, S.N. Shapka, Methacrylated Glycol Chitosan as a Photopolymerizable Biomaterial, Biomacromolecules 8(12) (2007) 3758-3766.
[150] J. Fan, H. Park, S. Tan, M. Lee, Enhanced osteogenesis of adipose derived stem cells with Noggin suppression and delivery of BMP-2, PLoS One 8(8) (2013) e72474.
[151] J. Fan, C.S. Im, M. Guo, Z.-K. Cui, A. Fartash, S. Kim, N. Patel, O. Bezouglaia, B.M. Wu, C.-Y. Wang, T.L. Aghaloo, M. Lee, Enhanced Osteogenesis of Adipose-Derived Stem Cells by Regulating Bone Morphogenetic Protein Signaling Antagonists and Agonists, Stem Cells Translational Medicine 5(4) (2016) 539-551.
[152] R.A. Muzzarelli, Human enzymatic activities related to the therapeutic administration of chitin derivatives, Cell Mol Life Sci 53(2) (1997) 131-40.
[153] M. Betz, J. H ormansperger, T. Fuchs, U. Kulozik, Swelling behaviour, charge and mesh size of thermal protein hydrogels as influenced by pH during gelation, Soft Matter 8 (2012) 2477-2485.
[154] G.D. Nicodemus, S.J. Bryant, Cell encapsulation in biodegradable hydrogels for tissue engineering applications, Tissue Eng Part B Rev 14(2) (2008) 149-65.
[155] X. Chen, F. Niyonsaba, H. Ushio, D. Okuda, I. Nagaoka, S. Ikeda, K. Okumura, H. Ogawa, Synergistic effect of antibacterial agents human beta-defensins, cathelicidin LL-37 and lysozyme against Staphylococcus aureus and Escherichia coli, J Dermatol Sci 40(2) (2005) 123-32.
[156] J. Heller, S.H. Pangburn, K.V. Roskos, Development of enzymatically degradable protective coatings for use in triggered drug delivery systems: derivatized starch hydrogels, Biomaterials 11(5) (1990) 345-50.

[157] J. Heller, S.Y. Ng, B.K. Fritzinger, K.V. Roskos, Controlled drug release from bioerodible hydrophobic ointments, Biomaterials 11(4) (1990) 235-7.
[158] Q.P. Hou, P.A. De Bank, K.M. Shakesheff, Injectable scaffolds for tissue regeneration, Journal of Materials Chemistry 14(13) (2004) 1915-1923.
[159] X. Zhao, H. Wu, B. Guo, R. Dong, Y. Qiu, P.X. Ma, Antibacterial anti-oxidant electroactive injectable hydrogel as self-healing wound dressing with hemostasis and adhesiveness for cutaneous wound healing, Biomaterials 122 (2017) 34-47.
[160] X. Xu, X. Liu, L. Tan, Z. Cui, X. Yang, S. Zhu, Z. Li, X. Yuan, Y. Zheng, K.W.K. Yeung, P.K. Chu, S. Wu, Controlled-temperature photothermal and oxidative bacteria killing and acceleration of wound healing by polydopamine-assisted Au-hydroxyapatite nanorods, Acta Biomater 77 (2018) 352-364.
[161] R. Dong, X. Zhao, B. Guo, P.X. Ma, Self-Healing Conductive Injectable Hydrogels with Antibacterial Activity as Cell Delivery Carrier for Cardiac Cell Therapy, ACS Appl Mater Interfaces 8(27) (2016) 17138-50.
[162] C. Mao, Y. Xiang, X. Liu, Z. Cui, X. Yang, Z. Li, S. Zhu, Y. Zheng, K.W.K. Yeung, S. Wu, Repeatable Photodynamic Therapy with Triggered Signaling Pathways of Fibroblast Cell Proliferation and Differentiation To Promote Bacteria-Accompanied Wound Healing, ACS Nano 12(2) (2018) 1747-1759.
[163] X. Chen, F. Niyonsaba, H. Ushio, D. Okuda, I. Nagaoka, S. Ikeda, K. Okumura, H. Ogawa, Synergistic Effect of Antibacterial Agents Human Beta-Defensins, Cathelicidin LL-37 and Lysozyme Against Staphylococcus Aureus and Escherichia Coli, J Dermatol Sci 40(2) (2005) 123-132.
[164] T. Wu, C. Wu, S. Fu, L. Wang, C. Yuan, S. Chen, Y. Hu, Integration of lysozyme into chitosan nanoparticles for improving antibacterial activity, Carbohydr Polym 155 (2017) 192-200.
[165] B.K. Tiwari, V.P. Valdramidis, C.P. O'Donnell, K. Muthukumarappan, P. Bourke, P.J. Cullen, Application of natural antimicrobials for food preservation, J Agric Food Chem 57(14) (2009) 5987-6000.
[166] A. Conte, M. Sinigaglia, M.A. Del Nobile, Antimicrobial effectiveness of lysozyme immobilized on polyvinylalcohol-based film against Alicyclobacillus acidoterrestris, J Food Prot 69(4) (2006) 861-5.

[167] J. Duan, S.I. Park, M.A. Daeschel, Y. Zhao, Antimicrobial chitosan-lysozyme (CL) films and coatings for enhancing microbial safety of mozzarella cheese, J Food Sci 72(9) (2007) M355-62.
[168] J.K. Branen, P.M. Davidson, Enhancement of nisin, lysozyme, and monolaurin antimicrobial activities by ethylenediaminetetraacetic acid and lactoferrin, Int J Food Microbiol 90(1) (2004) 63-74.
[169] J.S. Boland, P.M. Davidson, J. Weiss, Enhanced inhibition of Escherichia coli O157:H7 by lysozyme and chelators, J Food Prot 66(10) (2003) 1783-9.
[170] S. Kim, Z.K. Cui, P.J. Kim, L.Y. Jung, M. Lee, Design of hydrogels to stabilize and enhance bone morphogenetic protein activity by heparin mimetics, Acta Biomater (2018).
[171] B. Choi, S. Kim, B. Lin, K. Li, O. Bezouglaia, J. Kim, D. Evseenko, T. Aghaloo, M. Lee, Visible-light-initiated hydrogels preserving cartilage extracellular signaling for inducing chondrogenesis of mesenchymal stem cells, Acta Biomater 12 (2015) 30-41.
[172] J. Duan, S.I. Park, M.A. Daeschel, Y. Zhao, Antimicrobial Chitosan-Lysozyme (CL) Films and Coatings for Enhancing Microbial Safety of Mozzarella Cheese, Journal of Food Science 72(9) (2007) M355-M362.
[173] S.I. Park, M.A. Daeschel, Y. Zhao, Functional Properties of Antimicrobial Lysozyme-Chitosan Composite Films, Journal of Food Science 69(8) (2004) M215-M221.
[174] M.C. Giano, Z. Ibrahim, S.H. Medina, K.A. Sarhane, J.M. Christensen, Y. Yamada, G. Brandacher, J.P. Schneider, Injectable bioadhesive hydrogels with innate antibacterial properties, Nat Commun 5 (2014) 4095.
[175] J.C. Tiller, Antimicrobial Surfaces, in: H.G. Börner, J.-F. Lutz (Eds.), Bioactive Surfaces, Springer Berlin Heidelberg, Berlin, Heidelberg, 2011, pp. 193-217.
[176] S. Kim, Z.K. Cui, B. Koo, J. Zheng, T. Aghaloo, M. Lee, Chitosan-Lysozyme Conjugates for Enzyme-Triggered Hydrogel Degradation in Tissue Engineering Applications, ACS Appl Mater Interfaces (2018).
[177] J. Hu, Y. Hou, H. Park, B. Choi, S. Hou, A. Chung, M. Lee, Visible Light Crosslinkable Chitosan Hydrogels for Tissue Engineering, Acta Biomater 8(5) (2012) 1730-1738.
[178] K. Feng, H. Sun, M.A. Bradley, E.J. Dupler, W.V. Giannobile, P.X. Ma, Novel antibacterial nanofibrous PLLA scaffolds, J Control Release 146(3) (2010) 363-9.

[179] E. Ruoslahti, M.D. Pierschbacher, New perspectives in cell adhesion: RGD and integrins, Science 238(4826) (1987) 491-7.
[180] Q. Chen, M.S. Kinch, T.H. Lin, K. Burridge, R.L. Juliano, Integrin-mediated cell adhesion activates mitogen-activated protein kinases, J Biol Chem 269(43) (1994) 26602-5.
[181] U. Hersel, C. Dahmen, H. Kessler, RGD modified polymers: biomaterials for stimulated cell adhesion and beyond, Biomaterials 24(24) (2003) 4385-415.
[182] S.R. Caliari, S.L. Vega, M. Kwon, E.M. Soulas, J.A. Burdick, Dimensionality and spreading influence MSC YAP/TAZ signaling in hydrogel environments, Biomaterials 103 (2016) 314-323.
[183] S. Khetan, M. Guvendiren, W.R. Legant, D.M. Cohen, C.S. Chen, J.A. Burdick, Degradation-Mediated Cellular Traction Directs Stem Cell Fate in Covalently Crosslinked Three-Dimensional Hydrogels, Nat Mater 12(5) (2013) 458-465.
[184] K.M. Schultz, K.A. Kyburz, K.S. Anseth, Measuring dynamic cell-material interactions and remodeling during 3D human mesenchymal stem cell migration in hydrogels, Proc Natl Acad Sci U S A 112(29) (2015) E3757-64.
[185] B.M. Watson, T.N. Vo, A.M. Tatara, S.R. Shah, D.W. Scott, P.S. Engel, A.G. Mikos, Biodegradable, Phosphate-Containing, Dual-Gelling Macromers for Cellular Delivery in Bone Tissue Engineering, Biomaterials 67 (2015) 286-296.
[186] B.K. Sun, Z. Siprashvili, P.A. Khavari, Advances in skin grafting and treatment of cutaneous wounds, Science 346(6212) (2014) 941-5.
[187] S. Werner, R. Grose, Regulation of wound healing by growth factors and cytokines, Physiol Rev 83(3) (2003) 835-70.
[188] X. Liu, H. Wu, M. Byrne, S. Krane, R. Jaenisch, Type III collagen is crucial for collagen I fibrillogenesis and for normal cardiovascular development, Proc Natl Acad Sci U S A 94(5) (1997) 1852-6.
[189] J.J. Tomasek, G. Gabbiani, B. Hinz, C. Chaponnier, R.A. Brown, Myofibroblasts and mechano-regulation of connective tissue remodelling, Nat Rev Mol Cell Biol 3(5) (2002) 349-63.
[190] S.L. Schor, Cell Proliferation and Migration on Collagen Substrata In Vitro, J Cell Sci 41 (1980) 159-175.
[191] G.D. Nicodemus, S.J. Bryant, Cell Encapsulation in Biodegradable Hydrogels for Tissue Engineering Applications, Tissue Eng Part B Rev 14(2) (2008) 149-165.

[192] L.G. Ovington, The truth about silver, Ostomy Wound Manage 50(9A Suppl) (2004) 1S-10S.
[193] M.I. Hoq, H.R. Ibrahim, Potent antimicrobial action of triclosan-lysozyme complex against skin pathogens mediated through drug-targeted delivery mechanism, Eur J Pharm Sci 42(1-2) (2011) 130-7.
[194] M.I. Hoq, K. Mitsuno, Y. Tsujino, T. Aoki, H.R. Ibrahim, Triclosan-lysozyme complex as novel antimicrobial macromolecule: a new potential of lysozyme as phenolic drug-targeting molecule, Int J Biol Macromol 42(5) (2008) 468-77.
[195] C.C. Blake, D.F. Koenig, G.A. Mair, A.C. North, D.C. Phillips, V.R. Sarma, Structure of hen egg-white lysozyme. A three-dimensional Fourier synthesis at 2 Angstrom resolution, Nature 206(4986) (1965) 757-61.
[196] T.E. Miller, Killing and lysis of gram-negative bacteria through the synergistic effect of hydrogen peroxide, ascorbic acid, and lysozyme, J Bacteriol 98(3) (1969) 949-55.
[197] B. Masschalck, C.W. Michiels, Antimicrobial properties of lysozyme in relation to foodborne vegetative bacteria, Crit Rev Microbiol 29(3) (2003) 191-214.
[198] J.M. Wozney, The bone morphogenetic protein family and osteogenesis, Mol Reprod Dev 32(2) (1992) 160-7.
[199] Y. Okubo, K. Bessho, K. Fujimura, Y. Konishi, K. Kusumoto, Y. Ogawa, T. Iizuka, Osteoinduction by recombinant human bone morphogenetic protein-2 at intramuscular, intermuscular, subcutaneous and intrafatty sites, International Journal of Oral and Maxillofacial Surgery 29(1) (2000) 62-66.
[200] S. Govender, C. Csimma, H.K. Genant, A. Valentin-Opran, Y. Amit, R. Arbel, H. Aro, D. Atar, M. Bishay, M.G. Borner, P. Chiron, P. Choong, J. Cinats, B. Courtenay, R. Feibel, B. Geulette, C. Gravel, N. Haas, M. Raschke, E. Hammacher, D. van der Velde, P. Hardy, M. Holt, C. Josten, R.L. Ketterl, B. Lindeque, G. Lob, H. Mathevon, G. McCoy, D. Marsh, R. Miller, E. Munting, S. Oevre, L. Nordsletten, A. Patel, A. Pohl, W. Rennie, P. Reynders, P.M. Rommens, J. Rondia, W.C. Rossouw, P.J. Daneel, S. Ruff, A. Ruter, S. Santavirta, T.A. Schildhauer, C. Gekle, R. Schnettler, D. Segal, H. Seiler, R.B. Snowdowne, J. Stapert, G. Taglang, R. Verdonk, L. Vogels, A. Weckbach, A. Wentzensen, T. Wisniewski, B.S. Grp, Recombinant human bone morphogenetic protein-2 for treatment of open tibial fractures - A prospective, controlled, randomized study of

four hundred and fifty patients, Journal of Bone and Joint Surgery-American Volume 84A(12) (2002) 2123-2134.
[201] Q. Kang, M.H. Sun, H. Cheng, Y. Peng, A.G. Montag, A.T. Deyrup, W. Jiang, H.H. Luu, J. Luo, J.P. Szatkowski, P. Vanichakarn, J.Y. Park, Y. Li, R.C. Haydon, T.C. He, Characterization of the distinct orthotopic bone-forming activity of 14 BMPs using recombinant adenovirus-mediated gene delivery, Gene Ther 11(17) (2004) 1312-20.
[202] M.C. Manning, D.K. Chou, B.M. Murphy, R.W. Payne, D.S. Katayama, Stability of protein pharmaceuticals: an update, Pharm Res 27(4) (2010) 544-75.
[203] A. Hawe, M. Wiggenhorn, M. van de Weert, J.H. Garbe, H.C. Mahler, W. Jiskoot, Forced degradation of therapeutic proteins, J Pharm Sci 101(3) (2012) 895-913.
[204] M.V. Trivedi, J.S. Laurence, T.J. Siahaan, The role of thiols and disulfides on protein stability, Curr Protein Pept Sci 10(6) (2009) 614-25.
[205] I. El Bialy, W. Jiskoot, M. Reza Nejadnik, Formulation, Delivery and Stability of Bone Morphogenetic Proteins for Effective Bone Regeneration, Pharm Res 34(6) (2017) 1152-1170.
[206] M. Kisiel, M. Ventura, O.P. Oommen, A. George, X.F. Walboomers, J. Hilborn, O.P. Varghese, Critical assessment of rhBMP-2 mediated bone induction: an in vitro and in vivo evaluation, J Control Release 162(3) (2012) 646-53.
[207] L. Luca, M.A. Capelle, G. Machaidze, T. Arvinte, O. Jordan, R. Gurny, Physical instability, aggregation and conformational changes of recombinant human bone morphogenetic protein-2 (rhBMP-2), Int J Pharm 391(1-2) (2010) 48-54.
[208] H. Ohta, S. Wakitani, K. Tensho, H. Horiuchi, S. Wakabayashi, N. Saito, Y. Nakamura, K. Nozaki, Y. Imai, K. Takaoka, The effects of heat on the biological activity of recombinant human bone morphogenetic protein-2, J Bone Miner Metab 23(6) (2005) 420-5.
[209] A.W. James, G. LaChaud, J. Shen, G. Asatrian, V. Nguyen, X.L. Zhang, K. Ting, C. Soo, A Review of the Clinical Side Effects of Bone Morphogenetic Protein-2, Tissue Engineering Part B-Reviews 22(4) (2016) 284-297.
[210] D.A. Wong, A. Kumar, S. Jatana, G. Ghiselli, K. Wong, Neurologic impairment from ectopic bone in the lumbar canal: a potential complication of off-label PLIF/TLIF use of bone morphogenetic protein-2 (BMP-2), Spine Journal 8(6) (2008) 1011-1018.
[211] K. Irie, C. Alpaslan, K. Takahashi, Y. Kondo, N. Izumi, Y. Sakakura, E. Tsuruga, T. Nakajima, S. Ejiri, H. Ozawa, T. Yajima, Osteoclast differentiation in ectopic bone formation

induced by recombinant human bone morphogenetic protein 2 (rhBMP-2), J Bone Miner Metab 21(6) (2003) 363-9.
[212] J.P.A. van den Bergh, C.M. ten Bruggenkate, H.H.J. Groeneveld, E.H. Burger, D.B. Tuinzing, Recombinant human bone morphogenetic protein-7 in maxillary sinus floor elevation surgery in 3 patients compared to autogenous bone grafts - A clinical pilot study, Journal of Clinical Periodontology 27(9) (2000) 627-636.
[213] T.T. Tang, X.L. Xu, K.R. Dai, C.F. Yu, B. Yue, J.R. Lou, Ectopic bone formation of human bone morphogenetic protein-2 gene transfected goat bone marrow-derived mesenchymal stem cells in nude mice, Chin J Traumatol 8(1) (2005) 3-7.
[214] J. Fan, J. Pi-Anfruns, M. Guo, D.C.S. Im, Z.K. Cui, S. Kim, B.M. Wu, T.L. Aghaloo, M. Lee, Small molecule-mediated tribbles homolog 3 promotes bone formation induced by bone morphogenetic protein-2, Sci Rep 7(1) (2017) 7518.
[215] A.R. Poynton, J.M. Lane, Safety profile for the clinical use of bone morphogenetic proteins in the spine, Spine (Phila Pa 1976) 27(16 Suppl 1) (2002) S40-8.
[216] G.S. Schultz, A. Wysocki, Interactions between extracellular matrix and growth factors in wound healing, Wound Repair and Regeneration 17(2) (2009) 153-162.
[217] L. Macri, D. Silverstein, R.A. Clark, Growth factor binding to the pericellular matrix and its importance in tissue engineering, Adv Drug Deliv Rev 59(13) (2007) 1366-81.
[218] I. Capila, R.J. Linhardt, Heparin-protein interactions, Angew Chem Int Ed Engl 41(3) (2002) 391-412.
[219] S.P. Seto, M.E. Casas, J.S. Temenoff, Differentiation of mesenchymal stem cells in heparin-containing hydrogels via coculture with osteoblasts, Cell and Tissue Research 347(3) (2012) 589-601.
[220] S.P. Seto, T. Miller, J.S. Temenoff, Effect of Selective Heparin Desulfation on Preservation of Bone Morphogenetic Protein-2 Bioactivity after Thermal Stress, Bioconjugate Chemistry 26(2) (2015) 286-293.
[221] M. Simann, V. Schneider, S. Le Blanc, J. Dotterweich, V. Zehe, M. Krug, F. Jakob, T. Schilling, N. Schutze, Heparin affects human bone marrow stromal cell fate: Promoting osteogenic and reducing adipogenic differentiation and conversion, Bone 78 (2015) 102-113.
[222] B. Mulloy, M.J. Forster, Conformation and dynamics of heparin and heparan sulfate, Glycobiology 10(11) (2000) 1147-56.

[223] R.J. Linhardt, N.S. Gunay, Production and chemical processing of low molecular weight heparins, Semin Thromb Hemost 25 Suppl 3 (1999) 5-16.
[224] R.J. Linhardt, D. Loganathan, A. al-Hakim, H.M. Wang, J.M. Walenga, D. Hoppensteadt, J. Fareed, Oligosaccharide mapping of low molecular weight heparins: structure and activity differences, J Med Chem 33(6) (1990) 1639-45.
[225] S. Battistelli, A. Genovese, T. Gori, Heparin-induced thrombocytopenia in surgical patients, Am J Surg 199(1) (2010) 43-51.
[226] M. Schindewolf, E. Lindhoff-Last, R.J. Ludwig, W.H. Boehncke, Heparin-induced skin lesions, Lancet 380(9856) (2012) 1867-79.
[227] G. Le Templier, M.A. Rodger, Heparin-induced osteoporosis and pregnancy, Curr Opin Pulm Med 14(5) (2008) 403-7.
[228] F. Mussano, K.J. Lee, P. Zuk, L. Tran, N.A. Cacalano, A. Jewett, S. Carossa, I. Nishimura, Differential effect of ionizing radiation exposure on multipotent and differentiation-restricted bone marrow mesenchymal stem cells, J Cell Biochem 111(2) (2010) 322-32.
[229] Z.K. Cui, S. Kim, J.J. Baljon, M. Doroudgar, M. Lafleur, B.M. Wu, T. Aghaloo, M. Lee, Design and Characterization of a Therapeutic Non-phospholipid Liposomal Nanocarrier with Osteoinductive Characteristics To Promote Bone Formation, ACS Nano (2017).
[230] W.C. Kett, R.I. Osmond, L. Moe, S.E. Skett, B.F. Kinnear, D.R. Coombe, Avidin is a heparin-binding protein. Affinity, specificity and structural analysis, Biochim Biophys Acta 1620(1-3) (2003) 225-34.
[231] M.D. Wood, D. Hunter, S.E. Mackinnon, S.E. Sakiyama-Elbert, Heparin-Binding-Affinity-Based Delivery Systems Releasing Nerve Growth Factor Enhance Sciatic Nerve Regeneration, Journal of Biomaterials Science-Polymer Edition 21(6-7) (2010) 771-787.
[232] I.A. Silver, R.J. Murrills, D.J. Etherington, Microelectrode studies on the acid microenvironment beneath adherent macrophages and osteoclasts, Exp Cell Res 175(2) (1988) 266-76.
[233] A. Teti, Mechanisms of osteoclast-dependent bone formation, Bonekey Rep 2 (2013) 449.
[234] T.J. Sigurdsson, L. Nygaard, D.N. Tatakis, E. Fu, T.J. Turek, L. Jin, J.M. Wozney, U.M.E. Wikesjo, Periodontal repair in dogs: Evaluation of rhBMP-2 carriers, International Journal of Periodontics & Restorative Dentistry 16(6) (1996) 525-537.

[235] E.Y. Chi, S. Krishnan, T.W. Randolph, J.F. Carpenter, Physical stability of proteins in aqueous solution: mechanism and driving forces in nonnative protein aggregation, Pharm Res 20(9) (2003) 1325-36.
[236] A.P. Wohl, H. Troilo, R.F. Collins, C. Baldock, G. Sengle, Extracellular Regulation of Bone Morphogenetic Protein Activity by the Microfibril Component Fibrillin-1, J Biol Chem 291(24) (2016) 12732-46.
[237] G. Bhakta, B. Rai, Z.X.H. Lim, J.H. Hui, G.S. Stein, A.J. van Wijnen, V. Nurcombe, G.D. Prestwich, S.M. Cool, Hyaluronic acid-based hydrogels functionalized with heparin that support controlled release of bioactive BMP-2, Biomaterials 33(26) (2012) 6113-6122.
[238] M. Kisiel, A.S. Klar, M. Ventura, J. Buijs, M.K. Mafina, S.M. Cool, J. Hilborn, Complexation and Sequestration of BMP-2 from an ECM Mimetic Hyaluronan Gel for Improved Bone Formation, Plos One 8(10) (2013).
[239] O. Chaudhuri, L. Gu, D. Klumpers, M. Darnell, S.A. Bencherif, J.C. Weaver, N. Huebsch, H.-p. Lee, E. Lippens, G.N. Duda, D.J. Mooney, Hydrogels with tunable stress relaxation regulate stem cell fate and activity, Nature Materials 15 (2015) 326.
[240] S. Paine-Saunders, B.L. Viviano, A.N. Economides, S. Saunders, Heparan sulfate proteoglycans retain Noggin at the cell surface: a potential mechanism for shaping bone morphogenetic protein gradients, J Biol Chem 277(3) (2002) 2089-96.
[241] Y.G. Ko, H.J. Lee, S.S. Shin, U.S. Choi, Dipolar-molecule complexed chitosan carboxylate, phosphate, and sulphate dispersed electrorheological suspensions, Soft Matter 8(23) (2012) 6273-6279.